UNIVERSITY OF CALIFORNIA

Santa Barbara

Discovery and Delivery of Synergistic Chemotherapy Drug Combinations to Tumors

A dissertation submitted in partial satisfaction of the requirements for the degree

Doctor of Philosophy in Chemical Engineering

by

Kathryn Militar Camacho

Committee in charge:

Professor Samir Mitragotri, Chair

Professor Francis J. Doyle III, Harvard University

Professor Craig J. Hawker

Professor Michelle A. O'Malley

December 2015

The dissertation of Kathryn Militar Camacho is approved.

_____

Francis J. Doyle III

_____

Craig J. Hawker

_____

Michelle A. O'Malley

_____

Samir Mitragotri, Committee Chair

December 2015

Discovery and Delivery of Synergistic Chemotherapy Drug Combinations to Tumors

ACKNOWLEDGEMENTS

"Watching great people do what you love is a good way
to start learning how to do it yourself"
– Amy Poehler, *Yes Please*

I've been blessed to have had the support, camaraderie, and counsel of many amazing souls, without whom I would not have had the drive nor the intellect to complete this Ph.D. They each have distinct qualities I admire and try to adopt in my own life, and collectively have helped me grow throughout the past 5.5 years into a stronger, humbler, and happier version of myself.

To Samir, you taught me how to become a more efficient researcher - how to not get caught in rabbit holes when there was a bigger picture to find. As an advisor, you trusted me with an immense amount of creative freedom, an invaluable experience which has helped me become more curious and independent. Thank you for being patient when nothing worked, and for pushing me, but not too much. You have been incredibly supportive, and I think that's evident in the tremendous amount of growth each of your students achieves by the time they leave your lab.

To my committee, Frank Doyle, Craig Hawker, and Michelle O'Malley, thank you for your insightful feedback, constructive criticisms, and support throughout my journey. To Matt Metzger and Brenda Remy, the instigators behind my Ph.D., thank you for being great role models to a young, naive undergraduate, for believing in me, and for continuing to impart your wisdom. To Jenny Guerrero, Dan Coller, Gricelda Ramirez, Deepika Singh, Nicole de Vries, and Diana Wu thank you for heartwarming conversations and reminders of how to relax during incredibly stressful times.

To Tracy Hsu, thank you for generously welcoming me into lab, and for your kind words of encouragement throughout the way. To Vivek Gupta, Ming Chen, Sutapa Barua, Byeong Hee Hwang, Zhimin Zhou, Poornima Kolhar, Nishit Doshi, Jinwook Yoo, Jenny Lee, Vinu Krishnan, Michael Evans, Tyler Brown, Apoorva Sarode, Max Nowak, Gwen Zhang, and Dave Smith, thank you for helpful and kind conversations in lab. Lab environment can make all the difference, and your smiles and friendliness helped keep my morale during hectic research days. To Aaron Anselmo and Mike Zakrewsky, thank you for providing me with excellent research advice, even in the midst of your own busy schedules. I wish we could have collaborated more in our time here, but it doesn't mean we can't later!

To Sunny Kumar, thank you for helping develop the tumor model, an enormous challenge which certainly could not have been completed without you. To Amrita Banerjee, thank you for encouraging words during stressful times, and I will miss being lab bench neighbors. To Stefano Menegatti, thank you for sharing your chemistry knowledge with me, and helping accelerate my projects. To Zoë Fuchs, you are an incredibly fast learner and you helped move along my troubleshooting twice as fast had it been just myself. We had a very difficult problem to tackle, but having your help made it that much easier, and I will always be thankful for that.

To Doug Vogus, Izzy Jarvis, and Anusha Pusuluri, thank you for your help with *in vivo* studies. You were kind, hardworking, and helped calm my nerves during stressful experiments – a nontrivial feat. To Doug, thank you for helping

guide my experiments, and for also continuing the elephant that is my project, which I know you'll improve upon immensely.

To Renwei Chen, you have offered immense logistical and technical help towards the end of my Ph.D., and I only wish we had your help sooner! To Mary Raven, thank you for your expert advice with confocal microscopy, and making it a colorful tool in my research. Thank you Ronni Wynn and Manny Garcia at the ARC, who have both offered invaluable advice and kind smiles daily. To Jaya Nolt and Shamon Walker, thank you for your patience in teaching me about various forms of spectroscopy. To Laura Crownover, Carina Billigmeier, Kit Holmlund, Pat White, Erica Brunasso and Ruby Mojarro, thank you for all the immensely important behind-the-scenes work and placing rapid orders or shipments.

To Louis Jones, my lava and my light, you have taught me how to have passion in everything that I do (and to do it with a laugh if possible). Thank you for instilling confidence in me when I had the Imposter Syndrome, for challenging me to be kinder and smarter, and for being someone I will always look up to. I am blessed that our paths met here. You have made Santa Barbara even more of a paradise than it already is, and I can't wait to make many more with you! To Dash, you are the sweetest and most fun poochismo I've ever met, and thank you for keeping me warm and happy while thesis writing.

To my incredibly supportive family - I'm so, very fortunate. Although we were far apart, I always had someone to call. Thank you for listening to my issues, even if you couldn't quite understand them, giving constant love, and being the best role models a little sister/daughter/niece could ask for. To my older sisters, Ate Marie and Ate Trixia, who I always wanted to be growing up - you told me not to become the kind of doctors you are, so I chose to become the kind that doesn't really help people, instead. To my twin, Mads, thanks for never making it feel like there was 3,000 miles between us. I spent my Ph.D. discovering what I already knew from us - that 2 is (almost) always better than 1! To my Kuya, thank you for taking the time to write lengthy e-mails to still give me brotherly advice, despite the 15 hour time difference. To Sophies, Logan and Abby, thank you for silly play time which always erases stress. To Rich, Anthony, and Bobby, thank you for instant comic relief during family gatherings and through iPad photo sharing. To Lolamommy, thank you for teaching me and all of my siblings to be determined and kind; I hope to radiate your same energies one day! To Lolapacing, thank you for always being encouraging and supportive. To Mom and Dad, thank you for never forcing me to choose a certain path, and supporting me in every decision I've made. I know I've been in school too long now, but I'll finally have a job and won't have to ask for your help with the bills anymore! To the Jones, Aguila and Fuglevand families, thank you for making me a home in California, and always making sure I was well-fed for the energy demands of graduate school.

And finally, I thank God for showing me over and over again that everything happens for a reason, particularly when an experiment or timing (especially timing!) doesn't always go my way. I've learned to suck it up and pummel through because of it. To everyone acknowledged here, and anyone who has contributed even a kind hello during my time here...as they say in yoga: The light in me honors the light in each in every one of you. Namasté!

VITA OF KATHRYN MILITAR CAMACHO
December 2015

EDUCATION

2010-2015 Doctor of Philosophy in Chemical Engineering
University of California, Santa Barbara

2006-2010 Bachelors of Science in Chemical Engineering
Rutgers University, New Brunswick

PROFESSIONAL EXPERIENCE

2010-2015 Graduate Student Research and Teaching Assistant
Dept. of Chemical Engineering
University of California, Santa Barbara

2009 Undergraduate Fellowship
Pharmaceutical Commercialization Technology
Merck & Co., Inc.

2008 Undergraduate Research Assistant
Dept. of Chemical Engineering
Rutgers University, New Brunswick

PATENTS AND PUBLICATIONS

K. M. Camacho, S. Menegatti, D. Vogus, A. Pusuluri, Z. Fuchs, M. Jarvis, M. Zakrewsky, M. A. Evans, R. Chen, S. Mitragotri. "Tumor inhibition of low dose chemotherapy by synergistic co-encapsulation in liposomes" (*In preparation*).

S. Mitragotri, K. M. Camacho, S. Menegatti. "Drug formulations for cancer treatment" (*Patent in preparation, UC Case No. 2016-246*).

K. M. Camacho, S. Menegatti, S. Mitragotri. "Low molecular weight polymer-drug conjugates improve synergistic anticancer activity of CPT and DOX combinations" (*In Review*).

K. M. Camacho, S. Kumar, S. Menegatti, S. Mitragotri. “Polymer-drug conjugates for the co-delivery of synergistic chemotherapy drugs” (Provisional U.S.S.N. Patent No. 62/130,284*)*.

K. M. Camacho, S. Kumar, S. Menegatti, D. R. Vogus, A. C. Anselmo, S. Mitragotri, "Synergistic Antitumor Activity of Camptothecin-Doxorubicin Combinations and their Conjugates with Hyaluronic Acid", Journal of Controlled Release, 210: 198-207 (2015).

M. Masaeli, E. Sollier, H. Amini, W. Mao, K. Camacho, N. Doshi, S. Mitragotri, A. Alexeev and D. Di Carlo. "Continuous Inertial Focusing and Separation of Particles by Shape", Physical Review X, 2(3): 31017-30 (2012).

PRESENTATIONS

K. M. Camacho, S. Kumar, S. Menegatti, D. R. Vogus, A. C. Anselmo, S. Mitragotri. Synergistic Antitumor Activity of Camptothecin and Doxorubicin Hyaluronic Acid-Conjugates (poster). *Cancer Nanotechnology Gordon Research Conference* (2015-West Dover, VT)

K. M. Camacho and S. Mitragotri. Liposomal Co-encapsulation of 5-Fluorouracil and Doxorubicin for Synergistic Anticancer Activity. *American Institute of Chemical Engineers* (2013-San Francisco, CA).

K. M. Camacho, S. Rahmani, J. Lahann, S. Mitragotri. Nanoparticles for Dual Delivery of Synergistic Chemotherapy Drugs (poster). UCSB Chemical Engineering Clorox-Amgen Graduate Student Symposium (2012-Santa Barbara, CA).

K. M. Camacho and Alan R. Silverman. Film Coating Scale-Up in Dimensional and Dimensionless Contexts (poster). *Merck Design of Experiments Symposium* (2009-West Point, PA).

OUTREACH

Mar-Aug 2013	Institute for Science & Engineer Educators (ISEE) Professional Development Program
Jun 2011-2015	Research Mentor: Advised UCSB (5) undergraduate students on nanoparticles for drug delivery

AWARDS AND RECOGNITIONS

May 2010	Graduated Summa Cum Laude in Chemical Engineering
May 2008-2010	Omega Chi Epsilon Chemical Engineering Honor Society
Mar 2009, 2010	Merit Award (highest GPA) in Rutgers Chemical Engineering

ABSTRACT

Discovery and Delivery of Synergistic Chemotherapy Drug Combinations to Tumors

by

Kathryn Militar Camacho

Chemotherapy combinations for cancer treatments harbor immense therapeutic potentials which have largely been untapped. Of all diseases, clinical studies of drug combinations are the most prevalent in oncology, yet their effectiveness is disputable, as complete tumor regressions are rare. Our research has been devoted towards developing delivery vehicles for combinations of chemotherapy drugs which elicit significant tumor reduction yet limit toxicity in healthy tissue. Current administration methods assume that chemotherapy combinations at maximum tolerable doses will provide the greatest therapeutic effect – a presumption which often leads to unprecedented side effects. Contrary to traditional administration, we have found that drug ratios rather than total cumulative doses govern combination therapeutic efficacy. In this thesis, we have developed nanoparticles to incorporate synergistic ratios of chemotherapy combinations which significantly inhibit cancer cell growth at lower doses than would be required for their single drug counterparts.

The advantages of multi-drug incorporation in nano-vehicles are many: improved accumulation in tumor tissue via the enhanced permeation and retention effect, limited uptake in healthy tissue, and controlled exposure of tumor tissue to optimal synergistic drug ratios. To exploit these advantages for polychemotherapy delivery, two prominent nanoparticles were investigated: liposomes and polymer-drug conjugates. Liposomes represent the oldest class of nanoparticles, with high drug loading capacities and excellent biocompatibility. Polymer-drug conjugates offer controlled drug incorporations through reaction stoichiometry, and potentially allow for delivery of precise ratios. Here, we show that both vehicles, when armed with synergistic ratios of chemotherapy drugs, significantly inhibit tumor growth in an aggressive mouse breast carcinoma model. Furthermore, versatile drug incorporation methods investigated here can be broadly applied to various agents. Findings from our research can potentially widen the therapeutic window of chemotherapy combinations by emphasizing investigations of optimal drug ratios rather than maximum drug doses and by identifying appropriate nanoparticles for their delivery. Application of these concepts can ultimately help capture the full therapeutic potential of combination regimens.

TABLE OF CONTENTS

LIST OF FIGURES

LIST OF ABBREVIATIONS

5FU	5-Fluorouracil
5FUG	1-[(aminomethyl)-ester]methylene-5-fluorouracil
5FUR	5-Fluorouridine
5FURW	Tryptophan 5-fluorouridine ester
5FUW	Tryptophan 5-fluorouracil ester
Boc-glycine	N-(tert-Butoxycarbonyl)glycine
Chol	Cholesterol
CI	Combination index
CPT	Camptothecin
CPT-11	Irinotecan
D	Diffusivity
D_{50}	Concentration which inhibits 50% cell growth
Da	Dalton
Da_1, Da_2	Damköhler numbers
DCM	Dichloromethane
DIC	N,N′-Diisopropylcarbodiimide
DOC	Docetaxel
DOTAP	1,2-dioleoyl-3-trimethylammonium-propane
DOX	Doxorubicin
DMAP	4-(dimethylamino)pyridine
DMEM	Dulbecco's modified eagle's medium
DMSO	Dimethyl sulfoxide
DSPC	1,2-Distearoyl-sn-glycero-3-phosphocholine
EDC	N-(3-dimethylaminopropyl)-N′-ethylcarbodiimide hydrochloride
EPR	Enhanced permeability and retention
FBS	Fetal bovine serum
FdUMP	5-fluorodeoxyuridine monophosphate
FUMP	5-fluorouridine monophosphate
GEM	Gemcitabine
H&E	Hematoxylin and eosin

HA	Hyaluronic acid
HMFU	Hydroxymethyl-5-fluorouracil
HPMA	N-(2-hydroxypropyl)methacrylamide
i.v.	Intravenous
J	Mass flux
k_b	Reverse reaction rate
k_f	Forward reaction rate
k_m	Lipid membrane permeability
LAP	Lapatinib
MEBM	Mammary epithelial basal medium
mPEG-DSPE	1,2-dioleoyl-sn-glycero-3-phosphoethanolamine-N-[methoxy(polyethylene glycol)-2000]
MTD	Maximum tolerable dose
MW	Molecular weight
MWCO	Molecular weight cut off
NMWL	Nominal molecular weight limit
PEG	Polyethylene glycol
ppt	Precipitate
PVA	Poly(vinyl alcohol)
R	Molar ratio of drugs combined, in alphabetical order
RPMI	Roswell Park memorial institute medium
S-PVA	Succinylated poly(vinyl alcohol)
s.c.	Subcutaneous
$t_{1/2,R}$	Time for half of drug to release
τ_L	Residence time of one DOX molecule in liposome
T_m	Phase transition temperature of lipid membrane
TFA	Trifluoroacetic acid
Top I/II	Topoisomerase I/II
TPT	Topotecan

Chapter 1

Introduction

1.1. Cancer Therapies

Of the most common cancer treatments, chemotherapy unmistakably bears the greatest stigma. Surgery removal is often associated with high success rates, particularly when the cancer is confined to a primary tumor and can be easily located [1]. Radiation therapy can be honed in to only expose tumors to high energy beams, rendering the procedure effective at killing cancer cells and relatively painless to other areas of the body [2]. Chemotherapy, however, is at best described by the American Cancer Society as "strong drugs to treat cancer" [3], which is a slight euphemism for the reality: drugs which indiscriminately inhibit the growth of cells, be them cancerous or healthy, and often cause adverse side effects. Because of this inability to differentiate between which cells to kill, chemotherapy is often used when surgery or radiation alone is insufficient to treat the cancer. However, if chemotherapy were engineered in such a fashion to only destroy cancer cells and leave healthy cells unscathed, side effects would be diminished and chemotherapy may be just as potent of a therapeutic, if not more, than radiation or surgery. This is the motivation which drives thousands of labs, academic or industrial, private or public, across many disciplines and countries – the Mitragotri lab at UCSB being no exception. Where our lab has made our mark, specifically where my Ph.D. research

has aimed to contribute to this enormous field, is in the simultaneous delivery of multiple chemotherapy drugs to tumors.

1.2. Organization of the Dissertation

This dissertation explains the advantages of multi-chemotherapy treatment regimens, pitfalls in current chemotherapy combinations, and novel strategies we have developed to capture the therapeutic potential of potent chemotherapy combinations in animal models. In particular, we explore nanoparticles which can incorporate two chemotherapy agents, and can passively accumulate in tumor tissue by escaping blood circulation through tumor endothelium's characteristic leaky pores, known as the enhanced permeability and retention (EPR) effect [4, 5]. In Chapter 3, we present pairs of chemotherapy drugs which demonstrate high activity against cancer cell growth *in vitro*, and serve as model pairs for concurrent tumor delivery in subsequent studies. In Chapter 4, we explore the oldest chemotherapy nanoparticle vehicle, liposomes, and apply it to the delivery of potent drug pair 5-fluorouracil and doxorubicin. We then exploit a relatively new chemotherapy vehicle, polymer-drug conjugates, in Chapter 5, for the concurrent delivery of camptothecin and doxorubicin to 4T1 mammary tumors in mice. Chapter 6 addresses other nanoparticle properties apart from drug payload which vastly impact drug uptake into cells, and hence influence therapeutic efficacy.

Collectively, our studies expose the complexities of multi-drug delivery, elucidate the advantages and disadvantages of each nano-vehicle for clinical applicability, and provides a methodology for designing potent combination

chemotherapy therapeutics. While our work here focused on specific chemotherapy pairs and two major types of drug vehicles, the information gathered has allowed us to develop a multi-drug delivery approach which can be applied to different classes of chemotherapy agents and various vehicles. We hope that our findings can be absorbed and applied by other drug delivery and cancer researchers, in hopes to facilitate in the design of more effective and less formidable cancer therapeutics.

1.3. Current clinical chemotherapy combinations

Chemotherapy combinations have been clinically tried since the 1960s, and were initially inspired by the success of polychemotherapy in treating drug-resistant strains of tuberculosis [6, 7]. The "Holy Grail" of chemotherapy combinations promises a multi-mechanistic approach at killing malignant cells to treat the metastatic and chemotherapy-resistant cancers which single chemotherapy agents often fail at. Yet current clinical trials show mixed results. Some combinations are in fact more potent than single agents, but many are merely comparable or even less effective at prolonging cancer patient survival [8-12]. Often the combinations are associated with greater side effects [13], likely due to amplified toxicity in healthy tissues where both drugs accumulate. Despite the prevalence of multi-chemotherapy regimens in cancer therapies, there is a stark lacking of true success stories which consistently halt tumor progression and prolong patient survival. Inherently, this begs the question if there is true merit to their use in the clinic. Fundamentally, however, the poor efficacy and heightened toxicity of combinations pose two questions: 1. Are two drugs truly better than one at inhibiting

cancer growth? and 2. Is it possible to avoid augmented side effects with combinations? During the course of my Ph.D., I've aimed to address both questions, utilizing *in vitro* drug screens against cancer cells for the former, and engineering safe drug delivery vehicles for the latter.

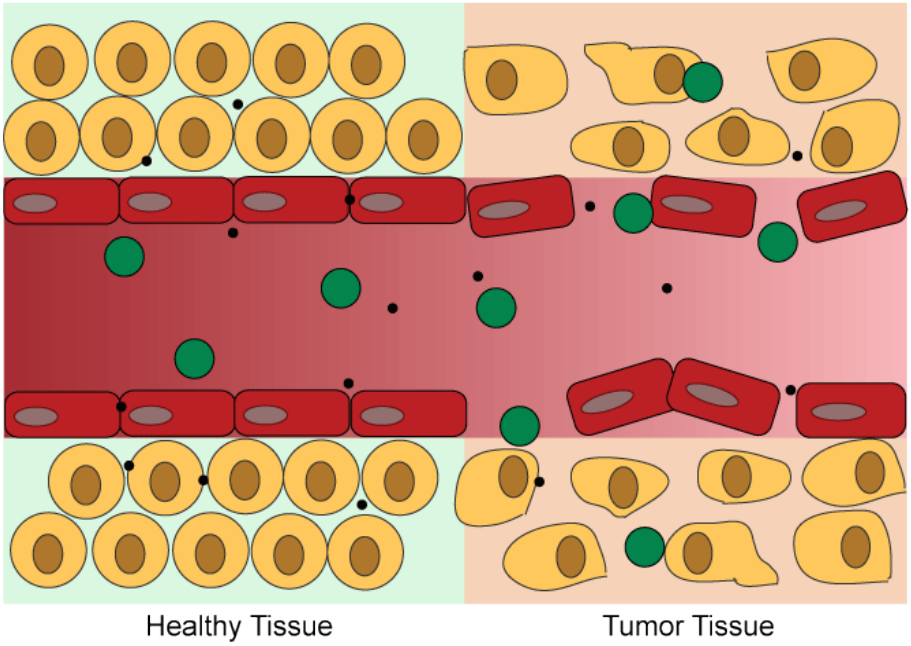

Figure 1.1. Schematic of the enhanced permeability and retention (EPR) effect.

Tumor vasculature, highlighted on the right, is characteristically leaky due to the wide fenestrae present between poorly aligned endothelial cells (red), a phenomena which occurs due to rapid angiogenesis. Nanoparticles (green) below 200 nm in diameter can passively escape blood circulation through these pores to access tumor tissue. On the contrary, healthy tissue consists of highly organized endothelium, whose tight junctions only small molecules (black) can diffuse through. Therefore, freely circulating small molecule chemotherapy drugs can passively accumulate in both healthy and malignant tissue, whereas nanoparticles preferentially localize in tumors.

The criteria which typically govern whether two chemotherapy agents are combined for clinical testing are if the drugs demonstrate some tumor reduction capabilities when used alone, and if their anticipated side effects do not overlap. If yes to both, the two drugs are considered a sound candidate for clinical trials. However, neither of these criteria guarantee that the combination will elicit better

tumor inhibition. Although drugs from different classes attack cancer cell growth via different mechanisms, unprecedented drug interactions can lead to antagonistic, additive, or synergistic cancer inhibition, which lead to reduced, identical, or enhanced therapeutic efficacy, respectively, with respect to the individual drugs. Because drug interactions are difficult to predict, these interactions are currently best studied empirically, in a petri dish of isolated cancer cells. Thus, the first efforts of my Ph.D. focused on identifying drug pairs which synergistically inhibit cancer cell growth *in vitro*. Even if drugs are more effective at inhibiting cancer cell growth *in vitro*, however, they may not necessarily perform the same *in vivo*.

Drugs of various classes possess unique chemical and physical properties, which govern their clearance and metabolization in the body. Hence, two drugs injected in free solutions will not necessarily co-localize in tumor tissue, and may not be able to simultaneously attack the cancer cells with multiple cell death mechanisms. For example, doxorubicin (DOX) and camptothecin (CPT) are both topoisomerase enzyme inhibitors, but their chemical structures differ in that DOX is an anthracycline and CPT is a quinone alkaloid. DOX has been reported to exhibit a clinical half life of 4 minutes [14], whereas that of CPT is much longer, 71-90 minutes [15]. Thus, their biodistribution to various tissues, not excluding the tumor, may vary drastically. Often clinical combinations are administered sequentially in order to avoid simultaneous occurrences of side effects, but this may also prevent concurrent drug delivery to tumors and potentially reduce combination therapeutic efficacy. It is noteworthy that the order of drugs as well as dose schedule can influence therapeutic efficacy [16-18], but only concurrent drug exposures were

considered herein, and the main focus was to identify synergistic drug ratios. Concurrent polychemotherapy delivery is not typically tried clinically, and is limited due to the presence of adverse side effects.

To overcome treatment-related side effects, nanoparticles have been utilized as a superior delivery alternative to free drug solutions. Unlike drug molecules which are small enough to diffuse through capillary walls into tissues, nanoparticles ranging between 10 nm and 200 nm in size can only passively diffuse into tissue through large pores in the endothelial wall [19]. Thus, tumor tissues which exhibit disordered blood vessel structure and leaky endothelial walls tend to passively uptake nanoparticles; furthermore, their poor lymphatic drainage prevents leakage of nanoparticles once accumulated [4, 20]. This phenomena is known as the enhanced permeability and retention effect (EPR) and is schematically demonstrated in Figure 1.1. Nanoparticles carrying chemotherapy payloads will hence allow the preferential accumulation of drugs in tumors. Moreover, nanoparticles can encapsulate and protect drugs from quickly becoming cleared from circulation or from metabolization into inactive forms. Drug clearance occurs within minutes from intravenous administration, owing to their small size and filtration through the kidneys. Nanoparticles, however, can be engineered to larger sizes than the renal filtration cutoff (~5nm) [21], and can instead act as a drug depot which slowly releases the drug and prolongs its circulation. Doxil™, for example, is a liposomal formulation of DOX which extends the drug's elimination half life from 4 minutes in its free form to 3 hours [14]. Longer drug circulation allows for greater number of passes through tumor endothelium, and more chances to escape and treat tumor

tissue. Hence, nanoparticles are multifunctional drug carriers which can not only prevent drug accumulation in healthy tissue, but can also direct therapies to tumors and, as a result, potentiate therapeutic efficacy while also reducing side effects.

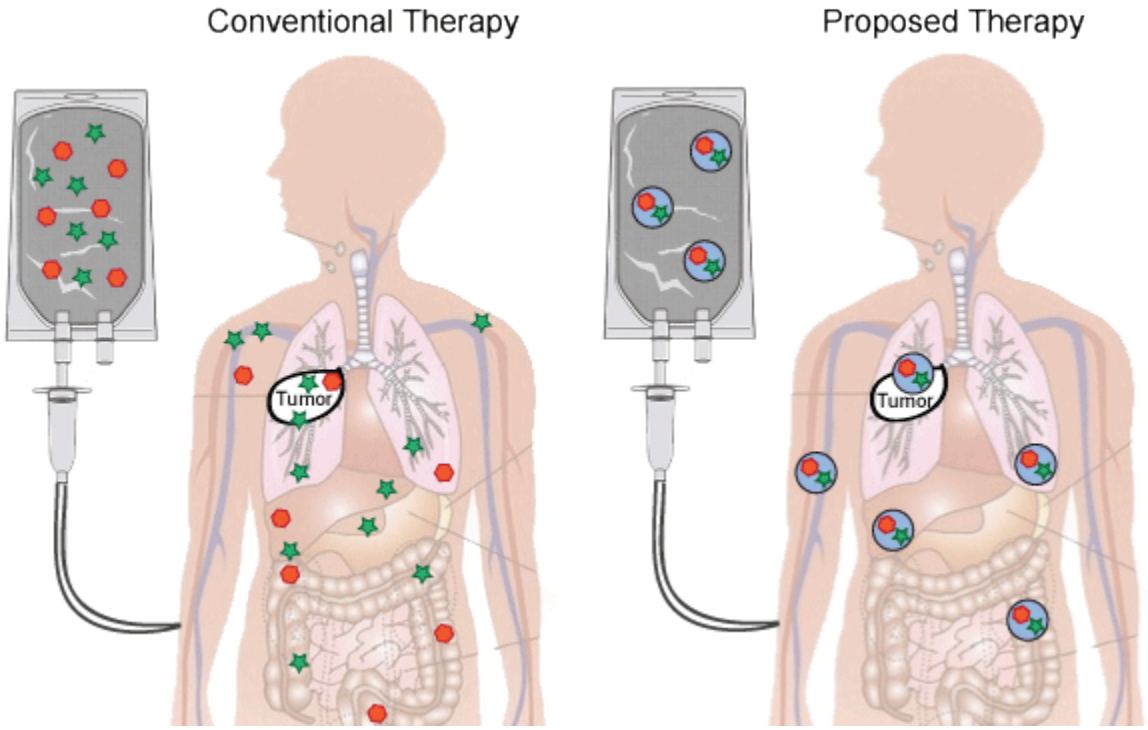

Figure 1.2. Proposed nanoparticle co-delivery of combination chemotherapy.

Conventional combination chemotherapy administration (left) involves infusions or bolus injections of drugs in free solution, often sequentially. Differences in drug pharmacokinetics result in distinct biodistributions and varied uptake in tumors. In contrast, the proposed nanoparticle co-delivery of polychemotherapy (right) encapsulates multiple drugs in a single carrier, unifies drug pharmacokinetics and ensures concurrent arrival in tumors. Hence, the administered drug ratio is also the ratio which is exposed to the tumor. Adapted from [23].

Nanoparticles for the concurrent delivery of multiple chemotherapy drugs is a particularly promising and burgeoning area of research [22]. Co-encapsulation of multiple drugs in a single nanoparticle will unify their pharmacokinetics and ensure simultaneous arrival in tumors (Figure 1.2). Nanoparticles can also alleviate the amplified toxic side effects associated with polychemotherapy by preventing

immediate drug distribution to healthy tissues. Thus, multi-drug loaded nanoparticles have the potential to both improve the survival rates and quality of life of patients treated with polychemotherapy.

1.4. Multi-Drug Delivery Carriers

Traditional nanoparticles which have been investigated for chemotherapy delivery are composed of three main materials: lipids, polymers, or organometallic compounds [20]. Of the three, lipid- and polymer-based particles have had the most prevalence clinically due to their biodegradability and safety, and have also been the most investigated for multi-drug encapsulations. Liposomes in particular have had the most clinical success in delivering multiple chemotherapy drugs. They consist of phospholipids which self-assemble to form an aqueous core surrounded by a lipid bilayer membrane, so multiple hydrophilic drugs can be trapped inside. Drugs can either be incorporated during liposome self-assembly, or post-fabrication by crossing the lipid bilayer and retaining in the inner aqueous environment. Celator Pharmaceuticals currently has three multi-drug loaded liposomes in clinical trials against various cancers. One formulation, CPX-351, achieves a 5:1 ratio of cytarabine and daunorubicin by incorporating cytarabine during liposome fabrication and daunorubicin post-fabrication. CPX-351 was able to elicit a whopping 9 complete responses of 43 patients with acute myeloid leukemia in Phase I clinical trials with acceptable tolerability, and is currently in ongoing Phase III trials [24]. Although this particular formulation has been met with great success, it is unclear

whether the same encapsulation methods can be universally applied to other chemotherapy combinations.

Polymeric nanoparticles are widely utilized for multi-drug delivery, owing to the versatile drug incorporation methods. Drugs can either be physically absorbed inside a polymeric nanoparticle, governed by hydrophobic-hydrophilic interactions, or chemically conjugated to functional groups on the polymeric backbone. One key advantage of polymeric nanoparticles over liposome-based carriers is controlled incorporation through reaction stoichiometry. In pre-clinical studies, gemcitabine (GEM) and DOX were co-conjugated to N-(2-hydroxypropyl)methacrylamide (HPMA) and were more potent at inhibiting tumor growth compared to their free drug counterparts [25]. HPMA conjugated to GEM and DOX were not able to completely eradicate the tumor, but the drug pair was not optimized to synergistically inhibit cancer cells in this study. Although polymeric nanoparticles carrying multiple chemotherapy agents have not entered clinical trials, polymer-drug conjugates bearing single drugs are in ongoing trials, and implicate the potential of these vehicles for improving polychemotherapy delivery.

Regardless of the nanoparticle type, the ultimate test for their applicability for multi-chemotherapy delivery is their ability to incorporate synergistic drugs. Multi-drug delivery only bears merit if the drugs enhance each others' potencies; otherwise, it's not economical or time-efficient to incorporate another drug which, at best, elicits the same survival rate as either of the individual drugs. It is also likely that the added drug will cause more adverse side effects, a sacrifice which may only be validated if therapeutic efficacy were significantly improved. However, drug

encapsulation may not easily be controlled, especially if one drug prefers conjugation or physical entrapment more than the other due to differences in chemical properties. Therefore, synergistic drug incorporation is a non-trivial feat, and it is not currently clear which particle type is more advantageous for these purposes.

1.5. Engineering combination chemotherapies

The approach we adopted to develop safe and effective chemotherapy combination delivery methods was to first empirically identify drug pairs which synergistically inhibit cancer cell growth, and to further encapsulate the model combinations in nanoparticles which can passively accumulate in tumors. Only drugs from different chemotherapy classes were assessed for synergistic cancer cell kill, in order to simultaneously attack different pathways of cell proliferation. Two nanoparticles were investigated for combination chemotherapy co-delivery, liposomes and polymer-drug conjugates. While liposomes are more conventional nanoparticles, water soluble polymers can exhibit hydrodynamic radii between tens and hundreds of nanometers to surpass kidney filtration and exploit the EPR effect [26, 27], thereby also classifying as nanoparticles. Liposomes typically encapsulate drugs through passive techniques, while polymer-drug conjugates incorporate drugs through chemical conjugation. Both types of nanoparticles have been shown to encapsulate high single drug payloads, and have demonstrated clinical efficacy at reducing tumor progression [28-30]. Herein, we elucidate their potential for combination chemotherapy delivery, while also uncovering disadvantages to each. Particular emphasis is given towards the applicability of each vehicle for various

classes of chemotherapy agents. A plethora of chemotherapy combinations have been investigated clinically, and even more pre-clinically; however, to advance these promising regimens forward to successful therapies, multi-drug delivery carriers which can be universally applied to drugs of various classes must be developed.

Chapter 2

Experimental Methods

2.1. Cell culture: All cell lines were purchased from ATCC (Manassas, VA, USA) and grown in a humidified incubator maintained at 5% CO_2 at 37˚C. BT-474 human breast cancer cells were cultured in Hybri-Care medium (ATCC) supplemented with 10% fetal bovine serum (FBS) , and 4T1 murine breast carcinoma cells were cultured in RPMI-1640 medium supplemented with 2.05 mM L-glutamine, 10% FBS and 1% penicillin/streptomycin. Murine brain endothelial cell line bEnd.3 was cultivated in DMEM medium supplemented with 4 mM L-glutamine, 4500 mg/L glucose, 1 mM sodium pyruvate, 1500 mg/L sodium bicarbonate (ATCC), 10% FBS and 1% penicillin/streptomycin. MCF 10A human breast epithelial cells were cultured in MEBM basal medium supplemented with 2 mL bovine pituitary extract, 0.5 mL hydrocortisone, 0.5 mL human epidermal growth factor, and 0.5 mL insulin, all of which were obtained from Lonza Walkersville Inc. (Walkersville, MD, USA). All other medium and medium supplements, unless otherwise noted, were obtained from Thermo Scientific (Waltham, MA, USA).

2.2. *In vitro* cell growth inhibition studies: To assess drug effects on cell proliferation, MTT (3-(4,5-dimethylthiazol-2-yl)-2,5-diphenyltetrazolium bromide; Life Technologies, Carlsbad, CA, USA) *in vitro* cell cytotoxicity assays were utilized. When living cells internalize MTT, they convert MTT to an insoluble formazan.2-4

dye. Thus the amount of living cells scales linearly with the intensity of the dye. The MTT protocol is as follows: In a 96-well plate, specified cell concentrations were mounted in a total volume of 100 μL full cell culture media/well and allowed to adhere overnight. For BT-474, bEnd.3, and MCF 10A studies, the initial cell seeding density was 1.0 x 10^4 cells/well. For 4T1 cytotoxicity studies, the cell seeding density was 1.0 x 10^3 cells/well. The media was then replaced with fresh media containing drug, nanoparticles, or drug-loaded nanoparticles. The cells were incubated with drug and/or nanoparticle solutions for designated times at 37°C and 5% CO_2. BT-474, bEnd.3, and MCF 10A cells were incubated with agents for 72 hours, whereas 4T1 cells were incubated for 48 hours. Initial cell concentrations and drug incubation times were chosen such that untreated cells reached 70% confluency after the designated time period. Afterwards, the media was replaced with 0.5 mg/mL MTT in media and returned to 37°C and 5% CO_2 for 4 hours. Media was then replaced with 100% dimethyl sulfoxide (DMSO) to solubilize intracellularly reduced MTT (formazan crystals), and formazan dye intensity was determined by absorbance measured at 570 nm in a Tecan Infinite M200 Pro plate reader (Männedorf, Switzerland). The fraction of inhibited cell growth, also known as fractional cell inhibition, was calculated by subtracting absorbance of live cells in experimental wells from that of control cells and normalizing against control cells. Experimental data was fit to the Median Effect (ME) model (Equation 2.1) developed by T.C. Chou and P. Talalay [31],

$$\frac{f_i}{f_u} = \left(\frac{D}{D_{50}}\right)^m \tag{2.1}$$

where f_i and f_u refer to fraction of cells inhibited and uninhibited, respectively, m dictates the shape of the drug dose-cell inhibition (also known as "dose-effect") relationship, D is the drug concentration which elicits f_i cell growth inhibition and D_{50} is the drug concentration required to inhibit 50% cell growth. D_{50} and m were derived for each drug by fitting experimental D, f_i values to linearized Equation 2.1 via linear regression analysis.

2.3. Synergy assessment, the Combination Index method: T.C. Chou and P. Talalay's Combination Index (CI) method was adopted to identify synergistic chemotherapy pairs. The CI is defined in Equation 2.2:

$$CI = \frac{D_1}{D_{x,1}} + \frac{D_2}{D_{x,2}} \qquad (2.2)$$

$D_{x,1}$ and $D_{x,2}$ represent doses of drug 1 and 2, respectively, which inhibit x% cell growth when used alone. On the other hand, D_1 and D_2 are the combination doses of drug 1 and drug 2, respectively, which also inhibit x% cell growth. Hence, the CI can be considered as the dose reduction achieved by combining the drugs compared to their single drug administration. A CI of less than 1 indicates synergy, a CI equal to 1 denotes the additive effect, and a CI greater than 1 occurs if the drugs are antagonistic. Graphs representing CI often include a solid black line which represents additivity (CI=1) in order to help visualize these regimes of interactions. To find $D_{x,1}$ and $D_{x,2}$ for CI evaluation, the dose D of each drug must be defined as a function of inhibition, x. For this, the ME model (Equation 2.1) determined for each individual drug was utilized, where x is simply fraction cell growth inhibition, f_i.

2.4. Confocal microscopy: Confocal laser scanning microscopy was utilized to visualize cells and any fluorescent markers, such as, but not limited to, internalized fluorescent drugs. Cells were seeded at a density of 80,000 cells per 300 μL media in a Nunc Lab-Tek 8-well chambered borosilicate coverglass (Thermo Scientific; Waltham, MA, USA), and were allowed to adhere overnight. Post-treatment with indicated fluorescent drugs, nanoparticles, or other specified markers, cells were washed twice with warmed PBS (pH 7.4), followed by staining with nuclear dyes at 37˚C, 5% CO_2. In the case of DOX-exposed cells, Hoechst nuclear dye was utilized at a concentration of 25 μg/mL for 30 minutes. For CPT-exposed cells, to avoid overlap fluorescence between CPT and nuclear marker, DRAQ5 was used to stain nuclei at a concentration of 5 μM in media for 60 minutes. Cells were washed twice more in warmed PBS and finally suspended in media immediately prior to imaging. All cells were imaged live with an Olympus Fluoview 1000 spectral confocal equipped with a 60X silicon oil objective and a 37˚C temperature-controlled imaging chamber. DOX, fluorescein, CPT, Hoechst and DAPI were excited with the following lasers: 488 nm 10 mW Argon gas (DOX or fluorescein), 405 nm 50 mW diode (CPT or Hoechst), and 635 nm 20 mW diode (DRAQ5). For general oxidative stress detection studies, carboxydichlorofluorescein and DOX were both excited utilizing a 488 nm 10 mW Argon gas laser and visualized with 492-560 nm and 574-674 nm optical filters, respectively. Z-stacks of 10 μm were captured and subsequently analyzed with ImageJ 1.47h software (NIH). Each z-stack was collapsed into an averaged image, and fluorescence intensity was reported as the raw integrated density divided by number of cells. An average of 25 cells was imaged in each field view. Where

provided, images are representative of all samples in the experimental group, and are shown as averaged z-stacks.

2.5. Apoptosis studies: Apoptosis assessment was made based on Annexin V and Sytox Green counterstaining. Studies followed the Life Technologies Apoptosis Assay protocol, with few modifications tailored to BT-474 cells. Briefly, cells were seeded at a concentration of 100 x 10^4 cells per 25 cm^2 cell culture flask in a total volume of 10 mL media, and allowed to adhere overnight. Cells were exposed to drug solutions for 72 hours, as previously described. After drug exposure, adherent and floating cells were harvested at a concentration of 1 x 10^6 cells/mL in Annexin V binding buffer, and 200 µL of each sample were incubated with 5 µL of Annexin V-647 and 1 µL of 1 µM Sytox Green. After 15 minutes of dye incubation, cells were diluted 5X in ice cold Annexin V Binding Buffer, and immediately analyzed via flow cytometry in a Becton Dickinson FACSAria cell sorter (Franklin Lakes, NJ, USA). To quantify Annexin V-647 and Sytox Green fluorescence, a 633 nm laser with 660 PMT and a 488 nm laser with 530 PMT, respectively, were utilized. Cells gated as –AV/-SG were live, cells with +AV/-SG were pre-apoptotic, and cells gated as +AV/+SG were either late apoptotic or necrotic.

2.6. Liposome Fabrication: Liposomes were fabricated utilizing the conventional thin film evaporation method [32], and all lipids were purchased from Avanti Polar Lipids (Alabaster, Alabama, USA). Specified lipids were co-dissolved in chloroform and methanol in a round-bottom flask, and organic solvent was removed

using a Buchi R-210 rotary evaporator at reduced pressure and 60˚C (5˚C above the lipid transition temperature) in order to form a thin lipid film. The film was subsequently hydrated in 250 mM ammonium sulfate at 60˚C to form large multilamellar vesicles. Small, monodisperse vesicles were produced by passing vesicles 21 times through an extruder (Avestin LiposoFast Extruder) with 100 nm polycarbonate filters. A transmembrane ammonium sulfate gradient was generated by passing the liposomes through a Sephadex G-25 PD-10 size exclusion column of molecular weight cut off (MWCO) 5000 Da (GE Healthcare Life Sciences; Piscataway, NJ, USA) equilibrated with PBS (pH 7.4) [45]. DOX was encapsulated by incubation with liposomes after generation of the transmembrane ammonium sulfate gradient for 30 minutes at 65°C. 5FU encapsulation methods are reported in the respective sections of Chapter 4. To remove free drug, liposomes were finally passed through a Sephadex G-25 PD-10 column.

To measure drug encapsulation, 50 μL of drug-loaded liposomes were dissolved in 950 μL methanol through vortexing and sonication. The dissolved liposomes were centrifuged at 12000 g for 20 minutes to allow the lipids to pellet. The supernatant was collected, diluted serially, and their absorbances were measured at 480 nm, 266nm, 264 nm, 268 nm, 268 nm, and 394 nm to quantify DOX, 5FU, 5FUG, 5FUW, 5FUR, and 5FURW concentrations, respectively.

2.7. Nanoparticle characterization: Nanoparticle sizes and ζ potentials were determined utilizing dynamic light scattering and electrophoretic light scattering, respectively, on a Malvern ZetaSizer Nano ZS. Samples were diluted at minimum

100X in distilled de-ionized water immediately prior to analysis, and each measurement is reported as an average of 3 independent sets of at least 13 runs each ± SD.

2.8. Liposome cancer cell growth inhibition: *In vitro* anticancer efficacy of drug-loaded liposomes was determined via calcein-AM cell viability assay. Cells were seeded overnight as described in Section 2.2, followed by liposome incubation with fresh media. Post-incubation with liposomes, media was aspirated and replaced with 1 μM calcein-AM in PBS for 30 minutes at room temperature. Fluorescence intensity of intracellularly hydrolyzed calcein-AM was measured using excitation and emission wavelengths of 490 nm/520 nm. Fractional cell inhibition, f_i, was calculated by subtracting fluorescence of live cells in experimental wells from those of untreated cells and normalizing against untreated cells. D_{50} and m were derived for each drug by fitting experimental D, f_i values to linearized Equation 2.1 (ME model) via linear regression analysis.

2.9. Drug release: Drug release of drugs from drug-loaded nanoparticles was achieved utilizing Slide-A-Lyzer MINI Dialysis Devices of 10,000 MWCO (Life Technologies, Grand Island, NY). Drug-loaded nanoparticles were placed in dialysis cups with fresh PBS buffer (pH 7.4), and were inserted into microcentrifuge tubes containing 1 mL PBS. Dialysis devices were placed at 37˚C and allowed to shake at 100 RPM. At indicated time points, concentrations of drug in the medium surrounding the dialysis cup were determined via absorbance. External PBS buffer

was replenished at each time point. Drug release was fit to exponential release profiles in order to estimate time required for half of the drug to release, indicated by $t_{1/2,R}$.

2.10. *In vivo* antitumor efficacy and toxicity: A mouse 4T1 breast tumor model was utilized to evaluate *in vivo* tumor reduction by combination chemotherapy formulations. All experiments were performed according to approved protocols by the Institutional Animal Care and Use Committee of the University of California, Santa Barbara. Six to eight week old female BALB/c mice were purchased from Charles River Laboratories (Wilmington, MA, USA). Tumor inoculation was achieved by subcutaneously (s.c.) injecting $1x10^5$ 4T1 cells in the abdominal mammary gland in order to prevent interference with normal bodily functions. Prior to injection, 4T1 cells were washed twice in PBS and re-suspended in sterile saline (0.9 wt/vol% NaCl). Tumor inoculation was designated as day "1". Mice were randomly assigned to experimental and control groups, and were treated every other day with specified formulations beginning on day 3 post-inoculation unless otherwise indicated. Treatments were administered via intravenous (i.v.) tail injections, and complete dosing schedules are specified for each study. Tumor growth inhibition was assessed with tumor volume, quantified by $V = ½ (l) x (w)^2$, where l is the longest tumor diameter and w is the shortest tumor diameter measured by a digital caliper. Mice were euthanized when tumor volumes exceeded 1000 mm^3, weight loss exceeded 15% of initial body weight, or if appeared moribound, and these dates were recorded for survival rate calculations. Kaplan–

Meier plots represent the percentage of animals remaining in each treatment group as a function of time following tumor inoculation.

Caspase-3 immunohistochemistry and hematoxylin and eosin (H&E) histology analyses were performed on excised tumors post-treatment in order to further assess tumor growth inhibition. Tumors were fixed and further sent to Mass Histology Services, Inc. (Worcester, MA, USA), where the tissues were paraffin-blocked, stained, and analyzed. To evaluate formulation toxicity, body weights were measured daily. Additionally, liver, spleen, heart, and lung organs were harvested at the end of the experiments, fixed and further analyzed by Mass Histology Services, Inc. via H&E staining.

2.11. Statistical analyses: Statistical significance was assessed via the two-tailed, unpaired Student's t-test in Microsoft Excel. One star indicates significance with $p < 0.05$, and two starts indicate $p < 0.01$.

Chapter 3

Synergistic Chemotherapy Pairs

3.1. Defining synergy

When two drugs are combined, one of three results occurs: synergy, the additive effect, or antagonism. Synergy implies mutual enhancement of both drugs, not simply an increase in therapeutic efficacy for only one drug. Antagonism is the opposite of synergism, where the combination results in lower efficacy. The additive effect occurs when neither efficacy of the drugs is altered, and the drugs can be thought of as non-interacting [31]. However, it is evidently difficult to assess synergy [33]. For example, if two drugs each provide 60% cell death when used alone, an additive effect would not be simple addition of their efficacies, as 120% cell growth inhibition is not possible. In the 1980s, T.C. Chou and P. Talalay derived a method for the ease of synergy assessment: the "Combination Index" (CI) method [31]. The CI is a measurement of synergy, and it can be calculated with a series of drug dose-effect experiments, such as cell inhibition assays. According to this method, $CI = 1$ indicates additivity, $CI > 1$ denotes antagonism, and $CI < 1$ describes synergy. Furthermore, the lower the CI, the more synergistic the pair.

Drugs which are synergistic can accomplish greater efficacy with smaller doses of either drug. Smaller doses can potentially lead to reduced side effects, provided that the drugs do not also synergistically inhibit healthy endothelial or epithelial cell growth, as well as slowed drug resistance due to less drug exposure.

Because harsh side effects and tumor resistance are notorious pitfalls of chemotherapy, cancer treatments can considerably benefit from chemotherapy synergy. Breast cancer in particular is the second most common cancer among women, counting for nearly 1 in 3 cancer cases in women in America [34]. Thus any advancements in breast cancer chemotherapy can potentially benefit millions. Moreover, combination chemotherapies are typical treatment regimes for carcinomas of the breast; some are already FDA-approved (capecitabine + docetaxel [35, 36], lapatinib + letrozole [37], cyclophosphamide + methotrexate + 5-fluorouracil [38]), and numerous others are in clinical trials. Therefore, the preliminary screen for synergistic pairs included four FDA-approved breast cancer drugs with different mechanisms: docetaxel (DOC; antimicrotubule agent), lapatinib (LAP; tyrosine kinase inhibitor), 5-fluorouracil (5FU; antimetabolite), and doxorubicin (DOX; topoisomerase II inhibitor). A thorough search for synergistic chemotherapy combinations helped to identify model drug pairs for nanoparticle encapsulation.

3.2. Single chemotherapy anticancer efficacy

First, individual drug activities were assessed for cancer cell growth inhibition. It was necessary to understand the capabilities of each drug alone so that they could later be compared to the therapeutic efficacies of drug combinations. DOC, LAP, 5FU, and DOX are all FDA-approved chemotherapy drugs for the treatment of breast cancer, proceed through different mechanisms, and are often included in combination chemotherapy regimens. The efficacies of single agents

were determined by exposing the drugs to BT-474 human breast cancer cells, followed by cell viability assessment via MTT cytotoxicity assays (Section 2.2). However, prior to determining the anticancer efficacies for all drugs, it was necessary to optimize general drug incubation conditions. Incubation time had to be long enough to allow drug internalization as well as sufficient interactions with its intracellular target, yet short enough that the cells could be healthily maintained. The incubation conditions also needed to ensure reproducible results between separate experiments.

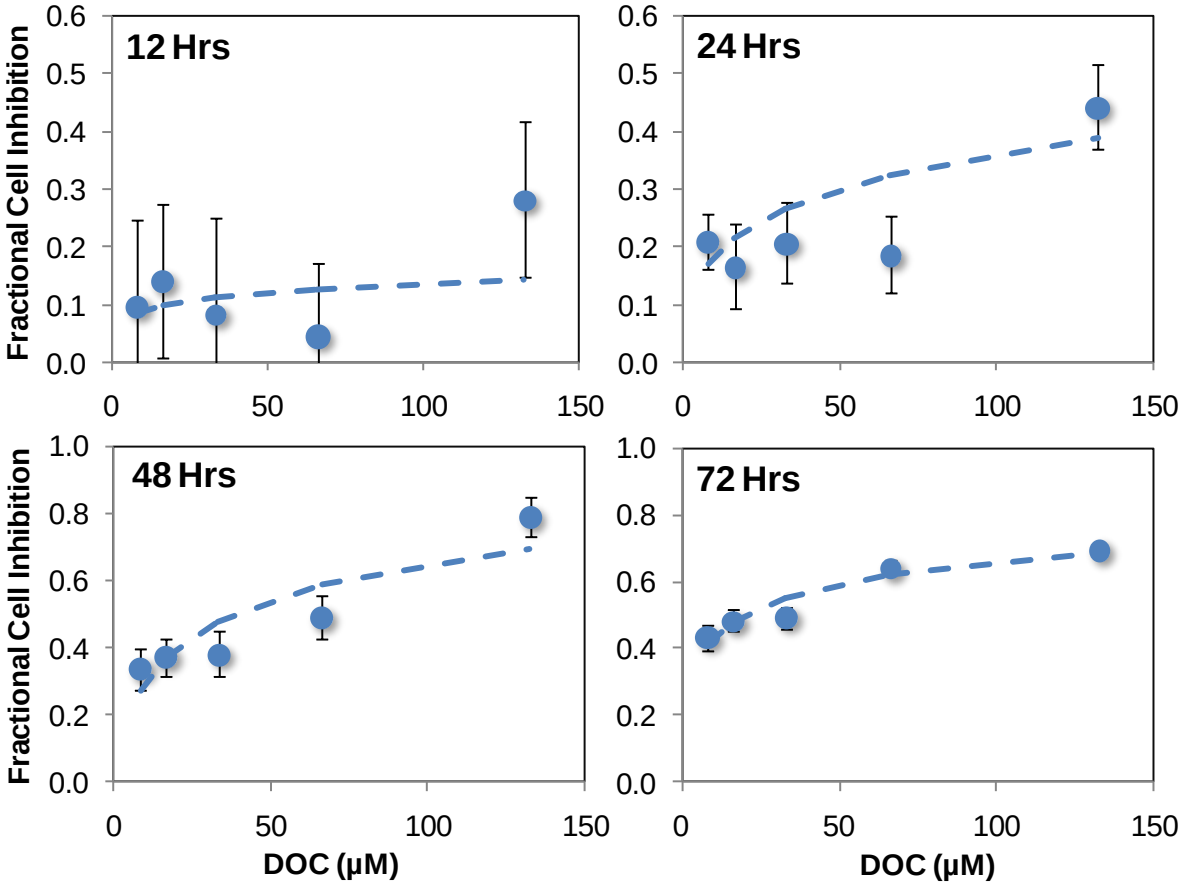

Figure 3.1. Effect of incubation time on DOC dose-effect reproducibility.

DOC was exposed to BT-474 for various incubation times, and cancer cell viability was assessed via MTT cytotoxicity assays. Dashed lines represent fits to the ME model. Data represented as mean ± SD (n ≥ 8). D_{50} (µM) and R^2 corresponding to the ME models for 12, 24, 48 and 72 hours were (1028114 ± 1.2E7, 0.08), (411 ± 428.3, 0.64), (38 ± 27.9, 0.75), and (23 ± 12.0, 0.89).

To determine a sufficient incubation time, a model drug, DOC, was exposed to BT-474 cells for 12, 24, 48, and 72 hours. Experimental data was then fitted to the median effect (ME) model (Equation 2.1), and all results are seen in Figure 3.1. Reproducibility seemed to improve with incubation time, as indicated by the reduced error bars, and the median effect model best fit data from 72 hour incubations, with R^2 closest to 1. The poor consistency observed at short incubation times is likely due to the lag time between drug internalization and drug action. Because DOC is highly hydrophobic, it can diffuse easily into cells through the cell membrane, and thus can be internalized *in vitro* within 4 hours [39]. However, it is commonly found that apoptosis only occurs many hours after taxane treatment on cancer cells, often 24 or 48 hours [40, 41]. Thus, literature suggests that DOC activation time is indeed multiple days, and the results obtained here correlate well with previous work. In addition, the D_{50} concentration (required to inhibit 50% cell growth) determined after 72 hour drug incubation, 23± 12.0 μM, was consistent with previously reported values (33.1 ± 9.3 μM) [42]. Therefore, a 72 hour incubation period was chosen for all future dose-effect studies.

The cancer cell growth inhibitory effects were further assessed for all single chemotherapy agents, and are shown in Figure 3.2. The doses required to impact cell growth evidently differ between each drug, and are an indication of their varied strengths. For example, the concentrations of LAP, 5FU, and DOX which inhibit 50% cell growth fluctuate by different orders of magnitude. LAP only requires 0.08 μM, while 5FU needs to be present in a 6000-fold greater concentration of 487 μM. DOX exhibits a potency between the two extremes, with a D_{50} concentration in the

tenths of μM, 0.3 μM. These D_{50} concentrations are also congruent with previous literature reports [43, 44], and validate our findings. It is clear that all the single drugs are capable of high efficacies (≥ 75% cancer cell growth inhibition), but only at doses much greater than their D_{50} concentrations. Combining these drugs could potentially decrease the doses needed for high efficacy, particularly if the drugs synergistically interact. This would yield a much more potent drug than either single agent because the pair could significantly reduce tumor growth at lower doses than are currently clinically effective.

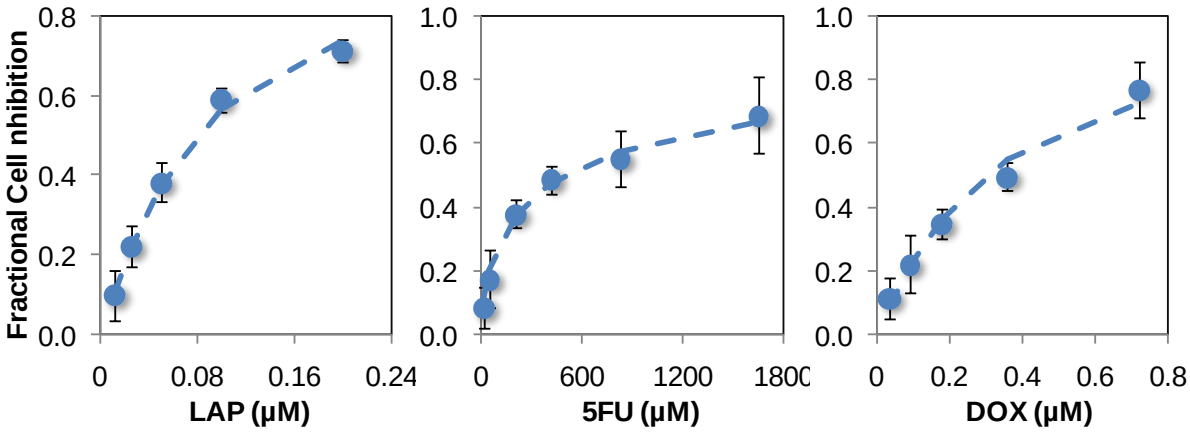

Figure 3.2. *In vitro* cancer cell growth inhibition of single chemotherapy drugs.

LAP, 5FU, or DOX were incubated with BT-474 human breast cancer cells for 72 hours, and cells were assessed for viability via MTT cytotoxicity assays. Dashed lines represent fits to the ME model. Data represented as mean ± SD (n ≥ 8). D_{50} (μM) and R^2 corresponding to the ME models for LAP, 5FU and DOX were (0.08 ± 0.01, 0.99), (487 ± 170.7, 0.98), and (0.30 ± 0.02, 0.98).

3.3. Synergy search

The completion of single drug treatments lead to combination studies, and with it, the exciting quest for synergy. An ideal drug pair would exhibit synergistic cancer cell kill at low doses of either drug because high doses of chemotherapy tend to cause toxicity in healthy tissue as well as tumor resistance. Thus, the highest

impact of polychemotherapy delivery would be achieved with a low dose drug combination. In ambition to find such a drug pair, any combination of the four drugs could be tested and tried. Additionally, each pair could be tested at varying concentrations of either drug. A six-drug pair screen could easily turn into an unmanageable number of experiments. To keep the screens at a reasonable amount, the first synergy trial consisted of drug pairs tested at equal potencies (Table 3.1).

Screen	1	2	3	4	5
Drug 1:Drug 2 dose	$\frac{1}{4}D_{50} : \frac{1}{4}D_{50}$	$\frac{1}{2}D_{50} : \frac{1}{2}D_{50}$	$1D_{50} : 1D_{50}$	$2D_{50} : 2D_{50}$	$4D_{50} : 4D_{50}$

Table 3.1. Equal potency combinations tested in first synergy trial.

For these equal potency experiments, doses were ranged between one-fourth- and four-fold the D_{50} concentrations for each drug. Two-drug combinations of LAP, 5FU, DOX and DOC were assessed for synergy using the Combination Index (CI) method (Section 2.3), and select pairs are shown in Figure3.3. LAP+DOC exhibit CI < 1 for all concentrations tested, implying high synergy, whereas LAP+5FU consistently yield CI > 1, indicating antagonism. LAP+DOX are antagonistic, apart from their highest concentration which appears additive (CI=1). The combination of 5FU+DOX is antagonistic for low concentrations, but becomes increasingly synergistic (decreasing CI values) with increasing dose. The most synergistic pair discovered was LAP+DOC, with CI values ranging between 0.08-0.35. While this pair represents an excellent candidate for inhibiting BT-474 cancer cells, LAP is considered a targeted therapy since it targets membrane receptors EGFR (epidermal growth factor receptor) and HER2/neu (human EGFR type 2). Hence, LAP, as well

as its combination with DOC, will only be effective against cancers which overexpress these receptors, which comprise only about 10% of all breast cancer cases [45]. In an effort to develop widely applicable multi-chemotherapy vehicles which can treat even the most challenging cancer cases, we chose not to conduct further studies on this drug pair. Therefore, 5FU+DOX, the second-most synergistic drug pair, with CIs ranging between 0.41-0.66 at the higher doses, was further investigated.

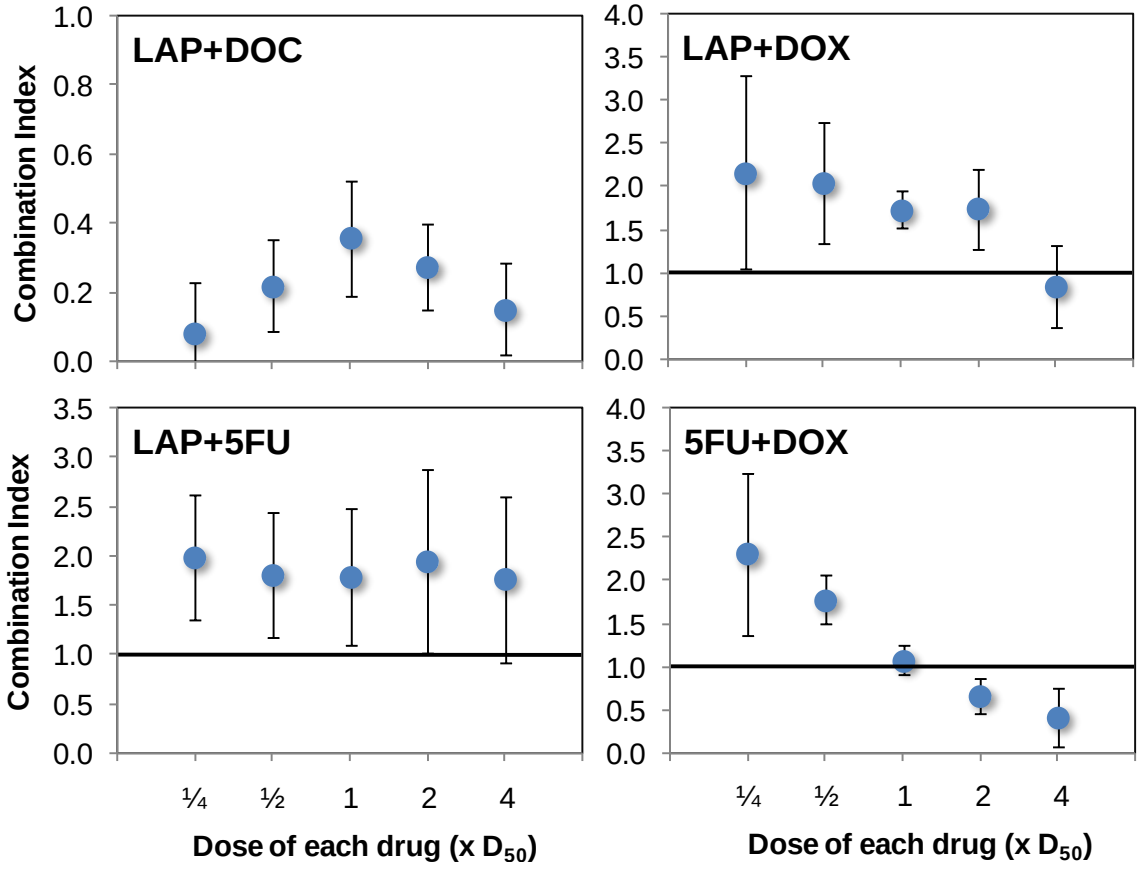

Figure 3.3. Synergy assessment for drugs combined in equal potencies.

Combination indices (CIs) calculated for drug combinations of LAP+DOC, LAP+DOX, LAP+5FU, and 5FU+DOX exposed for 72 hours to BT-474 cells. Drugs were combined in equal potencies, as outlined in Table 3.1. Black line (CI=1) indicates synergy cut-off, above which drugs exhibit antagonistic interactions. Data represented as mean ± SD (n ≥ 8).

3.4. Dependence of synergy on drug ratio

The initial synergy screen presented in the previous section combined drugs in varying total concentrations, while the ratio between the two drug concentrations (R) remained constant. However, it has been established in various literature reports that drug ratio can greatly impact CI, and hence synergy [46-49]. The same two drugs can elicit synergistic or antagonistic cancer cell kill depending on the ratio at which they are exposed to the cells. To improve synergistic interactions between the 5FU+DOX combination identified in Section 3.3, a second synergy screen was conducted whereby the molar ratio between 5FU and DOX (R, 5FU:DOX) was varied by changing DOX concentration. The drug doses used for this second screen are provided in Table 3.2. For low ratios ($R \leq 75$), DOX concentration was held constant at two-fold its D_{50}, 0.3 μM, while 5FU concentration was varied. For high ratios ($R \geq 409$), 5FU concentration was maintained at its D_{50}, 487 μM, while DOX dose was varied. These specific concentrations were utilized because the single drug efficacies at these concentrations should not elicit more than 60% cancer cell growth inhibition. This leaves a sufficient range for improvement in cancer cell kill, and allows for easier identification of synergistic interactions.

A strong dependence of 5FU and DOX interactions on R is evident in Figure 3.4. For $R \geq 3276$, where 5FU concentration dominates, CI is much greater than 1 and implies severe antagonism. CI values close to 1 occur for $75 \leq R \leq 409$, suggesting that the drugs are non-interacting for this regime. For $R \leq 19$, where DOX dose dominates, CI values less than 1 are calculated and indicate synergy. The greatest synergy between 5FU and DOX, however, occurs at $R = 819 \pm 64$, with CI =

0.34 ±0.12. Moreover, various total drug concentrations were tested at a constant R=819, and results in Figure 3.5a-b show that the pair consistently outperformed either 5FU or DOX alone. Various drug concentrations at the highly antagonistic ratio of R=6551 ± 170 were also tested, and the resulting cancer cell kill was consistently less than that of 5FU alone. Hence, for these representative synergistic and antagonistic drug ratios, R seemed to govern drug interactions more than total drug concentration. This finding is promising for the co-delivery of synergistic chemotherapy drugs, because it is difficult to control precise drug concentrations in tumor tissue, whereas ratios can be controlled via incorporation in nanoparticles. The nanoparticles can then unify the transport of a predetermined ratio of drugs specifically to the tumor, as alluded to in Figure 1.2.

Low R Screen	1	2	3	4
5FU:DOX dose	$0.0001D_{50}$: $2D_{50}$	$0.0006D_{50}$: $2D_{50}$	$0.023D_{50}$: $2D_{50}$	$0.092D_{50}$: $2D_{50}$
R (M:M 5FU:DOX)	0.1	0.5	19	75

High R Screen	5	6	7	8	9
5FU:DOX dose	$1D_{50}$: $4D_{50}$	$1D_{50}$: $2D_{50}$	$1D_{50}$: $1D_{50}$	$1D_{50}$: $½D_{50}$	$1D_{50}$: $¼D_{50}$
R (M:M 5FU:DOX)	409	819	1638	3276	6551

Table 3.2. Various R of 5FU+DOX investigated for synergy.

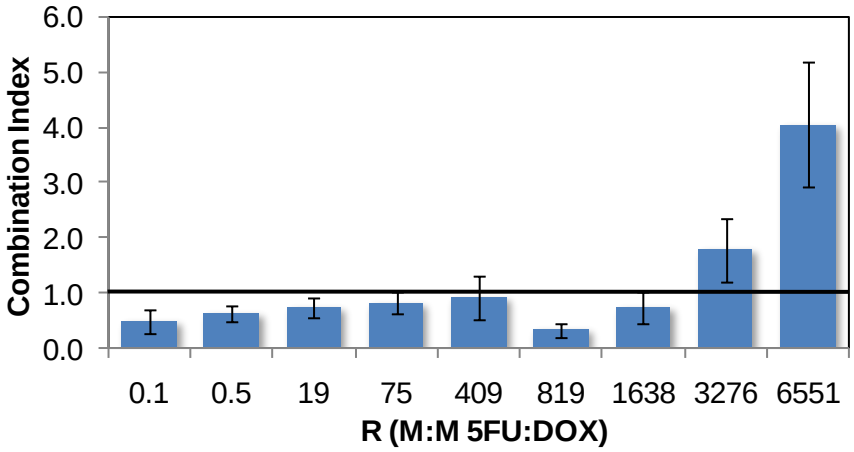

Figure 3.4. Synergy assessment for 5FU+DOX combined at various R.

Combination indices (CIs) calculated for various ratios of 5FU+DOX exposed for 72 hours to BT-474 cells. Drug doses used for this second synergy screen are provided in Table 3.2. For $R \leq 75$, DOX concentration was held constant at two-fold its D_{50}, 0.6 μM, while 5FU concentration was varied. For $R \geq 409$, 5FU concentration was maintained at its D_{50}, 487 μM, while DOX dose was varied. Black line (CI=1) indicates synergy cut-off, above which drugs exhibit antagonistic interactions. Data represented as mean ± SD ($n \geq 6$).

Another important factor which governs the clinical applicability of chemotherapy combinations is the adverse side effects that occur when multiple drugs accumulate in healthy tissue rather than tumors. Because chemotherapy drugs cannot distinguish between healthy and malignant cells, they can easily distribute throughout the body, and toxicity is an inherent challenge. Although nanoparticles can promote drug accumulation in tumors via the EPR effect, it does not eliminate uptake in healthy tissue. In fact, a common issue with nanoparticles is their retention in organs highly involved in the mononuclear phagocyte system (MPS), such as the liver and spleen [50, 51]. To assess potential toxic effects that may occur *in vivo*, 5FU+DOX was challenged *in vitro* against two representative healthy cell lines, bEnd.3 mouse brain endothelial cells and MCF 10A human breast epithelial cells. These cell types were chosen because any systemically-administered drug is susceptible to interactions and uptake by endothelial cells, as well as

epithelial cells in surrounding healthy tissue. 5FU+DOX were exposed to each cell line in the synergistic and antagonistic ratios of R=819 and R=6551, respectively, and toxicity was assessed via MTT assays. The combination toxicities were also compared to 5FU treatment alone and DOX treatment alone, and the results are shown in Figure 3.5.

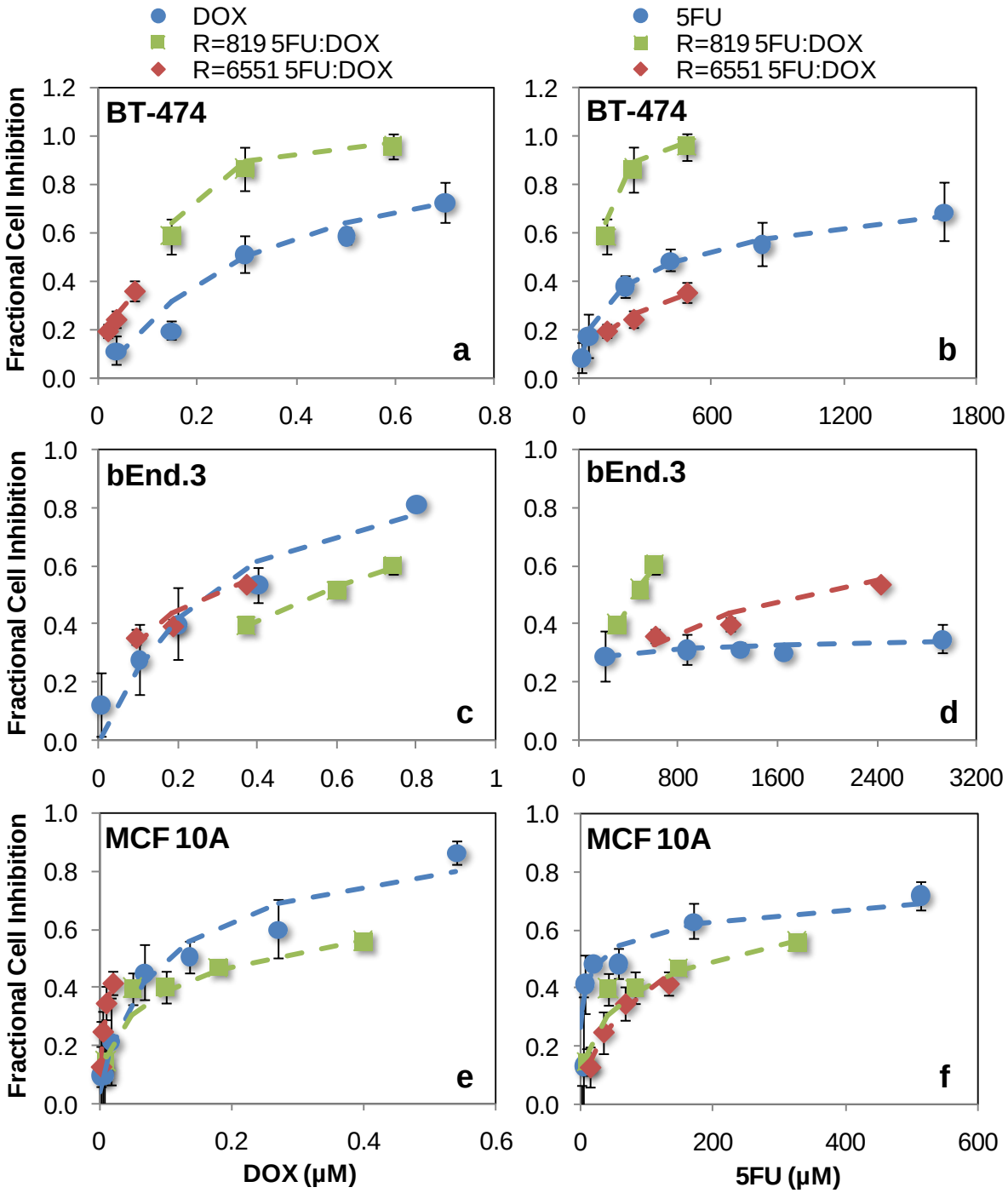

Figure 3.5. *In vitro* cytotoxicity of 5FU+DOX in cancerous and healthy cells.

5FU+DOX in the synergistic ratio R=819 ± 64 (squares) or antagonistic ratio R=6551 ± 170 (diamonds) were exposed to (a)-(b) BT-474 human breast cancer cells, (c)-(d) bEnd.3 mouse brain endothelial cells, or (e)-(f) MCF 10A human breast epithelial cells, and cell growth inhibition was evaluated via MTT cytotoxicity assays. Single drug treatments of DOX (left, circles) and 5FU (right, circles) are shown for comparison. Dashed lines represent fits to the ME model. Data expressed as mean ± SD (n ≥ 6).

Although 5FU+DOX combined at R=819 consistently inhibited more cancer cell growth than either 5FU or DOX alone, the same was not true for the endothelial or epithelial control cells investigated. For bEnd.3 cells (Figure 3.5c-d), R=819 inhibited less endothelial cell growth than DOX alone, and for MCF 10A cells (Figure 3.5e-f), the same ratio inhibited less epithelial cell growth than both DOX and 5FU alone. Similarly, 5FU+DOX combined in the antagonistic ratio of R=6551 was less toxic than 5FU when exposed to MCF 10A, and only as toxic as DOX when exposed to bEnd.3. The combination of 5FU+DOX actually reduced the toxicity in control cells, regardless of ratio, compared to 5FU or DOX administered alone. Figure 3.6 represents the same data in a different light. Here, the D_{50} concentrations for BT-474 cancer cells and MCF 10A epithelial cells are directly compared in a relative ratio. Higher D_{50} ratios indicate higher drug concentrations are required to kill cancer cells compared to epithelial cells, and hence greater toxicity to epithelial cells. Lower D_{50} ratios imply that low drug concentrations can significantly kill cancer cells, but can't effectively kill epithelial cells. In this manner, direct comparisons of D_{50} concentrations for cancer cells relative to healthy cells can act as a specificity metric. Relative D_{50} concentrations < 1 indicate that the treatment more selectively kills cancerous cells over epithelial cells, whereas ratios > 1 suggests the opposite and that the drugs are more toxic to healthy cells. As seen in Figure 3.6, the D_{50} ratio for both 5FU and DOX was reduced by simply combining them in the synergistic ratio R=819, relative to individual drug administrations. We were able to reduce the D_{50} ratio by 36-fold and 5-fold for 5FU and DOX, respectively. This suggests that the drugs are more toxic to healthy cells when used alone, but can be tuned to more

preferentially inhibit cancer cells if combined in an optimal ratio. Our findings introduce a new concept of creating chemotherapy specificity by unconventional methods; instead of incorporating antibodies or peptides which direct the toxic drugs to tumors, one can utilize combination chemotherapy at optimal drug ratios.

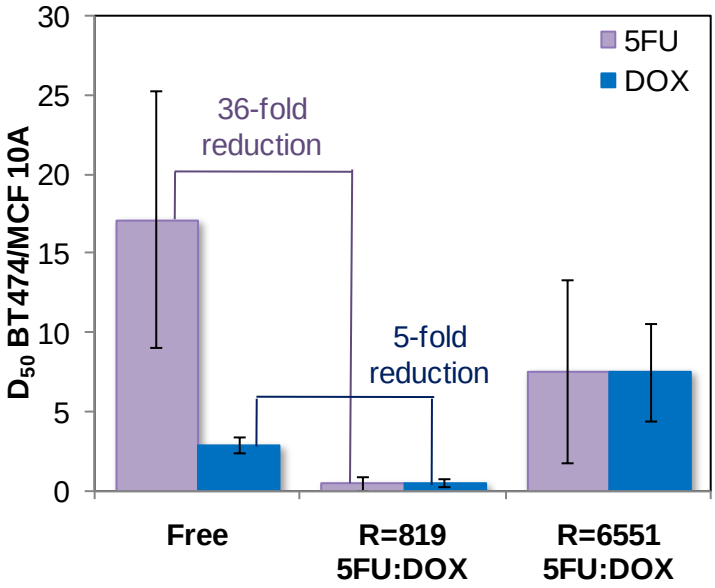

Figure 3.6. D_{50} ratios for BT-474 relative to MCF 10A.

Ratio of D_{50} (concentration required to inhibit 50% cell growth) for BT-474 breast cancer cells relative to MCF 10A breast epithelial cells. Relative D_{50} concentrations are reported for 5FU (purple, left bars) and DOX (blue, right bars). Relative $D_{50} < 1$ indicates greater specificity for cell inhibition of cancerous over epithelial cells. For synergistic R=819, relative D_{50} concentrations were 0.54 ± 0.21 and 0.47 ± 0.47 for DOX and 5FU, respectively. D_{50}s were determined from experimental fits of cell inhibition data to the ME model, and error is propagated from the standard error of the model fit.

This reduction in cell kill when incubated with healthy cells may be attributed to inherently different cytotoxicity mechanisms the drugs elicit depending on cell type. For instance, susceptibility to cell death by 5FU treatment greatly depends the activity of various enzymes responsible for RNA and DNA incorporation, such as uridine phosphorylase, orotate phosphoribosyl transferase and thymidylate synthase. The activities of these enzymes have been shown to differ between various

cancer cells and seemed to correlate with drug sensitivity [52]. Altered levels of these enzymes is one plausible reason for reduced combination activity in bEnd.3 and MCF 10A cells. More specifically, DOX has been previously reported to elicit apoptosis in endothelial cells and cancer cells via different pathways. DOX-mediated generation of hydrogen peroxide has been shown to play a pivotal role in endothelial cell apoptosis but not in tumor cell apoptosis [53]. Such differences in drug sensitivity may prevent the interactions between 5FU and DOX that are seen in cancer cells, and provides a probable cause for reduction in combination activity. Results from these studies suggest that the enhanced cell inhibition of 5FU+DOX at R=819 is specific for cancer cells, and is not as toxic to endothelial or epithelial cells. In fact, the combination may not be any more toxic than either 5FU or DOX when administered as a single agent because the combination, at best, only inhibits as much cell growth as DOX alone. This is a remarkable finding, since one challenge with combination chemotherapies is amplified adverse side effects due to co-localization of multiple drugs in essential organs. Our results suggest that this challenge can potentially be overcome by optimizing drug pair and ratio such that synergistic cell kill occurs in malignant cells, but not in healthy cells. Further *in vivo* or *ex vivo* studies, whereby 5FU+DOX are exposed to tissues in their natural environments, would need to be executed to assess this hypothesis.

3.5. Mechanistic study of 5FU and DOX enhanced cancer cell kill

To understand the cause of synergistic interactions between 5FU and DOX, one of the mechanisms DOX utilizes to induce cell death was investigated: reactive oxygen species (ROS) generation. DOX is known to induce apoptosis in endothelial and tumor cells by different mechanisms. In endothelial cells, DOX induces cell death by ROS generation, whereas in tumor cells, DOX induces apoptosis by activating the p53 tumor suppressor gene [53]. By comparing ROS generation in cancer cells exposed to 5FU and DOX rather than DOX alone, one can investigate the impact of 5FU on DOX cancer cell cytotoxicity. Post-incubation with either 5FU+DOX at R=819, 5FU alone, or DOX alone, BT-474 cells were treated with general oxidative stress indicator carboxy-H_2DCFDA (10 μM for 30 min), which forms carboxydichlorofluorescein upon acetate cleavage and oxidation. Cells were then imaged utilizing confocal microscopy, and representative images are included in Figure 3.7. Results demonstrate that negligible ROS generation was present in untreated cells and cells incubated with 5FU alone. Little ROS generation was visualized in cells incubated with just DOX; on the contrary, significantly more ROS was present in cells treated with the synergistic combination of 5FU+DOX. Quantification of the ROS fluorescence indicator (Figure 3.7) suggests that ROS generation is slightly more than doubled when 5FU is included in the treatment compared to DOX incubated alone. Therefore, the addition of 5FU amplifies the non-traditional mechanism by which DOX induces apoptosis in cancer cells, and enhanced ROS generation is a probable contribution to their synergistic anticancer activity. Moreover, ROS generation has been found to effectively inhibit cancer cells

that have previously grown resistant to DOX treatments [54, 55], demonstrating that ROS generation is indeed a powerful cell inhibitory mechanism. It seems plausible that heightened levels of ROS produced by 5FU+DOX lead to significantly greater cancer cell death than either drug alone, which produce lower levels of ROS.

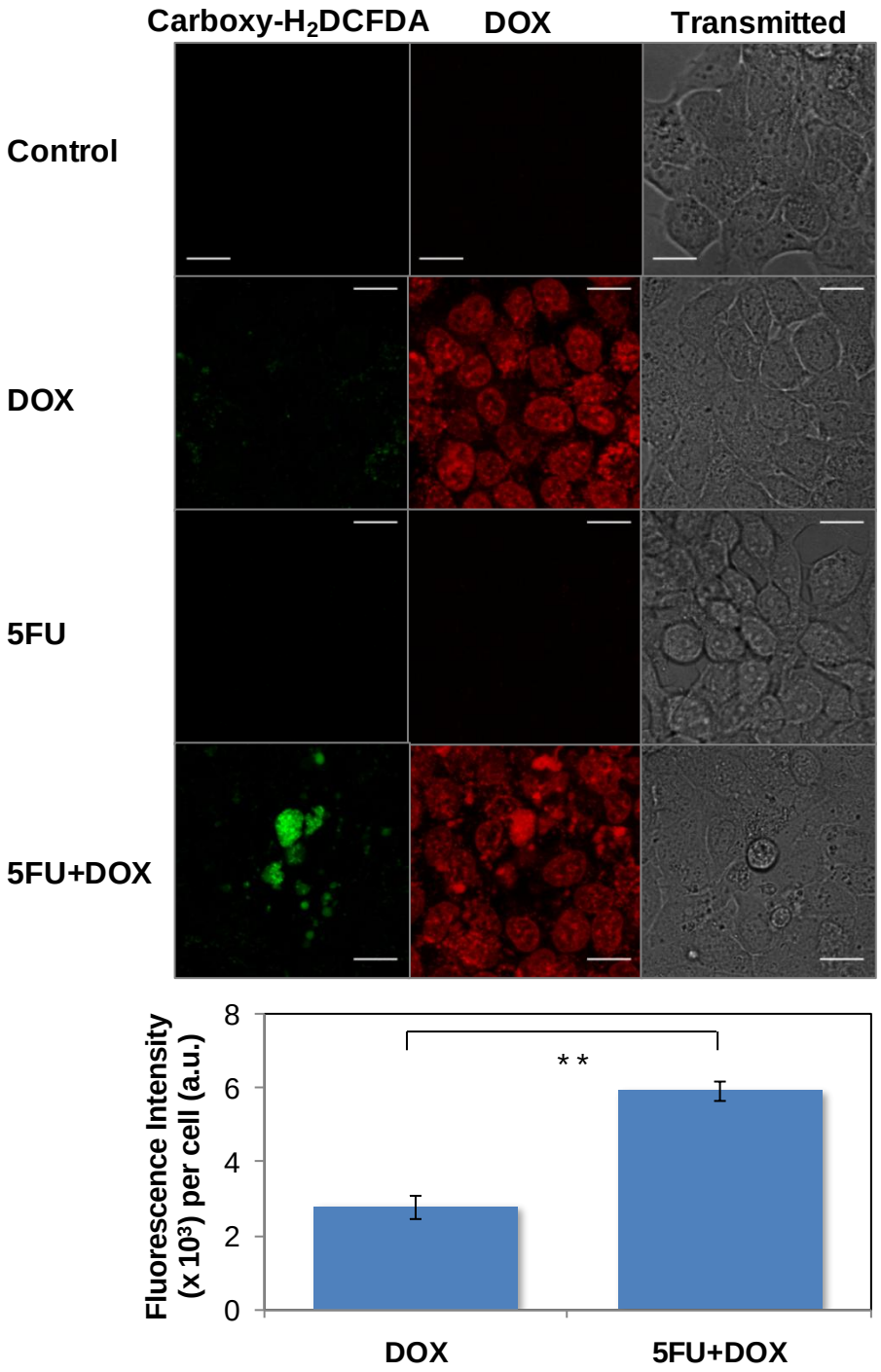

Figure 3.7. ROS detection in 5FU+DOX treatments.

Production of reactive oxygen species (ROS) in BT-474 cells exposed to no drug (top), 0.6 μM DOX (second from top), 487 μM 5FU (second from bottom), or 5FU+DOX at R=819 (bottom). Cells were exposed to free drug solutions for 24 hrs, incubated with 10 μM carboxy-H_2DCFDA (green) for 30 minutes, washed and imaged live immediately via confocal microscopy. DOX internalization is visualized in red. Scale bar=20 μm. Carboxy-H_2DCFDA fluorescence intensity is reported as mean ± SD (n=3).

The mechanism behind 5FU and DOX synergy may be multi-faceted, however, and cell cycle phase arrests may be another plausible cause for their combined anticancer potency. 5FU is considered to be a cell cycle-specific drug, as exposure to 5FU results in accumulation of cells in the G_1/S phases [56-59]; meanwhile, the classification of DOX as a cell cycle-nonspecific drug is controversial. One convincing report by Y. Ling and co-workers demonstrated that DOX-induced cytotoxicity can be significantly enhanced by synchronizing cells in the S phase prior to DOX treatment [60]. By incubating cancer cells with a double thymidine block, they were able to promote cell accumulation in the S phase, and subsequently inhibit 50% cell growth with ~3.28 fold lower DOX concentration than was necessary for asynchronized cells. This enhanced cytotoxicity seemed directly correlated to G_2/M phase arrest. The mechanism between 5FU and DOX synergy may be similar in our studies, since 5FU is (1) a thymidylate synthase inhibitor [61], which is consequently responsible for thymidine levels and hence similar to the thymidine block utilized by Y. Ling and co-workers, and (2) a proponent of S phase accumulation [56]. It is likely that 5FU first synchronizes cancer cells in the S phase, which further allows DOX to accumulate cells in the G_2/M phase, and consequently cause enhanced cell death compared to single drug treatments, where concentrated phase arrests would otherwise be absent. In a separate study, it was found that DOX anticancer synergy with silibinin, an active constituent of milk thistle seeds, was strongly correlated with enhanced G_2/M phase arrests [62]. DOX and silibinin treatments alone resulted in 19% and 41%, respectively, of cells in the G_2/M phases, whereas their combination suspended88% of cells in the G_2/M phases. This supplementary finding supports the

hypothesis that enhanced G_2/M phase arrest can cause synergistic drug interactions, and could be another probable cause of 5FU and DOX synergy.

Collectively, the results presented in Section 3.4-3.5 form a strong basis for the use of 5FU and DOX in combination chemotherapy regimens. This is far from the first time that the two have been identified as a potent anticancer pair, as 5FU and DOX is included in nearly all chemotherapy regimens for the treatment of gastric cancers [8, 63-69], and has been employed in many breast carcinoma therapies as [16, 70, 71], well. However, our studies elucidate the grave impact that ratio between 5FU and DOX can impose on drug interactions; the drugs can either enhance cancer cell kill or significantly reduce it, depending on the ratio utilized. As a result, R can have vast implications on therapeutic efficacy. On the contrary, synergistic R was less toxic to both endothelial and epithelial cells compared to treatment with DOX alone, suggesting that the combination is specifically potent at killing cancer cells, and may be well-tolerated *in vivo*. Controlled nanoparticle encapsulation of 5FU+DOX will allow the pair to simultaneously arrive in tumors at the prescribed synergistic ratio, and may be able to mimic the synergistic cancer cell kill so consistently demonstrated *in vitro*. Therefore, 5FU+DOX at R=819 was chosen as one of the model drug pairs investigated for multi-drug encapsulation and delivery in nanoparticles.

3.6. Topoisomerase inhibitor combination

All combinations previously explored for synergy consisted of FDA-approved drugs that are often used in polychemotherapy regimens. However, there is a vast repertoire of drugs which have failed clinically due to toxicity or solubility issues, yet may have strong potential for comprising potent combinations. Incorporation in nanoparticles can alleviate the challenges associated with these problematic anticancer drugs by prolonging systemic circulation and improving tumor uptake. To investigate whether these disreputable drugs can be made clinically relevant by multi-drug nanoparticle delivery, one FDA-approved drug was screened for synergy with one that is non-FDA-approved.

In particular, the drug pair chosen for synergistic screening was one that has a strong basis for enhanced therapeutic efficacy, that is, topoisomerase I and II inhibitors. Topoisomerase (top) I and II are enzymes are essential for cell proliferation, as they alleviate DNA tension during replication. Inhibitors of top I and II enzymes have been found to synergistically reduce cancer cell growth *in vitro* [72-76], and their combined anticancer potency is attributed to collateral drug sensitivity; top I-exposed cancer cells compensate the obstruction of DNA replication by enhancing top II activity, which further sensitizes the cancer cells to top II inhibitors [77, 78]. However, their clinical applicability has been questionable due to little improvements in tumor reduction [9, 79, 80] and heightened side effects [80-83]. DOX is the conventional FDA-approved topoisomerase II inhibitor which is consistently used in cancer treatments due to its well-established liposomal administration and marked efficacy. In contrast, camptothecin (CPT) is the

archetypal non-FDA-approved topoisomerase I inhibitor which exhibits significant anticancer efficacy *in vitro*, but has failed clinically due to extreme gastrointestinal toxicity and myelosuppresion in phase II trials [84-86]. Various analogues of CPT have been developed to mitigate these unpredictable drug toxicities, with substantial focus on improving its water solubility. Two successful CPT analogues, topotecan (TPT) and irinotecan (CPT-11), were able to improve the drug's water solubility, adverse side effects, and efficacy against human tumor xenografts in mice models [84]. Both are FDA-approved for various cancers, however they are notably less effective at cancer cell kill *in vitro* compared to the original CPT drug [87, 88]. Despite this, their improved efficacy *in vivo* is likely attributed to their enhanced tolerability yielding higher maximum tolerable doses (MTDs) and hence a larger therapeutic window than the original CPT. Therefore, in an effort to find a potent anticancer combination top I and II inhibitor, our synergistic screen included both the FDA-approved analogue CPT-11 and the original, more cytotoxic CPT.

Single drug treatments of CPT or CPT-11 on BT-474 cells (Figure 3.8a) verify that CPT-11 is less active than CPT at inhibiting cancer cell growth. To assess if synergistic interactions exist between these top I inhibitors and DOX, various ratios of the combinations were exposed to cancer cells. CPT+DOX consistently outperformed the cancer cell kill of either drugs when used alone (Figure 3.8b). The enhancement of cancer cell kill seemed to increase with increasing R (CPT:DOX); similarly, CI decreased with increasing R (Figure 3.8c). These results indicate that CPT+DOX become more synergistic with increasing R, with the greatest synergy occurring when $R > 2$ ($0.01 < CI < 0.08$). The highest CI was 1 ± 0.07, indicating

that CPT and DOX interactions were never worse than additive. For molar ratios > 2, the reported CI values are among the lowest, and therefore most synergistic, of reported drug interaction studies evaluated by the CI method [42, 46, 48, 62, 76, 89-91]. This remarkable synergy renders CPT+DOX highly desirable for co-delivery to tumors. Previous reports found CPT and DOX to be only additive in wild type rat C6 glioma cells, but slightly synergistic in a CPT-resistant C6 cell line [89]. BT-474 human breast cancer cells which were utilized in this study were found to be inherently resistant to CPT, with a D_{50} of 100 μM, nearly 50 times that of CPT-resistant C6 cell lines reported in the literature. However, when BT-474 cells were treated here with CPT and DOX at a molar ratio of R = 4.5, the pair was able to inhibit 95% cell growth at a CPT concentration 100-fold less than the D_{50}. Hence, the finding of CPT and DOX synergy in CPT-resistant cells is consistent with previous studies, and suggests that CPT and DOX are most potent when used against highly CPT-resistant tumor cells.

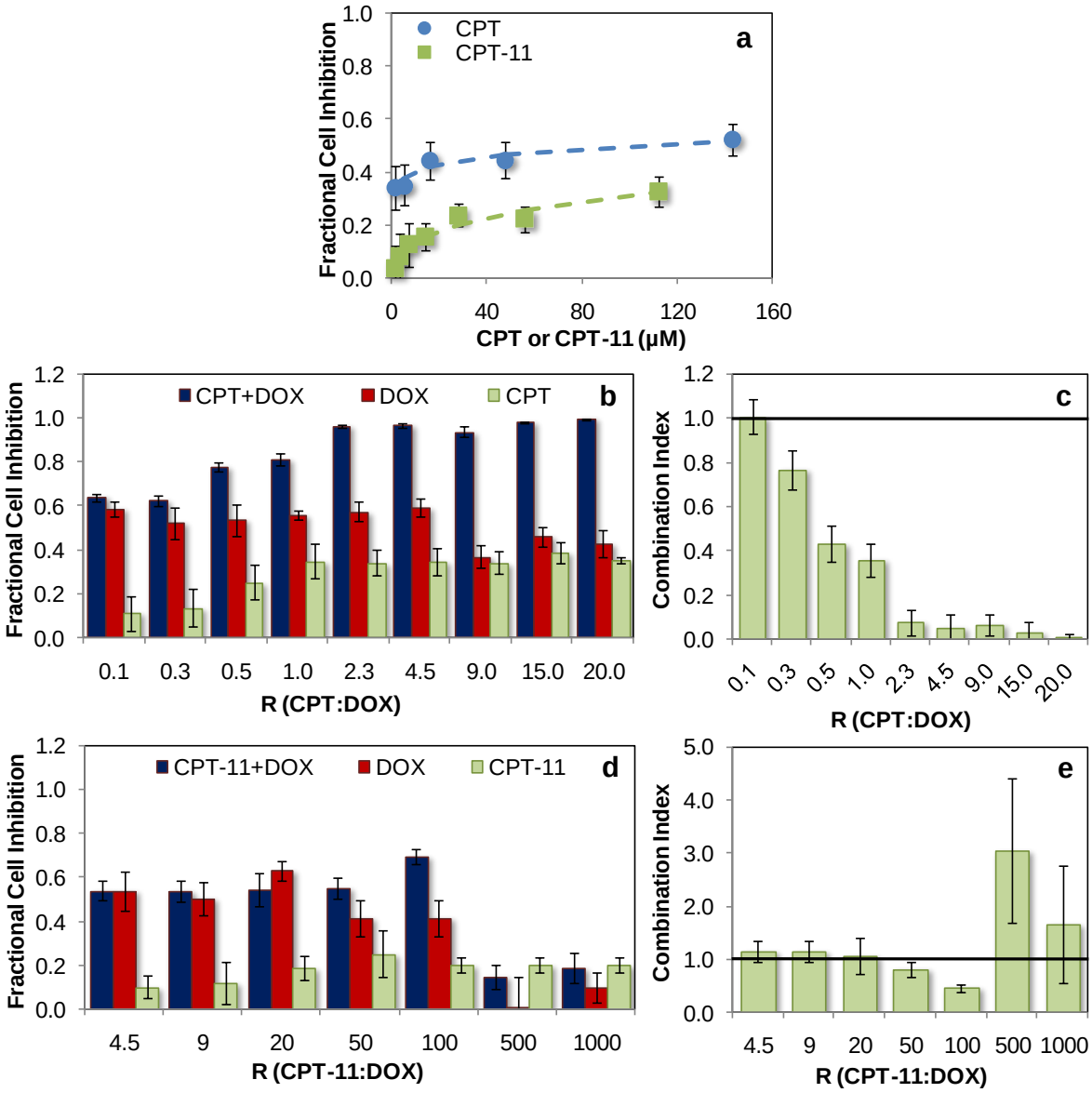

Figure 3.8. Top I + Top II inhibitors synergy screen.

(a) Cell growth inhibition of BT-474 cells exposed to CPT (circles) or CPT-11 (squares). Dashed lines represent fits to the ME model. D_{50} (μM) and R^2 values corresponding to CPT and CPT-11 respectively are (104 ± 42, 0.93) and (570 ± 206, 0.95). Cell inhibition elicited by combinations (blue, left) (b) CPT+DOX or (d) CPT-11+DOX combined at various R. Single drug treatments of DOX (red, middle) and CPT (green, right) at concentrations which make-up the combinations are juxtaposed for direct comparison. CPT and DOX concentrations (μM) in (b) corresponding to each R were: 0.1 (0.05, 0.5), 0.3 (0.1, 0.36), 0.5 (0.2, 0.4), 1.0 (0.4, 0.4), 2.3 (0.9, 0.4), 4.5 (1.35, 0.3), 9.0 (2.0, 0.22), and 15.0 (5.0, 0.33). CPT-11 and DOX concentrations in (d) corresponding to each R were: 4.5 (1.75, 0.39), 9 (3.5, 0.39), 20 (7.0, 0.35), 50 (14.0, 0.28), 100 (28.0, 0.28), 500 (28.0, 0.056), 1000 (28.0, 0.028). Drug concentrations were chosen such that at least one of the individual drug doses inhibited between 40-60% cell growth. CIs for each R of (c) CPT+DOX and (e) CPT-11+DOX. Data expressed as mean ± SD (n ≥ 6).

Most ratios of CPT-11+DOX, on the other hand, were only as effective at cancer cell kill compared to single DOX treatments, as seen in Figure 3.8d. Consequently, CIs ranged between 0.8-1.15 for $4.5 < R < 50$ (Figure 3.8e), indicating that the drugs were additive and non-interacting. The only synergy was observed at $R = 100$ ($CI = 0.45$), approximately two orders of magnitude higher than that needed for CPT+DOX synergy. Thus, a much larger concentration of CPT-11 is required in combination with DOX compared to CPT in order to induce synergistic interactions. This is likely due to the lower efficacy of CPT-11, whose D_{50} is 5.5 fold higher than that of CPT. CPT-11 is a pro-drug analogue of CPT which requires hydrolysis into its active ingredient SN-38, and this necessary metabolization, while helpful for *in vivo* applications, may be the root cause of reduction in therapeutic efficacy. This reduction in CPT-11 *in vitro* efficacy is congruent with previous studies [87, 88], however our report of reduced synergy with DOX is an additional finding.

The more potent anticancer drug pair CPT+DOX was tested in two additional cell lines: the highly metastatic murine mammary cancer cells 4T1, and healthy murine brain endothelial cells bEnd.3. These extensive cytotoxicity studies assess the applicability of CPT+DOX to aggressive forms of cancer, as well as its toxicity in healthy cells. As seen in Figure 3.9a-b, CPT+DOX synergy was maintained in the aggressive 4T1 cell line, and with a slight shift in optimal synergistic ratios. When CPT+DOX was exposed to 4T1 cells, $CI < 1$ occurred for $R > 2.25$, which is higher than the $R > 0.3$ threshold in BT-474 cells. In stark contrast, however, the combination consistently inhibited less endothelial cell growth than CPT or DOX alone (Figure 3.9c-d), suggesting that the pair is considerably more toxic to cancer

cells than endothelial cells. CI evaluation revealed extreme antagonism, regardless of ratio, in bEnd.3 cells, with CIs occurring at a minimum of 25, and as high as 3×10^9. This vastly reduced combination activity in endothelial cells may be attributed to the distinctly different cytotoxicity mechanisms the drugs elicit in endothelial cells, as alluded to in Section 3.4. As described earlier, hydrogen peroxide is a major mechanism by which DOX induces apoptosis in endothelial cells, but not in cancer cells [53]. Furthermore, top I enzymes present in endothelial cells exhibit higher resistance to CPT-induced oligonucleotide cleavage compared to those expressed in cancer cells [92, 93]. Such differences in drug sensitivity may prevent synergistic interactions between CPT+DOX when exposed to endothelial cells, and provides a probable cause for reduction in combination activity. Synergistic CPT+DOX interactions in 4T1 cells suggests that the combination can be broadly applied to metastatic and aggressive cancers, and their antagonistic interactions in bEnd.3 cells suggest that the potent pair will be less toxic than their free drug counterparts while in blood circulation. Because the synergistic interaction between DOX and CPT seems specific to tumor cells, the pair may be less toxic *in vivo* compared to the higher doses of free drug that are required to inhibit tumor growth. This concept of utilizing chemotherapy combinations to direct toxicity towards cancerous rather than healthy cells is consistent with our findings with 5FU+DOX in Section 3.4.

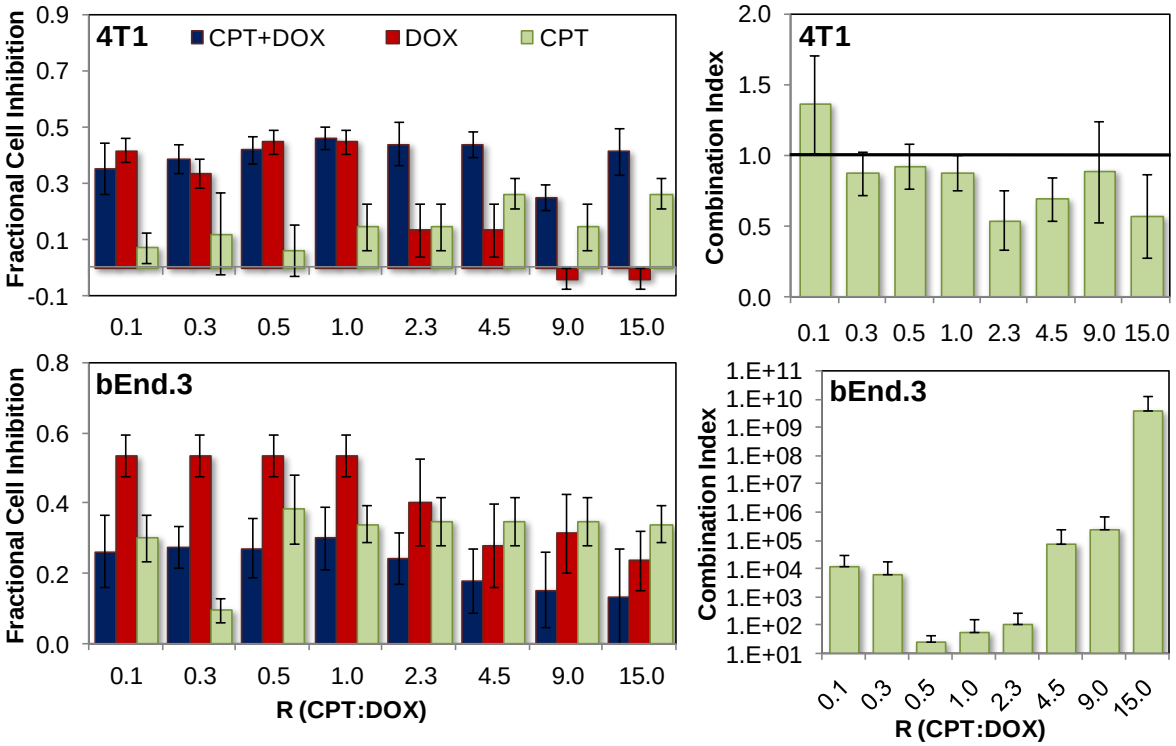

Figure 3.9. CPT+DOX interactions in 4T1 and bEnd.3 cells.

Cell inhibition of 4T1 (top, left) or bEnd.3 (bottom, left) elicited by various R of CPT+DOX (blue, left), DOX (red, middle) or CPT (green, right) at concentrations which make-up the combinations. CPT and DOX concentrations (μM), respectively, exposed to 4T1 cells (R, CPT:DOX) were: 0.1 (0.005, 0.05), 0.3 (0.01, 0.03), 0.5 (0.02, 0.04), 1.0 (0.04, 0.04), 2.3 (0.04, 0.018), 4.5 (0.08, 0.018), 9.0 (0.04, 0.004), 15.0 (0.075, 0.005). In the case of bEnd.3 cells, CPT and DOX concentrations respectively utilized corresponding to each R ratio were: 0.1 (0.04, 0.4), 0.3 (0.11, 0.4), 0.5 (0.2, 0.4), 1 (0.4, 0.4), 2.3 (0.45, 0.2), 4.5 (0.45, 0.1), 9 (0.45, 0.05), 15 (0.3, 0.02). Drug concentrations were chosen such that at least one of the individual drug doses inhibited between 20-60% cell growth. CIs for each R of CPT+DOX are shown on the right. Data expressed as mean ± SD (n ≥ 6).

Although CPT's poor water solubility limits its clinical use, results reported here demonstrate that it is a better match for DOX than its FDA-approved analogue, CPT-11. Not only is the CPT+DOX synergy among the lowest of those reported in literature, but it occurs over a broad range of ratios. Therefore, their encapsulation in nanoparticles for tumor co-delivery may not need to be stringently controlled. Further, incorporation of CPT+DOX in a nano-carrier, much like the pro-drug CPT-11, can improve drug solubility in aqueous solution, and can act as a drug depot

which slowly releases drug rather than exposes the body to large, bolus amounts of it. The toxicity of CPT can also be alleviated just by co-administration with DOX, as indicated by CPT+DOX extreme antagonism in bEnd.3 cells. In this manner, the unpredictable, adverse side effects often associated with CPT may be overcome; meanwhile, the antitumor efficacy of the drug can be significantly improved by combining it with DOX.

3.7. Mechanistic study of CPT and DOX enhanced cancer cell kill

Since CPT and DOX inhibit DNA top I and II, respectively, which are required to relieve DNA supercoiling during transcription and replication, exposure of either drug to cancer cells results in DNA damage and can induce apoptosis. To understand the enhanced cancer cell capabilities of CPT+DOX, cells were quantified for pre-apoptotic and late-apoptotic populations with Annexin V/Sytox Green counterstaining (Section 2.5) after incubation with the drug pair or individual agents. Scatter plots obtained from flow cytometry of Annexin V/Sytox Green counterstained cells are seen in Figures 3.9a-f. These plots were utilized to quantify early apoptotic and late apoptotic/necrotic populations in Figure 3.10g-h. Cells stained with low levels of Annexin V and Sytox Green (-AV/-SG) were live, with high levels of Annexin V and low levels of Sytox Green (+AV/-SG) were early apoptotic, and high levels of both were necrotic and/or late apoptotic. Flow cytometry data indicated a significant increase in apoptosis when the drug pair was given in a synergistic ratio relative to treatment with DOX alone, and only little enhancement when provided in an additive ratio. Cells exposed only to CPT exhibited low

percentages of apoptotic cells, incomparable to those treated with DOX alone, likely due to BT-474's inherent resistance to CPT. However, at a synergistic ratio (R = 4.5, CI=0.05 ± 0.01), CPT + DOX induced a 24% increase in early apoptotic population (Figure 3.10), whereas cells exposed to additive ratio (R = 0.1, CI = 1.00 ± .07) resulted in only a 2% increase. This significant increase in early apoptotic populations improves the cancer cell inhibition of CPT+DOX at synergistic ratios, and facilitates potent efficacy at low drug concentrations.

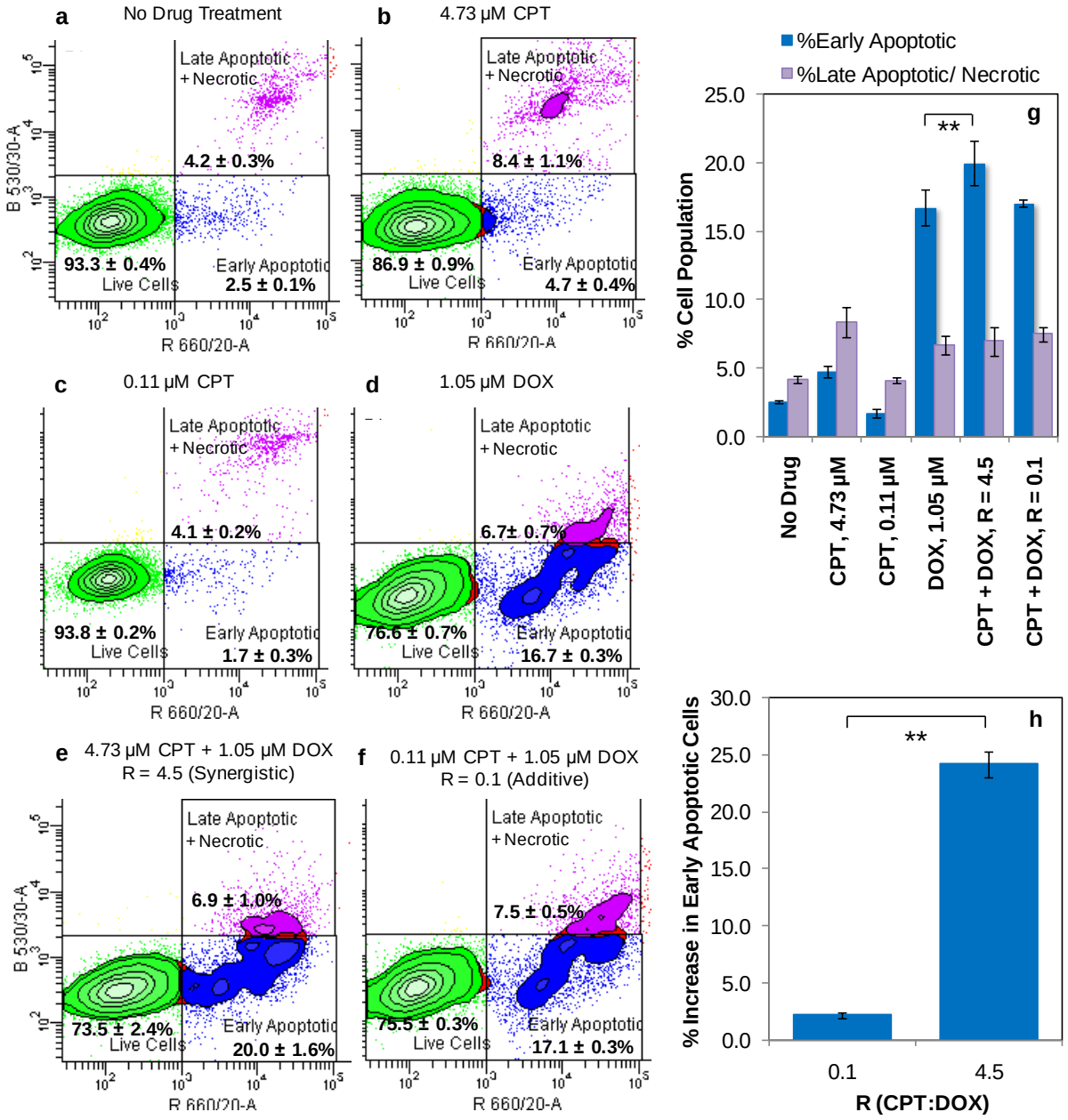

Figure 3.10. Apoptotic assessment of CPT+DOX-treated cancer cells.

Annexin V/Sytox Green assay was utilized to detect percentage of early apoptotic cells in various drug-treated BT-474 cells. Cells were treated with the following drugs for 72 hours prior to staining and analysis via flow cytometry: (a) No Treatment (b) 4.73 µM CPT (c) 0.11 µM CPT (d) 1.05 µM DOX (e) 4.73 µM CPT and 1.05 µM DOX (R = 4.5, representative synergistic dose) (f) 0.11 µM CPT and 1.05 µM DOX, in a molar ratio of (R = 0.1, representative additive dose). Representative flow cytometry plots are shown. Juxtaposed % cell populations represent averages ± SD (n=3). (g) Cell populations were quantified via flow cytometry as follows: early apoptotic (left, blue bars), and necrotic and/or late apoptotic (right, purple bars). (h) Percent enhancement of early apoptotic cells relative to treatment with DOX alone. Data represents mean ± SD (n=3).

CPT+DOX studies reported here, in agreement with previous 5FU+DOX results, also underscore the importance of drug ratios in determining potency. At R=0.1, no improvement in cancer cell inhibition was seen (additive effect), but at R=2, significant synergistic potency was apparent. This study verifies that precise drug ratios can govern combination synergy, as others have established [47, 48], and emphasizes the need for controlled combination delivery to tumor tissue. Further, clinical trials of top I and II combinations utilize the less cytotoxic, FDA-approved analogues of CPT (CPT-11 or TPT); however, CPT-11 was demonstrated here to only exhibit synergy with DOX at a single ratio (R=100), while all other ratios investigated elicited additive drug interactions. This use of a non-interacting drug pair may be the cause for the poor clinical efficacy of top I and II combinations. The inclusion of the more cytotoxic, original CPT at R>2 with DOX in nanoparticles may help enhance overall responses and reduce adverse side effects currently elicited by top I and II combinations. Therefore, CPT+DOX was chosen as a second model drug pair for multi-drug encapsulation in nanoparticles and to promote their simultaneous arrival in tumors.

3.8. Summary of chemotherapy combination studies

Through extensive *in vitro* combination studies, we have identified two chemotherapy pairs which synergistically inhibit cancer cell proliferation. 5FU+DOX were found by conducting synergy screens among FDA-approved drugs of distinct classes. CPT+DOX were discovered though deliberate investigation of collaterally sensitive top I and II inhibitors, with the foresight that the most potent pair may not

consist of FDA-approved agents. In both cases, drug ratio governed anticancer potency. For 5FU+DOX, R ≥ 3276 resulted in antagonistic interactions and hence reduction in cancer cell kill upon combination, whereas R ≤ 1638 synergistically inhibited cancer cell growth. The effect on ratio was less dramatic for CPT+DOX; R=0.1 elicited additive interactions, while all other investigated ratios were synergistic. These results illustrate the same conclusion: ratio plays a pivotal role in antitumor efficacy, and validates the need for multi-drug vehicles which can deliver precise ratios to tumors in order to capture the pair's full therapeutic potential.

Also noteworthy is the marked reduction in combination potency when exposed to control endothelial or epithelial cells. This finding was consistent for both drug pairs, and suggests that the combination selectively kills cancer cells rather than healthy cells. While more thorough studies are required to validate this concept, it proposes a new, unconventional methodology for tumor targeting therapies. Rather than including antibodies or peptides which can recognize cancer cell surface markers, one can simply tune chemotherapy by delivering combinations at ratios that are more toxic to cancer cells than healthy cells. This can be an incredibly powerful approach which modernizes nanoparticle therapies. Nanoparticle stigma is associated with its uptake in MPS organs such as the liver and spleen, and can cause adverse side effects if the drug payload is released or if it is non-biodegradable. Thus, by improving drug payload specificity through combinations, one may still be able to reduce adverse side effects even if the nanoparticles accumulate in healthy tissue.

The combinations discovered in this chapter are not entirely surprising, as variations of them have been used clinically. 5FU+DOX combined with methotrexate, collectively tokened as FAMTX, is considered one of the standard regimens for gastric cancer patients [8, 63]. Top I and II inhibitors CPT-11 and liposomal DOX have been combined in clinical trials for the treatment of ovarian and lung cancers [9, 94, 95]. Both of these combinations have shown slight improvements in partial responses (decrease in tumor size), but complete responses (disappearance of tumor) still remain rare [8, 9, 68, 94, 96]. Furthermore, the clinical applicability of top I and II inhibitors has become questionable due to heightened side effects [80, 81, 83]. Collectively, clinical data and our CI results demonstrate the high therapeutic potential of 5FU+DOX and top I+II inhibitor combinations. However, there is a clear unmet need for improving their tumor reduction and side effects. We have thus far demonstrated the ability to improve cancer cell kill by optimizing combination ratios, and hope to further reduce side effects by incorporation in nanoparticles.

Chapter 4

Liposomes for combination chemotherapy co-delivery

4.1. Advantages of liposomes

Liposomes represent the oldest class of nanoparticles for chemotherapy delivery. It pioneered the field by becoming the first FDA-approved nanoparticle chemotherapy formulation in 1995 for DOX delivery [28], and has since been a staple in drug delivery for its numerous advantages over free drugs; to name a few, enhanced biocompatibility, extended systemic circulation, and ability to accumulate in tumor endothelium via the EPR effect [97, 98]. Scientists even proclaimed the properties of liposomes through poetry upon their discovery in 1962, such as the verse below:

> "Little fatty vesicles of bilayer fame
> protean and elusive, fragile all the same,
> aloof and enigmatic beneath your many skins,
> unyielding to the vigour of thousands of spins,
> descended from the pastures of Babraham we are told,
> you never ceased to wrinkle, expand and then to fold
> embracing sodium ions and such electrolytes.
> Twinkling guide stars to throngs of acolytes
> desirous of your membranous semi-barriers.
> Precursors of bion, potential drug carriers. '
> - Gregory Gregoriadis [99]

Moreover, liposomes have been shown to significantly reduce cardiotoxicity associated with DOX treatments [100-102], the main adverse side effect which has

earned DOX's tokened name of "red death". For all of these acclaimed advantages of liposomes, they were the first nanoparticle we sought to investigate for the co-delivery of chemotherapy combinations.

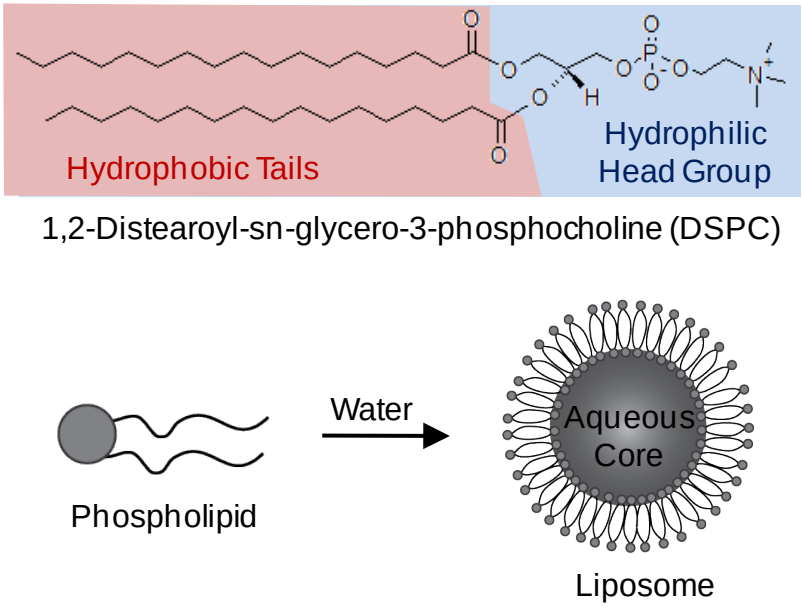

Figure 4.1. Phospholipid and liposome schematic.

A representative phospholipid, 1,2-Distearoyl-sn-glycero-3-phosphocholine (DSPC), is pictured, with its hydrophobic tails highlighted in red, and its hydrophilic headgroup shown in blue. The tails consist of two 18-carbon saturated fatty acids, which is connected to the phosphocholine head via a glycerol group. Phospholipids can vary depending on tail length, saturation, and charge of the headgroup. Liposome formation occurs via self-assembly of phospholipids in water, where a phospholipid bilayer membrane entraps an aqueous pocket.

As alluded to in G. Gregoriadis' poem, liposomes consist of phospholipids which self-assemble in water to form a lipid bilayer membrane enclosing an aqueous core [98, 103]. The building block of these nanoparticles, phospholipids, contain hydrophobic fatty acid tails and hydrophilic head groups, as depicted in Figure 4.1, and this amphipathicity is the driving force behind self-assembly of lipid bilayers. Because liposomes consist of both a hydrophobic compartment (lipid bilayer) and a hydrophilic core, they can potentially incorporate both water-soluble and lipophilic

drugs during the self-assembly process. Phospholipids also come in various sizes and charges, just by modification of the carbon chain lengths or the headgroups. These seemingly small modifications have vast implications for their fate *in vivo*, and can be tuned for different purposes [50, 104]. Phospholipids which mimic those present in our very own cell membranes can be utilized for liposome fabrication, rendering the nanoparticles biocompatible and biodegradable. Altogether, the ease of fabrication, versatility of drug payloads, and biocompatibility make for a coveted drug carrier which is exploited throughout the pharmaceutical industry.

4.2. Our approach for chemotherapy co-delivery

Here, we hoped to implement the advantages of liposomal drug delivery for chemotherapy combinations, specifically the synergistic pair 5FU+DOX identified in Section 3.4. Through multi-drug co-encapsulation in liposomes, we aimed to not only enhance the clinical therapeutic efficacies of 5FU+DOX, but we also proposed to improve upon the generation of liposomes in use today. The current standard, of course, is Doxil™, polyethylene glycol (PEG)-coated liposomal doxorubicin. Although Doxil™ revolutionized drug delivery for cardiotoxic chemotherapy drug DOX by alleviating adverse side effects, it remains unclear whether liposomal DOX elicits superior antitumor efficacy compared to free DOX. Some clinical trials reported little or only comparable therapeutic efficacy [105-109], whereas other studies showed that liposomal DOX merely increased the tolerable dose, making it difficult to decipher whether liposomal entrapment actually enhanced antitumor efficacy [110, 111]. By including another drug (5FU) which synergistically enhances

DOX's activity against cancer cells, we aimed to obtain greater therapeutic efficacies than are currently possible with single drug-loaded liposomes. However, the well-established method of liposomal DOX encapsulation involves a transmembrane ammonium sulfate gradient, which was specifically designed for anthracycline entrapment. Therefore, to incorporate DOX and 5FU simultaneously in liposomes, we developed a method for 5FU encapsulation which is compatible with the transmembrane ammonium sulfate gradient. This method is not unique to 5FU, but can be applied to its general class of chemotherapy drugs, nucleobase analogues, and hence can be a powerful tool for evaluating many chemotherapy drug pairs.

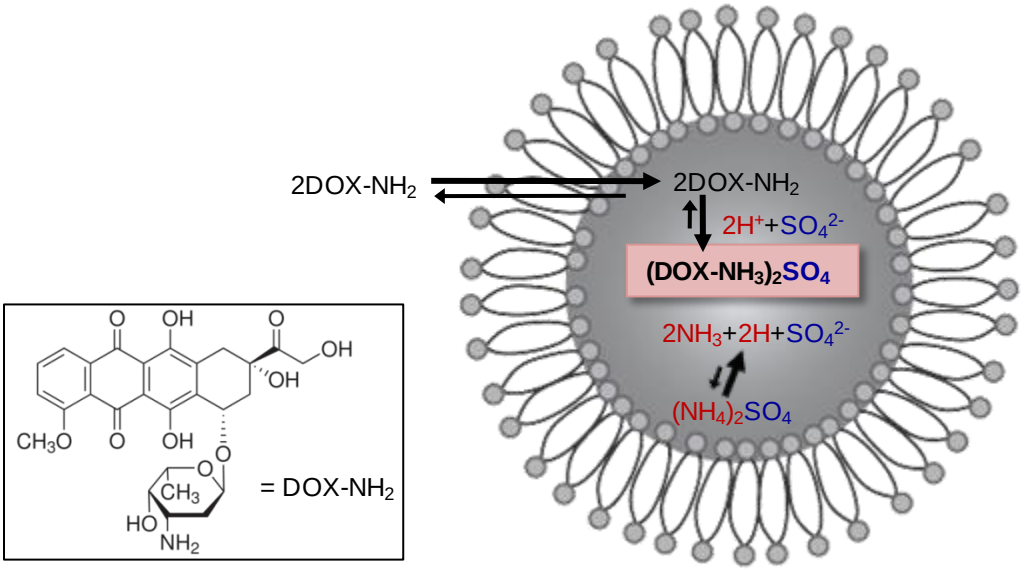

Figure 4.2. Mechanism for loading DOX into liposomes.

A transmembrane ammonium sulfate gradient is established in liposomes in order to encapsulate DOX into the aqueous core. Free base DOX, designated as DOX-NH_2, forms dimers with itself, and easily passes through the lipid easily as a neutral entity. Inside the liposome, the high ammonium sulfate concentration allows constant exchange into protons and sulfate anions. DOX-NH_2 dimers become protonated, and form a precipitate with sulfate anion, which is highlighted in pink. Adapted from [112].

Apart from increasing drug payload potency, promoting drug leakage is another effort which can enhance current liposomal efficacies. As seen in Figure 4.2, the transmembrane ammonium sulfate gradient loading mechanism promotes the formation of DOX precipitates in the liposomal core. This mechanism relies on the amphipathic weakly basic nature of DOX. Neutral-charged DOX can form dimers with itself via Π electron stacking of planar aromatic rings, can then easily pass through the lipid bilayer into the core, where it becomes protonated, and finally forms a precipitate with excess sulfate anions. While this mechanism facilitates high DOX encapsulations, it is nearly irreversible, and in order to completely release the drug, the ammonium sulfate gradient must be collapsed [28, 112, 113]. To that end, we explored cationic liposomes for improved intracellular drug release. Cationic liposomes can associate easily with cell membranes via ionic interactions [114], and can further fuse with cell membranes by flip-flopping with native anionic phospholipids [115, 116]. This fusion allows liposome drug payloads to escape and release into the cytoplasm or even nucleus [114, 117], where chemotherapy drugs can then attack their targets. We proposed that the improvement of both drug release (via positively-charged lipids) and drug payload potency (via chemotherapy combinations) will afford a second generation of liposomes which both ameliorates toxicity and augments therapeutic efficacy.

4.3. Effect of cationic charge on liposomal DOX activity

Cationic lipids were previously shown to improve both cell uptake and drug payload release compared to zwitterionic and negatively-charged lipids [114, 115,

117]. Poor DOX release is an inherent issue when incorporated via the strong, nearly irreversible transmembrane ammonium sulfate gradient (Figure 4.2), so cationic lipids offer a means to enhance DOX intracellular concentrations and thereby facilitate drug-target interactions. Because cationic liposomes exhibit the unique abilities to fuse with cell membranes and intracellularly release payloads, they have often been exploited for transfection purposes [118-120]. Transfecting liposomes typically contain a high content of positively-charged liposomes, 1:1 neutral:cationic lipids, and have been shown to be highly toxic [121]. Thus, to obtain the favorable properties of drug release while minimizing toxicity issues, only a small fraction of cationic lipids (10%) were embedded in the liposome membrane. Positively-charged liposomes also exhibit high affinity for the negatively-charged fenestrae in tumor vasculature [122-124], and can thereby provide additional tumor-targeting, complementary to the EPR effect.

Zwitterionic liposomes (DOX-L) studied here were composed of 1,2-distearoyl-sn-glycero-3-phosphocholine (DSPC) and cholesterol (Chol; Sigma-Aldrich; St. Louis, MO, USA) in a molar ratio of 55:45, while cationic liposomes (+DOX-L) consisted of DSPC, 1,2-dioleoyl-3-trimethylammonium-propane (DOTAP), and Chol in a ratio of 80:10:10. Properties of neutral and cationic DOX-liposomes are provided in Table 4.1. Incorporation of 10 mol% DOTAP lipids shifted the zeta potential from -9.55 mV (zwitterionic liposomes) to +39.93 mV, without affecting liposome size or drug encapsulation. Drug activity (Figure 4.3), however, was drastically enhanced upon cationic lipid incorporation. The DOX-equivalent D_{50} concentration was reduced 5-fold, from 33.5 μM to 6.7 μM, between the zwitterionic

and cationic liposomal formulations, respectively. Both DOX-L and +DOX-L were less active compared to free DOX (D_{50} = 0.3 μM), which is expected since liposomes must first overcome the added barrier of active cell internalization before the drug can interact with its intracellular target.

Liposome Formulation	Liposome Composition	Size (nm)	Zeta Potential (mV)	Drug Incorporation (mol%)
DOX-L	55:45 DSPC:Chol	154.5 ± 5.0	-9.55 ± 3.56	~1.08 ± 0.16
+DOX-L	80:10:10 DSPC:DOTAP:Chol	155.6 ± 5.3	39.93 ± 4.81	~0.96 ± 0.13

Table 4.1.Physical and chemical properties of DOX-loaded liposomes (n≥3).

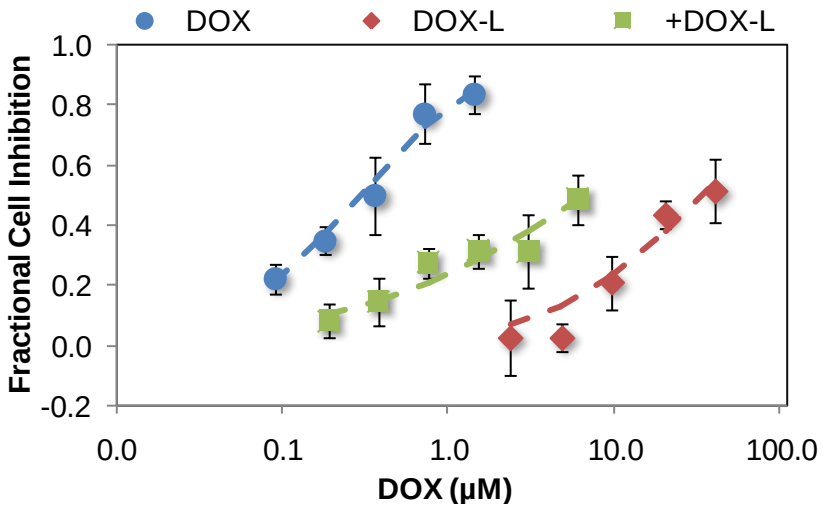

Figure 4.3. Cell inhibitory effects of DOX-L or +DOX-L.

BT-474 cell viability after incubation with DOX in free solution (circles), DOX-L (diamonds), or +DOX-L (squares). Cells were incubated with drug for 72 hrs then analyzed via calcein AM assay. Data expressed as mean ± SD (n≥6). Dashed lines represent dose-effect curves fit to the median-effect model, with D_{50} and R^2 of DOX, DOX-L and +DOX-L corresponding to (0.30 ± 0.02 μM, 0.98), (33.5 ± 19.2 μM, 0.92) and (6.7 ± 1.01 μM, 0.91), respectively.

To comprehend the improvement in DOX activity in +DOX-L compared to DOX-L, drug internalization studies were conducted. BT-474 cells were incubated

with free DOX, DOX-L or +DOX-L at drug-equivalent concentrations of 1 μM and subsequently imaged via confocal microscopy in order to visualize and quantify internalized DOX. Representative images in Figure 4.4a-d demonstrate similar intracellular DOX concentrations when cells were exposed to either free DOX or DOX-L. However, cells incubated with +DOX-L exhibited greater DOX fluorescence than those exposed to DOX or DOX-L. Quantification of fluorescence intensities is provided in Figure 4.4e, and indeed shows no statistical difference between DOX- and DOX-L-treated cells, but a 12-fold enhancement for cells treated with +DOX-L compared to DOX-L. These results elucidate that cationic lipids improve DOX uptake and intracellular concentration, and verify the use of positively-charged lipids to promote DOX release. All liposome formulations thereafter included 10% cationic lipids in order to facilitate drug release and to better preserve anticancer activity.

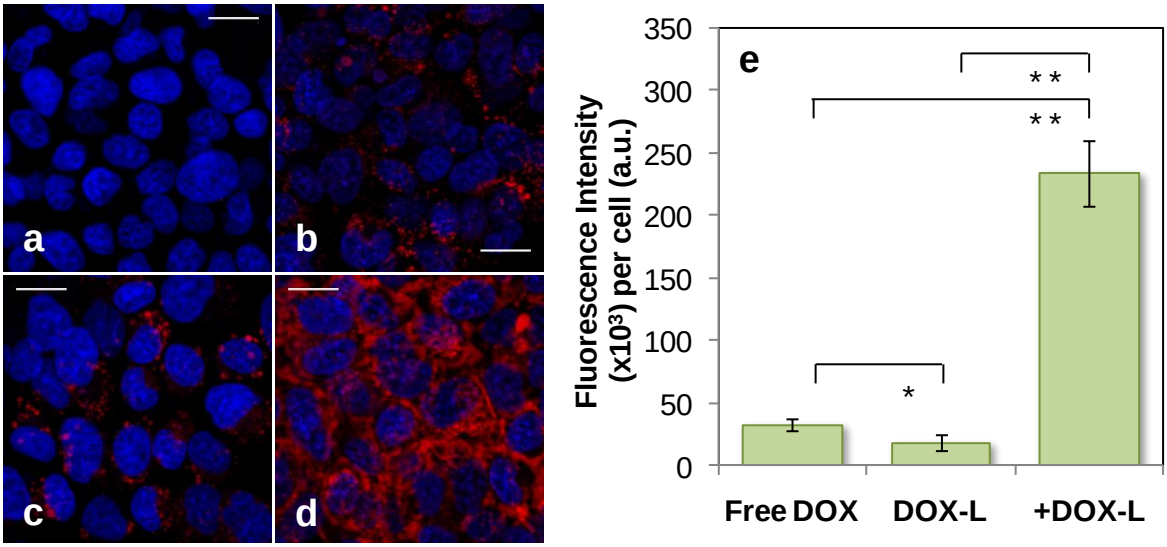

Figure 4.4. DOX internalization post-incubation with DOX, DOX-L or +DOX-L.

BT-474 cells imaged via confocal microscopy after 24 hr incubation with (a) no drug, or 1 μM drug-equivalent concentration of (b) DOX in free solution (c) DOX-L (d) +DOX-L. After drug incubation, cells were washed, stained with Hoechst (blue), and immediately imaged live. (e) DOX fluorescence (red) intensity is reported as mean ± SD (n=3). Scale bars=20 μm.

4.4. Synthesis of 5FU analogues for liposome entrapment

To maintain synergistic drug ratios *in vivo*, both drugs should be entrapped in the same vehicle so as to circulate systemically as one unit in the prescribed ratio. The transmembrane ammonium sulfate gradient, however, was developed for the incorporation of amphipathic weak bases, geared specifically for anthracycline chemotherapy drugs, and presents difficulty for the entrapment of agents from different drug classes. Thus, to incorporate 5FU and DOX in the same liposome, various modifications of 5FU were introduced and investigated for compatibility with the transmembrane ammonium sulfate gradient. Each 5FU analogue modified the native drug's chemical properties to facilitate incorporation in liposomes. This section describes the synthesis of each of these 5FU analogues, and Section 4.5 provides the methodology behind each chemical modification.

The preparation of 5FUG, 1-[(aminomethyl)-ester]methylene-5-fluorouracil, was performed similarly to the procedure presented by T. Ouchi and co-workers [125], as shown in Reaction Scheme 4.1. Briefly, 80 µL (1.07 mmol) of aqueous 37 w/w% formaldehyde was added to 100 mg (0.769 mmol) of 5FU and the reaction was kept at 60°C overnight under mild stirring. The resulting solution was then concentrated using a Buchi R-210 rotary evaporator at 45°C and 30 mbar for 2 hours, to obtain an viscous oil comprising a mixture of three products demonstrated in Reaction Scheme 4.1. The hydroxymethyl-5FU (HMFU) contained therein was recrystallized with ethanol and dissolved in dry DMSO, to which 180 µL of N,N′-Diisopropylcarbodiimide (DIC; Sigma-Aldrich), 160 mg of N-(tert-Butoxycarbonyl)glycine (Boc-glycine; Sigma-Aldrich), and 190mg of 4-

(Dimethylamino)pyridine (DMAP; Sigma-Aldrich) were added. The reaction was allowed for 6 hours at room temperature under vigorous stirring to yield the products shown in Reaction Scheme 4.1. The solution was then copiously washed with 1N HCl and brine. The organic layer thus formed was dried with anhydrous sodium sulfate and evaporated to return an oily liquid. The 5FU-Glycine(Boc) was then precipitated and thoroughly washed with abundant ice-cold methyl isopropyl ether. To remove the Boc protection, 5FU-Glycine(Boc) was dissolved in 5 mL of 50% trifluoroacetic acid (TFA) in dichloromethane (DCM) and the solution stirred for 1 h at room temperature. 5FUG was crystallized by solvent evaporation and purified using Sep-Pack 2mL C-18 columns (Waters; Milford, MA, USA), to separate the fraction containing the desired product. Mass spectrometry analysis (Figure 4.6a) verified that the desired product, 5FUG (m/z = 217),was present in high yield.

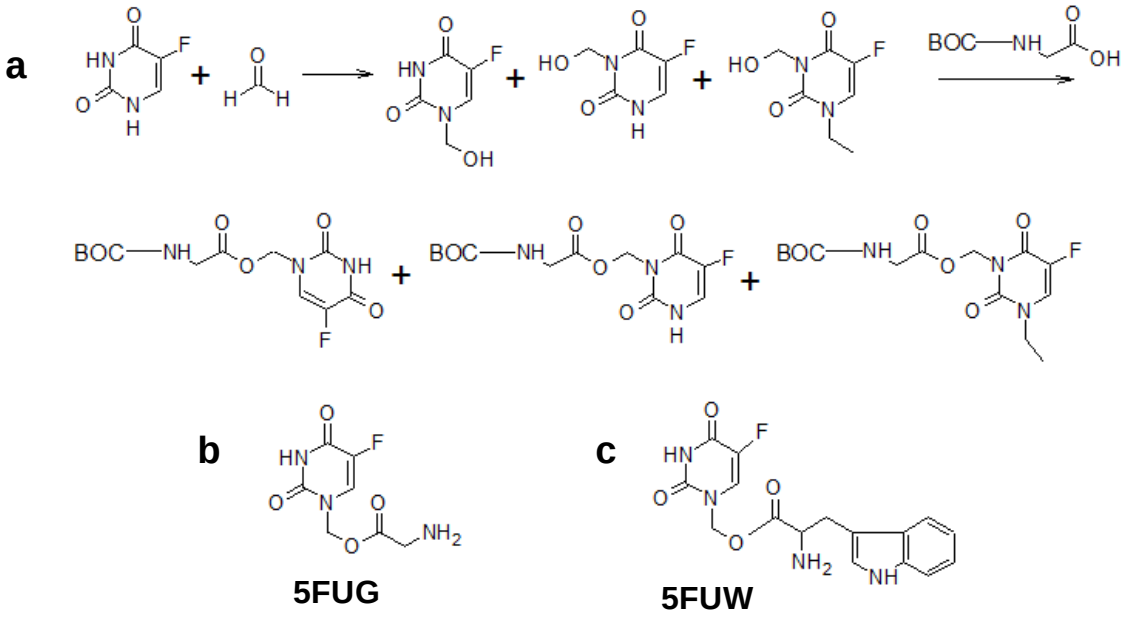

Reaction Scheme 4.1. Chemical synthesis of 5FUG or 5FUW.

(a) Reaction of 5FU and formaldehyde to form HMFU, followed by esterification with BOC-glycine. Three possible products are shown for each step. (b) Final 5FUG obtained after BOC removal with 1:1 TFA:DCM, and purification via Sep-Pak C-18 columns. (c) Replacement of BOC-glycine with tryptophan results in the formation of 5FUW.

5FUW, tryptophan 5-fluorouracil ester, was synthesized similarly. Tryptophan hydrochloride (Sigma-Aldrich) and N-(3-dimethylaminopropyl)-N′-ethylcarbodiimide hydrochloride (EDC; Sigma-Aldrich) were separately dissolved in dry DMSO in a proportion 1:1.1. The activated tryptophan was then added to the HMFU synthesized above, and allowed to react overnight at room temperature under mild stirring, to form an ester of tryptophan and HMFU. The product was precipitated in ice-cold water and the resulting crystals washed with acetone and dried. The 5FU-tryptophan ester was purified via reverse phase chromatography using Sep-Pack C18 cartridges and dried under vacuum.

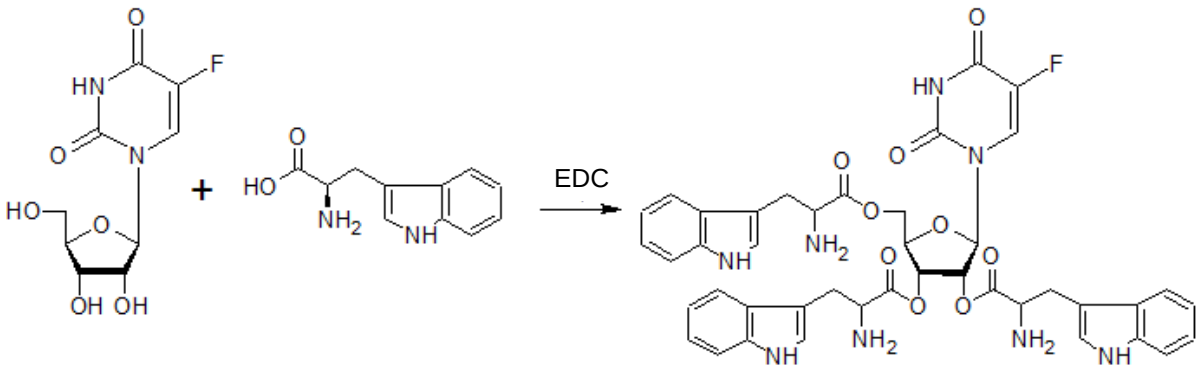

Reaction Scheme 4.2. Chemical synthesis of 5FURW.

5FURW was synthesized by esterification of 5FUR and tryptophan.

The synthesis of 5FURW, tryptophan 5-fluorouridine ester, was achieved by Reaction Scheme 4.2. 5-Fluorouridine (5FUR; Sigma-Aldrich), tryptophan hydrochloride, DMAP and EDC were mixed in a proportion of 1:3:3.5:3.5 in 1:1 DMSO:water, pH 6.5, and reacted overnight at 60 °C under mild stirring. The resulting 5FURW was purified via reverse phase chromatography using Sep-Pack

C18 cartridges and dried under vacuum. Nuclear magnetic resonance (NMR) spectra of the reactants and final product is provided in Figure 4.5b, acquired on a Varian 600 MHz magnet. Characteristic chemical shifts of both 5FUR (a-c) and tryptophan (e-f) were present in 5FURW, with a noticeable spread in chemical shift compared to unreacted reagents. These shifts are likely attributed to the significant change in electronic environment caused by the closer proximity of multiple aromatic moieties. The disappearance of (d) chemical shifts relative to unreacted 5FUR suggests the near-complete reaction of ribose hydroxyl groups. Furthermore, integration of chemical shifts shows an average ratio of 1:2.95 for single protons corresponding to 5FUR and tryptophan, respectively. NMR characterization therefore confirms the reaction of 5FUR with tryptophan, in a molar ratio of 1:3.

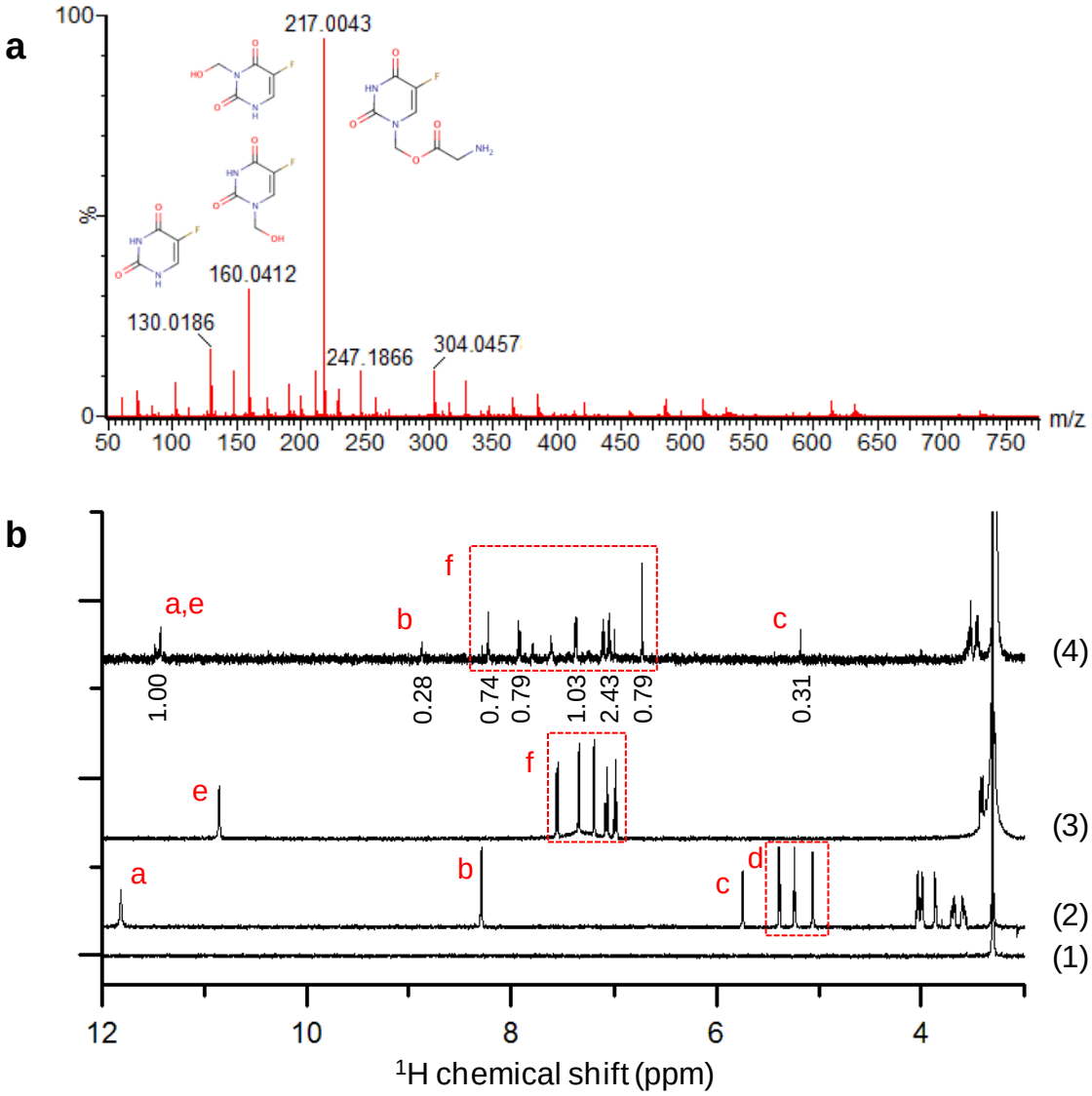

Figure 4.5. Characterization of 5FU analogues.

(a) Mass spectrometry analysis of the fraction containing 5FUG, obtained by Reaction Scheme 4.1. (b) NMR spectroscopy of reactants and product of Reaction Scheme 4.2. Spectra of d_6-DMSO, 5FUR, tryptophan, and 5FURW are designated as (1), (2), (3), and (4), respectively. Characteristic peaks are labeled as a-f, and integrations are provided for the final product 5FURW.

4.5. Liposome encapsulation of 5FU analogues

All 5FU analogues were methodically designed to improve drug encapsulation in liposomes. Contrary to DOX, 5FU is small (130 Da vs. 543 Da) and neutral, which

allows it to permeate in and out of the lipid bilayer easily, further resulting in poor liposomal retention. The overarching concept of all analogues was to synthesize prodrugs of 5FU, wherein the cleavable component vested similar chemical properties as DOX, such as amphipathicity, aromaticity and weak basicity. To optimize 5FU encapsulation in cationic liposomes bearing a transmembrane ammonium sulfate gradient, each pro-drug was incorporated at various stages of liposome fabrication. Only the method which yielded highest entrapment of each analogue is reported, and Table 4.2 summarizes the findings from these studies. Unmodified 5FU was best incorporated when introduced in the organic phase, and only resulted in 0.7 mol% relative to lipid. This poor retention substantiated the need for a novel 5FU liposomal encapsulation method. It is noteworthy that 5FU incorporation in liposomes bearing a transmembrane ammonium sulfate gradient was previously tried, also to no avail [126].

The first attempt aimed to improve the basicity of 5FU through the incorporation of a free amine. The free amine in DOX governs its ability to form a salt in the presence of ammonium sulfate. To incorporate a free amine which is inherently non-toxic, the simplest amino acid, glycine, was conjugated to 5FU as described in the previous section. The highest yield of 5FUG encapsulation in liposomes was 1.4 mol%, double that of unmodified 5FU, and was achieved by incorporation in the ammonium sulfate lipid film hydration solution. However, to be able to fine-tune ratios in liposomes co-loaded with DOX, the yield of 5FU encapsulation should be similar to that of DOX, ~14-24 mol% drug with respect to

lipids [127]. Despite the free amine addition to improve drug basicity, 5FUG was still poorly incorporated at ten-fold lower encapsulations compared to DOX.

5FU Analogue	Drug Incorporation (mol%)	Size (nm)	Zeta Potential (mV)
5FU 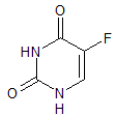	0.7 ± 0.2	173.5 ± 43	41.7 ± 9.8
5FUG 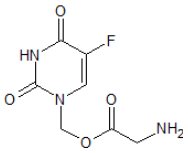	1.4 ± 0.5	161.8 ± 10.8	41.2 ± 1.8
5FUW 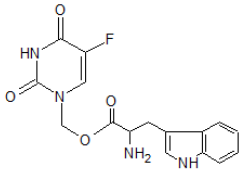	3.2 ± 0.4	167.4 ± 1.8	19.6 ± 0.6
5FUR 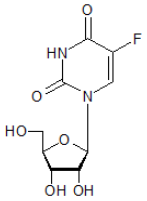	3.7 ± 0.2	177.4 ± 2.8	37.9 ± 1.0
5FURW 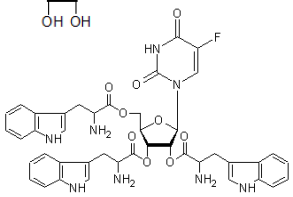	26.6 ± 2.4	163.8 ± 17.2	32.2 ± 6.5

Table 4.2. Physical and chemical properties of liposomes containing 5FU analogues with lipid composition of 80:10:10 DSPC:DOTAP:Chol (n≥3).

The next derivative investigated was tryptophan conjugated to 5FU (5FUW), utilizing the same chemistry as 5FUG. Tryptophan is weakly basic due to its free amine, but contrary to glycine, is also aromatic due to its indole moiety. Aromaticity plays a crucial role in liposomal DOX encapsulation, as the intra-liposomal oligomerization of DOX is attributed to the Π electron stacking of planar aromatic

rings [128]. The integration of planar aromatic rings in a 5FU prodrug can facilitate Π electron stacking to other 5FU prodrugs as well as to DOX, and can potentially improve the retention of 5FU. 5FUW was best encapsulated when exposed to liposomes after generation of the transmembrane ammonium sulfate gradient, for 2 hours at 65°C. The addition of the free amine and aromaticity in the 5FU analogue 5FUW slightly improved drug incorporation to 3.2 mol%, and additional 5FU analogues were further investigated to enhance encapsulation.

5-fluorouridine (5FUR) is the ribosylated nucleoside analogue of 5FU, and is both a metabolite and precursor of the original drug. 5FU can be converted to 5FUR and vice versa *in vivo* through uridine phosphorylase, and thus both 5FUR and 5FU are metabolized to the same active products, 5-fluorouridine monophosphate (FUMP) and 5-fluorodeoxyuridine monophosphate (FdUMP) to elicit both RNA and DNA damage, respectively [54-56]. Because of this, 5FUR is projected to behave similarly to 5FU, including its synergistic interaction with DOX, and was investigated for encapsulation in liposomes. 5FUR is commonly utilized as a plant growth regulator and is therefore commercially available. Unmodified 5FUR was also best incorporated post-generation of the ammonium sulfate gradient for 2 hours at 65°C. As seen in Table 4.2, 5FUR can be entrapped in liposomes to a greater extent than the original 5FU, about a five-fold enhancement to 3.7 mol% drug encapsulation. The more attractive advantage of utilizing 5FUR rather than 5FU, however, is that it inherently contains three hydroxyl groups for multiple conjugations of amino acids.

The next derivate investigated for 5FU, consequently, was 5FUR triply conjugated to tryptophan (5FURW) via the hydroxyl groups (Section 4.4). This modification should enhance both the basicity and aromaticity compared to the 5FUG and 5FUW analogues, and was projected to improve drug incorporation in liposomes. Like unmodified 5FUR, 5FURW yielded the greatest encapsulation when introduced after generation of the ammonium sulfate gradient for 2 hours at 65°C. As seen in Table 4.2, 5FURW achieved the greatest entrapment out of all the 5FU analogues considered, a 38-fold enhancement to 26.6 mol%, which is very similar to the encapsulation yields of DOX. The methodology to synthesize a 5FU analogue similar to DOX in both basicity and aromaticity resulted in encapsulation yields identical to that of DOX. Therefore, 5FURW served as the 5FU analogue for further co-encapsulation with DOX in liposomes.

To the best of our knowledge, there is no reported method for encapsulating 5FU in liposomes bearing a transmembrane ammonium sulfate. In fact, it was previously reported that the exact opposite approach, utilizing basic media (~pH 8.6), is required for liposomal encapsulation of 5FU [129]. A possible reason for this is that 5FU lacks a charge, and can therefore easily pass through the lipophilic bilayer to escape the liposome.5FU has only been reported to exist in anionic forms, which occur at neutral pH [130], and hence not in liposomes bearing an acidic pH gradient. Thus, for the purpose of simultaneously co-delivering 5FU+DOX, it was imperative that we develop our own method. By employing the nucleoside analogue of 5FU, we were able to attach chemical moieties bearing the two key properties of DOX drive its liposomal incorporation: a free amine and aromaticity. These

modifications were also designed to be hydrolyzable in order restore the active drug which is synergistic with DOX. While this approach was demonstrated only for 5FU, it can be theoretically applied to the entire class of nucleobase analogue chemotherapies, such as cytarabine, gemcitabine, and decitabine, all of which contain pendant hydroxyl groups that can be conjugated to tryptophan. Tryptophan modification has implications not only for delivering agents that previously could not be liposomally entrapped, but also for combination co-delivery of the many drugs that can be compatible with this encapsulation method.

4.6. Synergistic activity of 5FURW and DOX

Retaining drug synergy, however, is of the utmost importance next to feasible encapsulations of both drugs. Prior to incorporating both 5FURW and DOX in liposomes, optimal synergistic ratios between the new 5FU analogue and DOX were identified. BT-474 cells were exposed to various ratios of 5FURW and DOX, and synergistic interactions were assessed utilizing the CI method. 5FURW and DOX were tested in a broader range than the initial 5FU and DOX studies in order to identify multiple synergistic ratios, with the hindsight that some ratios may not feasibly be incorporated in liposomes. The dependence of anticancer synergy on ratio is seen in Figure 4.6a. Slight synergy occurred when low doses of 5FURW were combined with high doses of DOX (R=0.1), and extreme synergy was observed when high doses of 5FURW were combined with low doses of DOX ($R \geq 75$). These synergistic regimes are similar to the original synergistic interactions observed with unmodified 5FU and DOX, which occurred at $R \leq 0.5$ and $R = 819$.

Since 5FURW hydrolyzes directly to its precursor, 5FUR, synergistic interactions were also investigated between 5FUR and DOX. As seen in Figure 4.6a, 5FUR and DOX exhibit synergy at extreme ratios (R ≤ 1 and R = 600), as well. While the exact synergistic ratios are slightly different, the regimes of synergy are similar across the various analogues of 5FU tested, and attests to the potent interactions between this particular combination. It appears that low doses of 5FU combined with high doses of DOX and high DOX doses combined with low 5FU doses are synergistic regardless of whether the 5FU analogue is immediately active or requires metabolization first. The discrepancies between exact ratios may be attributed to the need for hydrolytic cleavage or metabolization prior to the interactions of the active forms of both drugs.

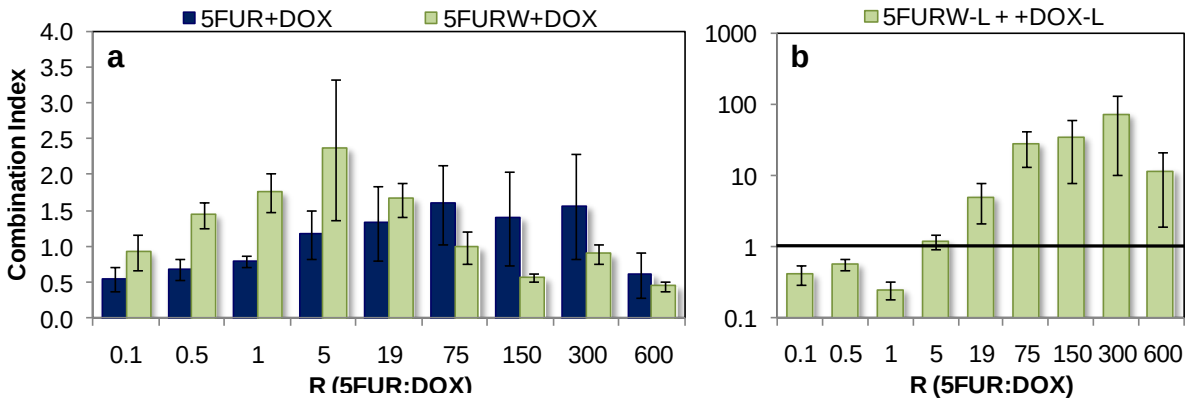

Figure 4.6. CIs for 5FUR+DOX, 5FURW+DOX, and 5FURW-L+DOX-L.

(a) CI for 5FUR+DOX (blue, left bars) or 5FURW+DOX (green, right bars). Drug concentrations for 5FUR and DOX, respectively, corresponding to each R were: 0.1 (0.06, 0.60), 0.5 (0.15, 0.3), 1.0 (0.3, 0.3), 5.0 (1.5, 0.3), 19 (2.9,0.15), 75 (11.25, 0.15), 150 (22.5, 0.15), 300 (22.5, 0.075), 600 (45, 0.075). Drug concentrations for 5FURW and DOX, respectively, corresponding to each R were: 0.1 (0.06, 0.60), 0.5 (0.15, 0.30), 1 (0.30, 0.30), 5 (1.50, 0.30), 19 (5.60, 0.30), 75 (22.50, 0.30), 150 (45.00, 0.30), 300 (45.00, 0.15), 600 (90.0, 0.15). (b) CIs calculated for various ratios of 5FURW-L and +DOX-L. Drug concentrations for 5FURW and DOX, respectively, corresponding to each ratio were: 0.1 (0.30, 2.40), 0.5 (0.60, 1.20), 1 (1.20, 1.20), 5 (22.50, 4.70), 19 (45.00, 2.40), 75 (180.00, 2.40), 150 (180.00, 1.20), 300 (180.00, 0.60), 600 (360.00, 0.60). BT-474 cells were exposed to combinations for 72 hours. Data shown as average ± SD (n≥6).

After verifying that 5FURW was both easily incorporated in liposomes and synergistic with DOX, single-drug loaded liposomes were tested for synergy to assess whether particle encapsulation compromises drug synergy. Combination indices were calculated for 5FURW-L and +DOX-L exposed to BT-474 cells, and the results are provided in Figure 4.6b. Contrary to the free drug counterparts, the single drug-loaded liposomes only synergistically inhibited cancer cell growth at one extreme regime, $R \leq 1$. Although the free drugs were synergistic for $R > 75$, the liposome-encapsulated forms were highly antagonistic ($CI \gg 1$), with CIs two orders of magnitude greater than those of the synergistic ratios. While this was a surprising finding, it is not unusual since particle encapsulation can impact drug internalization and intracellular concentrations, which can further alter drug-drug interactions. These results elucidate an added challenge of combination chemotherapy co-delivery, that the ratios at which free drugs are synergistic are not necessarily the same as those of the liposome-encapsulated form. Since 5FU and DOX consistently elicited synergistic cancer cell kill at $R \leq 1$, regardless of whether they were entrapped in liposomes, this was the regime that was sought for their dual encapsulation in liposomes.

4.7. Co-encapsulation of 5FURW and DOX in liposomes

Finally, both 5FURW and DOX were simultaneously encapsulated in liposomes in order to create a nanoparticle that can conserve their synergistic ratio *in vivo*. To achieve co-encapsulation, 5FURW was first introduced to liposomes bearing an ammonium sulfate gradient for 2 hours, followed by DOX loading for 30

minutes. Two ratios, one synergistic and one antagonistic, were incorporated in liposomes, and a third formulation of PEGylated liposomes with the synergistic ratio was fabricated for *in vivo* studies. PEGylated liposomes were prepared using DSPC:1,2-distearoyl-sn-glycero-3-phosphoethanolamine-N-[methoxy(polyethylene glycol)-2000] (mPEG-DSPE):DOTAP:Chol in a ratio of 75:5:10:10. The physical and chemical properties of all three liposome formulations are listed in Table 4.3. Liposomes encapsulated with a ratio of 12.2 were designated as ant-L, as their free drug contents exhibited CI > 1 and should be antagonistic (Figure 4.6a). Similarly, liposomes carrying a ratio of 0.18 were designated as syn-L, as their free drug contents elicited CI < 1 and should be synergistic. The ability to incorporate various ratios of 5FURW+ DOX, spanning multiple orders of magnitude, verifies that the tryptophan modification developed in the previous section is a robust liposome incorporation method. The sizes and diameters of ant-L and syn-L are very similar (156.9 nm vs. 149.8 nm and 36.2 mV vs. 35.7 mV, respectively); the primary difference between the two formulations is the ratio of their drug payloads.

Liposome Formulation	R (5FURW:DOX)	DOX Incorporation (mol%)	5FURW Incorporation (mol%)	Size (nm)	Zeta Potential (mV)
ant-L	12.2	0.45 ± 0.02	5.47 ± 0.94	156.9 ± 5.7	36.2 ± 0.5
syn-L	0.18	7.75 ± 0.09	1.41 ± 0.47	149.8 ± 15.1	35.7 ± 4.3
DAFODIL	0.15	14.82 ± 0.69	2.17 ± 0.23	168.8 ± 18.7	-23.0 ± 3.0

Table 4.3. Physical and chemical properties of liposomes containing 5FURW and DOX.

Lipids composition for all liposomes was 80:10:10 DSPC:DOTAP:Chol, except for DAFODIL, which consisted of 75:5:10:10 DSPC:mPEG-DSPE:DOTAP:Chol. Drug loadings and DLS measurements are reported as mean ± SD (n≥3).

However, this single difference in ratio dictates their anticancer activities, which is evident in the comparison of their 4T1 cancer cell growth inhibition. In Figure 4.7a, ant-L exhibits similar cancer cell growth inhibition as liposomes containing only 5FURW. On the contrary, syn-L exhibits superior cell inhibition compared to either 5FURW or DOX-loaded liposomes (Figure 4.7a-b). To quantitatively compare the liposome formulations, CIs were calculated and averaged for all concentrations tested of ant-L and syn-L. Indeed, ant-L elicited CI = 1.92 ± 1.21, indicating antagonistic cancer cell kill, and syn-L resulted in CI = 0.31 ± 0.24, implying synergistic cell kill. Thus, drug interactions in co-loaded liposomes were consistent with free drug interactions found in Figure 4.6a.

PEGylation of liposomes, especially positively charged, is necessary for prolonged systemic circulation because it prevents opsonization, allowing the nanoparticles to evade the immune system [104, 131]. Therefore, a PEGylated version of syn-L was fabricated and designated as DOX And 5FU Optimally Delivered In Liposomes (DAFODIL). For DAFODIL, a small fraction (5 mol%) PEG2000-DSPE was incorporated in the lipid bilayer, and resulted in a slightly larger size of 168.8 nm compared to syn-L (149.8 nm), as well as a change in ζ potential. Upon PEGylation, the cationic lipids became shielded, as was evident in the ζ potential of -23.0 mV. Drug encapsulations and ratios were only slightly altered. The inclusion of PEG allowed twice as much DOX retention compared to non-shielded liposomes, and may be a result of the added barrier of long, hydrophilic polymeric chains which must be overcome for drug release. Despite this increase in drug incorporation, encapsulated drug ratio was only slightly shifted from R=0.18 to

R=0.15, in favor of greater free drug synergy. The anticancer activity of DAFODIL surpassed that of syn-L, as seen in Figure 4.6a-b, which may be a consequence of the more favorable synergistic ratio DAFODIL carries. Lastly, differential dug release from DAFODIL was measured via dialysis. Results in Figure 4.6c show that 5FURW is released slightly faster than DOX, and that acidic conditions accelerate drug release. Therefore, the effective free drug ratio which is exposed to cancer cells is slightly higher than the ratio encapsulated in liposomes, but is evidently still potent at inhibiting cell growth. Fundamentally, these results show that the synergistic activity of 5FUR and DOX can be preserved when co-loaded in liposomes, with or without PEGylation, and provides promise for translating this combination *in vivo*.

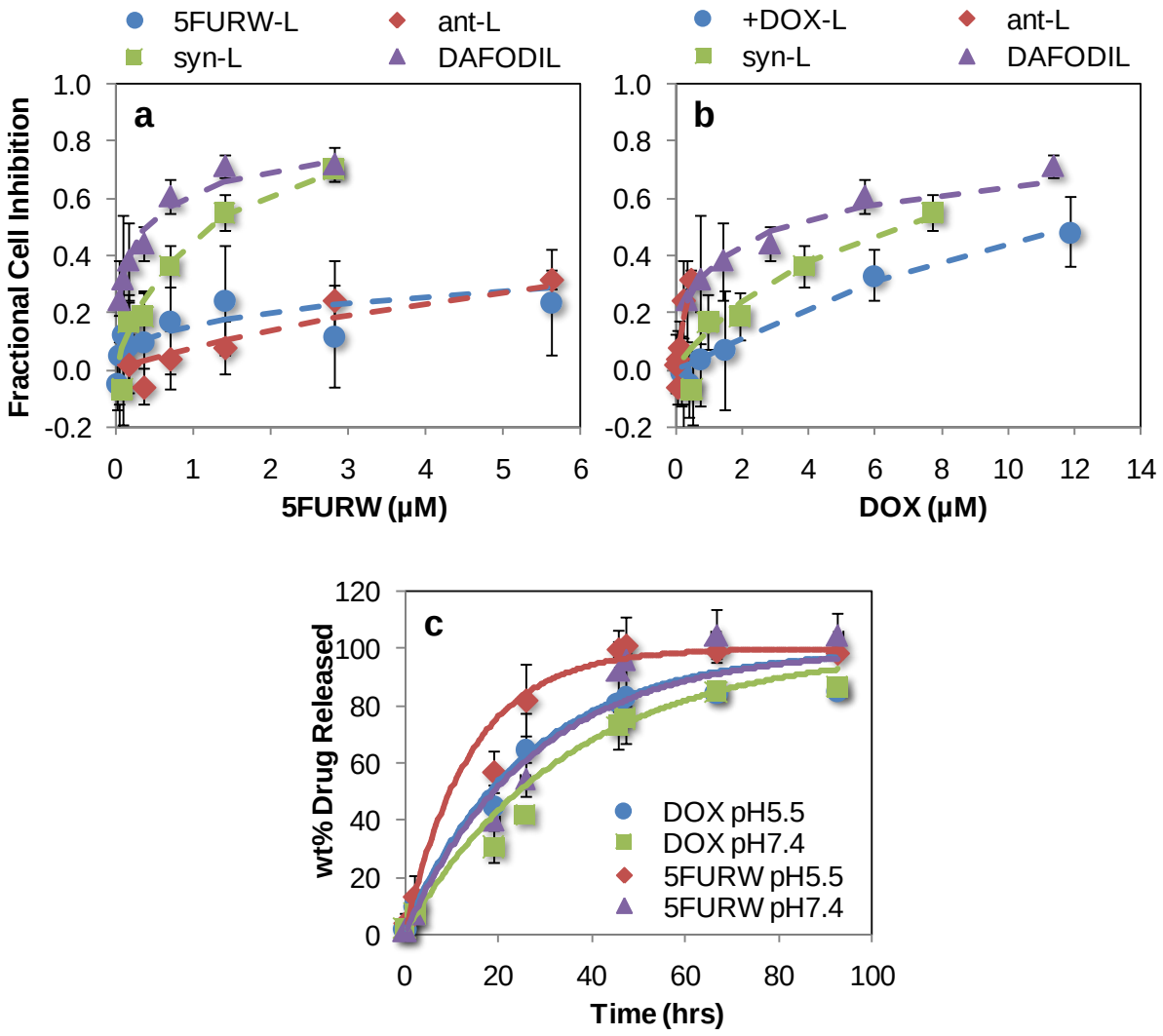

Figure 4.7. *In vitro* anticancer activity of 5FURW and DOX co-loaded liposomes.

4T1 cancer cell growth inhibition by various 5FURW- and DOX- co-encapsulated liposomes. (a) Comparison of 5FURW single-loaded liposomes (circles) to ant-L (R=12.2, diamonds), syn-L (R=0.18, squares), and DAFODIL (R=0.15, triangles). (b) The same co-loaded liposomes in (a) are compared to +DOX-L (circles). Dashed lines represents fits to the median effect model. Average calculated CI for the cell inhibition data of ant-L and syn-L are 1.92 ± 1.21 and 0.31 ± 0.24, respectively. Data reported as average ± SD (n≥6). (c) Drug release of 5FURW at pH 5.5 (diamonds) and pH 7.4 (triangles) or DOX at pH 5.5 (circles) and pH 7.4 (squares) from DAFODIL in PBS. Data shown as average ± SD (n=3). Lines represent exponential fits to release profiles ($t_{1/2,R}$ = 14.1, 27.7, 26.9, and 35.3 for 5FURW pH 5.5, 5FURW pH 7.4, DOX pH 5.5, and DOX pH 7.4 respectively).

4.8. *In vivo* efficacy of 5FURW and DOX co-loaded liposomes

To investigate if the drug delivery advantages of liposomes can be utilized to improve the efficacy of combination chemotherapies, liposomes co-loaded with a synergistic ratio of 5FURW and DOX were finally challenged against an animal tumor model *in vivo*. The highly metastatic and aggressive 4T1 mouse breast cancer model was adopted to challenge the formulations with more advanced, difficult to treat cancers. This model was also chosen for its robust tumor formation in immuno-competent BALB/c mice, which allows for a more accurate depiction of nanoparticle clearance and efficacy compared to models in immuno-incompetent mice. As seen in Figure 4.7a-b, liposomes co-loaded with a synergistic ratio of 5FURW+DOX are effective at inhibiting 4T1 cancer cell growth *in vitro*. However, this synergy may be difficult to capture *in vivo* due to uncoordinated drug pharmacokinetics and fast plasma clearance of the small molecule drugs when injected intravenously (i.v.) as free solutions. Clinical studies have shown that 5FU and DOX exhibit elimination half lives of 8-22 minutes [132] and 4-5 minutes [14], respectively. These rapid clearance rates demonstrate a clear need for nanoparticle delivery to ensure concurrent delivery to tumors. *In vivo* tumor growth inhibition studies comparing the efficacy of liposome and free drug formulations of 5FURW+DOX will elucidate if liposomes are capable of overcoming the drug delivery challenges of combination chemotherapies.

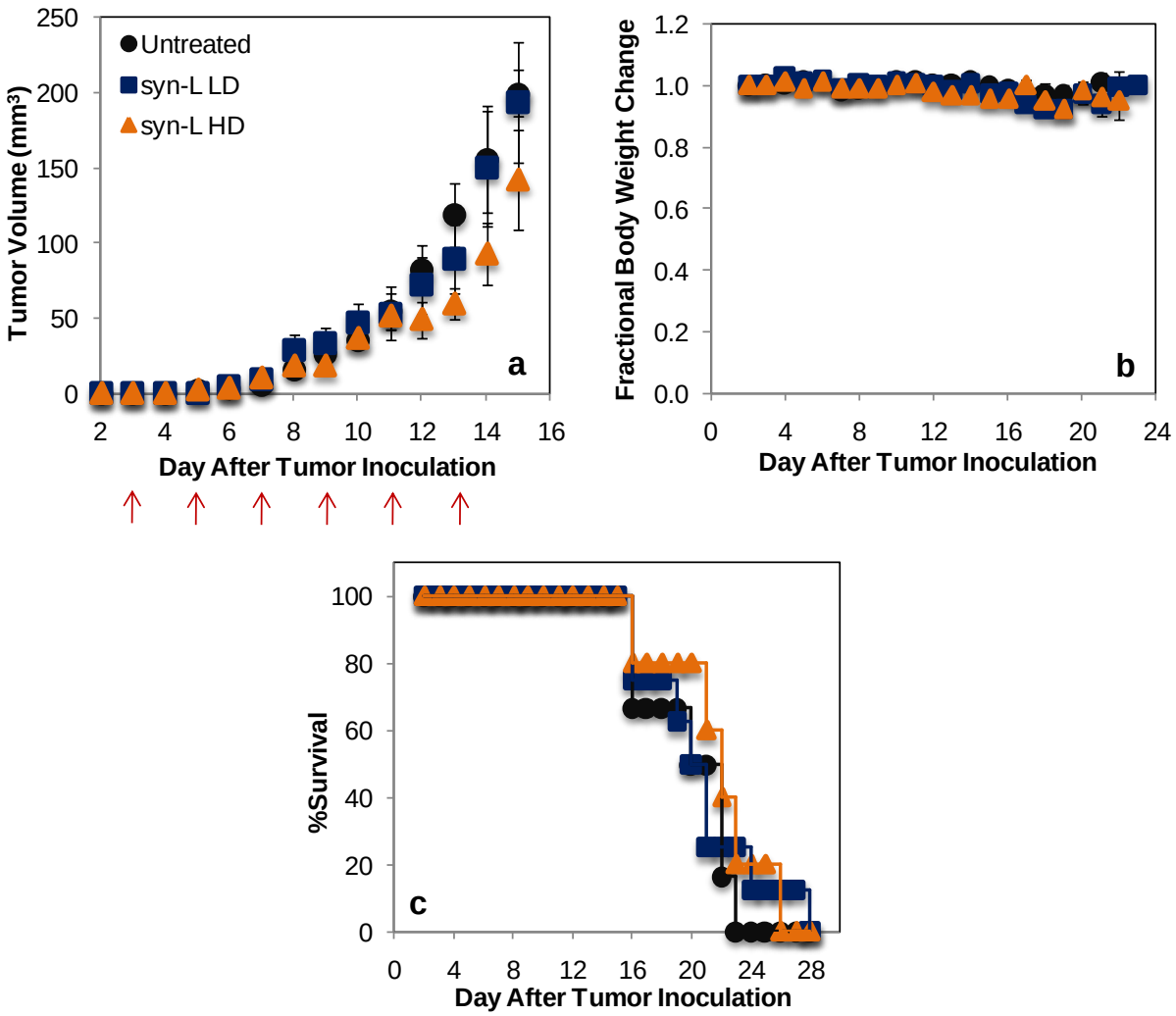

Figure 4.8. Tumor growth inhibition of syn-L.

(a) Tumor growth of mice bearing 4T1 breast cancer tumors, without treatment (circles), with i.v. injections of low dose syn-L (squares), or high dose syn-L (triangles). Low dose syn-L treatments consisted of drug-equivalent doses of 1 mg/kg DOX + 0.3 mg/kg 5FURW, while high dose syn-L treatments consisted of 4 mg/kg DOX + 1.1 mg/kg 5FURW. Arrows indicate days of treatment. (b) Effect of treatment on body weight fluctuations. Data is reported as mean ± SE (n≥5). (c) Survival rates for all treatment groups.

Initial studies investigated the efficacy of non-PEGylated syn-L. Mice we retreated with low dose (1 mg/kg DOX + 0.3 mg/kg 5FURW) or high dose (4 mg/kg DOX + 1.1 mg/kg 5FURW) syn-L via i.v. tail vein injections on Days 3, 5, 7, 9, 11, and 13 post tumor-inoculation. Control tumor-bearing mice were untreated. Tumor

volumes were recorded daily as a measure of therapeutic efficacy (Figure 4.8a), and body weight changes were reported (Figure 4.8b) as a measure of formulation tolerability. Results showed no significant difference in tumor growth between syn-L-treated mice and untreated mice, regardless of dose. There was also no significant difference in body weight changes, suggesting no evident treatment-related toxicity. All three groups, however, displayed similar survival rates. Comparisons of tumor growth and survival rates between liposome-treated and untreated mice demonstrate that the non-PEGylated liposome formulations are ineffective at reducing tumor burden. Although syn-L is potent at inhibiting cancer cell growth *in vitro*, it is incapable of doing so *in vivo*. This was not surprising, since cationic liposomes are rapidly cleared by the MPS system [51, 104, 131, 133], thereby reducing the likelihood of accumulation in tumor tissue.

In order to manifest the potency of 5FURW+DOX *in vivo*, mPEG-DSPE was incorporated in the lipid bilayer. PEG serves as a water soluble polymer that prevents protein opsonization and effectively disguises liposomes from MPS clearance [104, 131]. This further allows liposomes to circulate longer and increases the likelihood of tumor accumulation via the EPR effect. The PEGylated version of syn-L, DAFODIL, was challenged against 4T1 murine breast carcinoma *in vivo*, at drug-equivalent doses of 3 mg/kg DOX + 0.62 mg/kg 5FURW for a total of 7 alternating injections starting on Day 3. The resultant tumor growth curves are seen in Figure 4.9a.

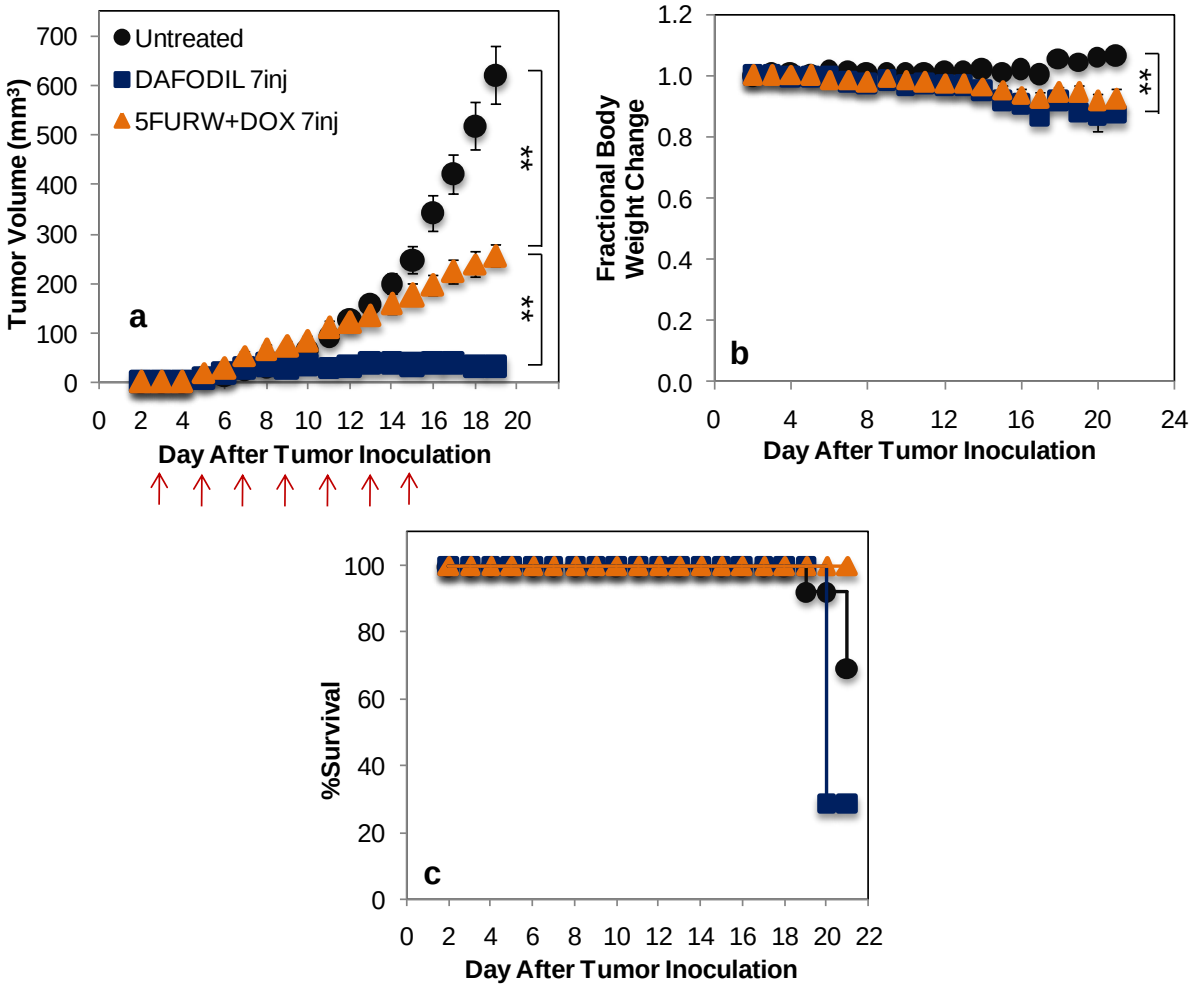

Figure 4.9. Tumor growth inhibition of 7 injections of DAFODIL.

(a) Tumor growth of mice bearing 4T1 breast cancer tumors, without treatment (circles), with i.v. injections of DAFODIL (squares), or free 5FURW+DOX (triangles), for a total of 7 injections (n≥10). Mice were administered liposomes or free drugs in drug-equivalent doses of 3 mg/kg DOX + 0.62 mg/kg 5FURW. Arrows indicate days of treatment. (b) Effect of treatment on body weight fluctuations. Data is reported as mean ± SE. Mice were provided daily Diet Gel supplements starting on Day 17 in hopes to revert weight loss. (c) Survival rates for all treatment groups.

In stark contrast to its non-PEGylated counterpart, DAFODIL was able to significantly inhibit tumor growth by a remarkable 95% (31 vs. 623 mm^3) compared to untreated tumors. At 59% (256 vs. 623 mm^3) tumor growth reduction, the free drug-equivalent administration was significantly less effective than the liposomal formulation. These results are drastically different than those seen for the syn-L,

and emphasize the importance of stealth properties for chemotherapy drug delivery. Unfortunately, DAFODIL at the 7 injection high dosing schedule was toxic as evident by >10% body weight loss (Figure 4.9b). Diet gel supplements were provided daily starting on Day 17, the onset of noticeable weight loss; however, the toxicity seemed irreversible. Therefore, although DAFODIL reduced tumor burden, it did not improve overall survival rates (Figure 4.9c), and the study was terminated to prevent additional treatment-related toxicities.

Drug optimizations are common in the clinic, and often initial drug doses must be reduced in order to find a well-tolerated therapeutic window of drug formulations. To see if a high therapeutic effect could be achieved with a lower, more tolerable dose of DAFODIL, the study was repeated with half the injections. Mice were injected at the same dose (3 mg/kg DOX + 0.62 mg/kg 5FURW) starting on Day 3 for a total of 4 injections. As seen Figure 4.10a-b, significant tumor reduction was maintained at the 4 injection schedule without a reduction in body weight. By day 23, the last day of >50% untreated mice survival, liposomes elicited 91% (77 vs. 904 mm^3) tumor growth inhibition, whereas free 5FURW+DOX at the same doses were only capable of inhibiting 39% tumor growth (547 vs. 904mm^3). Moreover, all tumors treated with free 5FURW+DOX eventually grew to the same sizes as control mice, and hence were only able to extend average survival of untreated mice by 4 days (24 vs. 28 days).

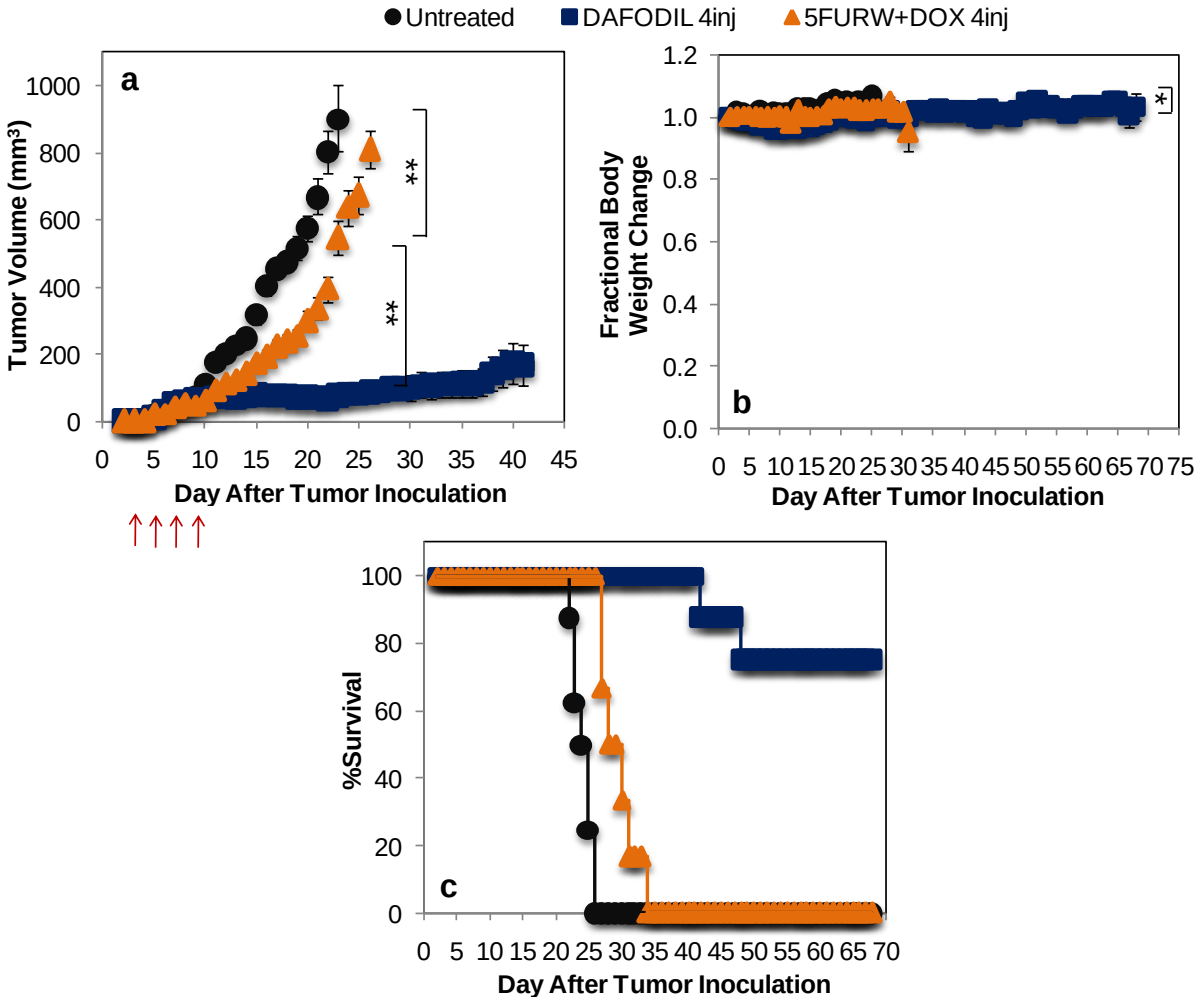

Figure 4.10. Tumor growth inhibition of 4 injections of DAFODIL.

(a) Tumor growth of mice bearing 4T1 breast cancer tumors, without treatment (circles), with i.v. injections of DAFODIL (squares), or free 5FURW+DOX (triangles), for a total of 4 injections (n=8 except for last two control data points where n≥5). Mice were administered liposomes or free drugs in drug-equivalent doses of 3 mg/kg DOX + 0.62 mg/kg 5FURW (same as study in Figure 4.9). Arrows indicate days of treatment. (b) Effect of treatment on body weight fluctuations. Data is reported as mean ± SE. Significance is reported for Day 23. (c) Survival rates for all treatment groups.

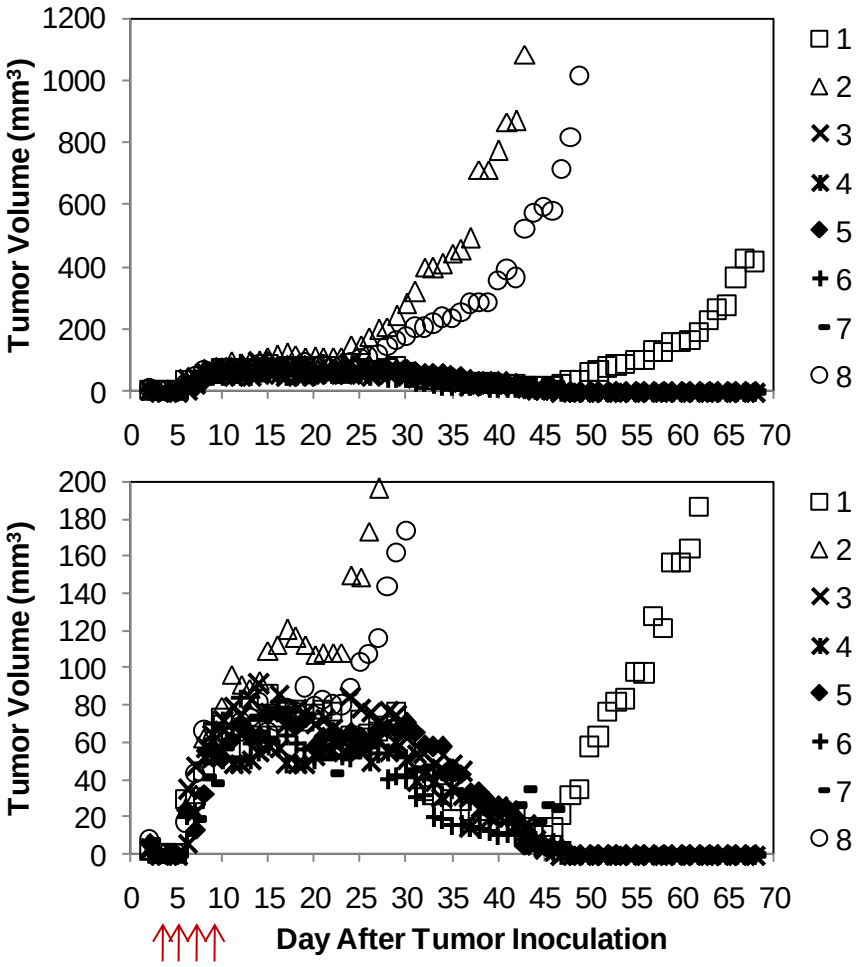

Figure 4.11. Tumor growth profiles of mice treated with DAFODIL.

Individual tumor growth profiles of mice bearing 4T1 breast cancer tumors, treated with 4 i.v. injections of DAFODIL. Mice were administered DAFODIL in drug-equivalent doses of 3 mg/kg DOX + 0.62 mg/kg 5FURW (same as Figure 4.10). Arrows indicate days of treatment. Bottom graph is a smaller scale version of the top graph, to provide greater detail.

Figure 4.11 shows the individual tumor growth profiles for each mouse treated with DAFODIL. Contrary to free drug-treated mice, the majority of DAFODIL-treated mice maintained low tumor sizes while 3/8 eventually developed recurring tumors. Figure 4.11 shows that most liposome-treated mice reached a peak tumor volume between 50-80 mm^3 on Day 28, followed by tumor regression and finally, complete eradication. No detectable tumors in 5/8 mice was observed for the

remainder of the study. The 3/8 liposome-treated mice with recurring tumors experienced significantly slowed tumor growth; all untreated mice had 1000 mm^3 tumors by Day 26, whereas the first liposome-treated mouse to reach 1000 mm^3 tumor volume occurred at Day 44. Because of these immense therapeutic effects, treatment with highly synergistic DAFODIL significantly extended average survival by at least 44 days relative to untreated mice. On the contrary, free 5FURW+DOX only extended median survival by 4 days relative to untreated mice. *To the best of our knowledge, this is the first time that 4T1 tumor growth was inhibited by >90% at a cumulative DOX dose < 15 mg/kg, either used as a single agent or combined with another chemotherapy drug* [46, 134-141]. This enhanced therapeutic efficacy is likely attributed to the synergistic interactions between 5FURW+DOX, compounded with tumor accumulation due to cationic liposomal delivery.

In addition to successful tumor treatments, 4 injections of DAFODIL demonstrated good safety in tumor-bearing mice. Unlike the higher dose schedule of 7 injections, the low dose schedule of 4 injections did not result in weight loss. Figure 4.10b shows that untreated tumor-bearing mice exhibited 5% increase in body weight, while liposome-treated mice gained 2% in body weight. Overall growth is anticipated as the mice are only 6-8 weeks of age at time of tumor inoculation, and this difference in growth between treatment groups was found to be statistically significant. However, it is likely that the increased weights of control mice was actually the tumor weights due to their large volumes. In fact, it has been shown in literature that tumor volume can encompass up to 28% of total body weight [142-144]. In addition, liposome-treated mice did not exhibit signs of pain or distress,

such as ruffled hair or reduced physical activity. Therefore, mice treated with 4 injection DAFODIL did not elicit any obvious signs of adverse side effects. Mice treated with free 5FURW+DOX at the same doses, however, lost 5% body weight shortly before euthanasia.

To the best of our knowledge, this was the first instance of 5FU-incorporated liposomes *in vivo* which were well-tolerated and effective at inhibiting tumor growth. Previously, liposomal 5FU encapsulation has been too low to allow injections of therapeutically active doses [123], or 5FU liposomes elicited ~20% body weight reduction and were toxic [145]. In the latter study, toxicity was attributed to fast leakage of 5FU from liposomes post-administration. Altogether, our studies demonstrate that PEGylated liposomal administration of 5FURW+DOX is more therapeutically effective and better tolerated than free 5FURW+DOX, and arguably compared to any liposomal of combination formulation of 5FU or DOX. PEGylation was required to extend circulation of and enhance tumor accumulation of cationic liposomes, while dose optimization was necessary to reduce side effects. With these modifications, 5FURW+DOX co-loaded liposomes delivered a potent therapeutic which reverted aggressive 4T1 tumor growth in most mice, while also maintaining overall health.

4.9. Summary of liposomes for synergistic chemotherapy delivery

Here, we sought to co-deliver the synergistic drug pair 5FU+DOX which is commonly employed in many gastric and breast cancer treatment regimens, in an effort to improve upon their therapeutic efficacy. Although they encompass an

archetypal chemotherapy combination, they rarely achieve complete eradication of tumors [8, 96]. Cationic liposomes were investigated for multiple reasons: their ability to direct drugs to tumors via the EPR effect and negative fenestrae present on tumor endothelium [122-124], their ionic interaction with cell membranes which facilitate uptake and drug release [114-117], as well as for the general ability of liposomes to alleviate adverse side effects [100-102]. Single-drug loaded liposomes, such as Doxil™, consistently reduce cardiotoxicity thereby increasing the maximum tolerable dose of DOX. However, this extension of safe DOX doses does not necessarily improve antitumor efficacy. By combining the power of combination chemotherapies with the targeting and stealth abilities of liposomes, we were able to administer low dose, yet potent payloads to tumors and achieve remarkable tumor reduction in a highly aggressive mouse breast cancer model.

This chapter elucidated the complexities in liposomal drug encapsulations. Because liposomes entrap and are surrounded by aqueous medium, water soluble drugs can diffuse easily in and out of the nanoparticles. Transmembrane gradients which favor the encapsulation of a particular drug, such as the ammonium sulfate gradient, can be applied, but often are geared towards the retention of one drug and offer poor encapsulation of another. 5FU and DOX, for example, are easily incorporated in liposomes with drastically different acidities. 5FU is best entrapped in liposomes with pH 8.6 [129], while DOX is best encapsulated at liposomes bearing pH 4-5 [127]. To incorporate multiple drugs into a single liposome, novel driving mechanisms which are compatible with their differing chemical properties must be developed. Celator Pharmaceuticals, Inc. has developed multi-drug loaded liposomes

with huge success; cytarabine+daunorubicin loaded-liposomes (CPX-351) is in Phase III clinical trials for secondary acute myeloid leukemia, and two other formulations are in Phase II studies. However, this is the first report, to our knowledge, which applied the well-established transmembrane ammonium sulfate gradient to nucleobase analogues, specifically 5FU. Using a methodological approach, we were able to incorporate the chemical moieties which facilitate DOX incorporation into a hydrolyzable prodrug analogue of 5FU. Furthermore, the modification required a non-toxic addition of tryptophan, and did not compromise synergy between 5FU+DOX.

Although this study only focused on 5FU+DOX encapsulations, this same approach can be applied to many other ribosylated nucleobase analogues, provided that they possess hydroxyl groups for esterification with tryptophan. What was once only useful for anthracycline incorporation into liposomes, the well-established pH gradient encapsulation method could now be utilized for multi-drug incorporation of numerous chemotherapy pairs. Compounded with cationic stealth liposomes, combination chemotherapies could be delivered *in vivo* specifically to tumors at prescribed synergistic ratios. This concurrent tumor drug delivery can result in amplified tumor reduction compared to free drug treatments. Our multi-faceted approach could be implemented to evaluate a plethora of anthracycline and nucleobase analogue combinations, in hopes to translate effective and safe anticancer therapeutics to the clinic.

Chapter 5

Polymer-drug conjugates for chemotherapy co-delivery

5.1. Advantages of polymer-drug conjugates

Conjugation to polymers can help achieve clinical efficacy of chemotherapy combinations by promoting drug accumulation in tumors rather than essential organs via the EPR effect [146-149], and by ensuring that the tumors are exposed to synergistic ratios of the drug pair. Polymer-drug conjugates are actively explored for the administration of single chemotherapy agents and have already shown clinical benefits over free drug injections [30, 150]: reduced liver accumulation, enhanced drug localization in tumors, and improved drug circulation times [151]. Furthermore, since multi-drug incorporation is governed by chemical reactions as opposed to traditional hydrophobic encapsulations, precise ratios of the drugs can be conjugated to the polymer and delivered to tumor tissue. This characteristic distinguishes polymer-drug conjugates from most nanoparticles, and is crucial since drug ratios can govern whether the combination is synergistic or antagonistic, as demonstrated in Chapter 3. Hence, this class of nano-vehicles presents an elegant method to preserve drug ratios after administration *in vivo*. To investigate polymer-drug conjugates for polychemotherapy delivery, the model synergistic drug pair CPT+DOX identified in Chapter 3 was employed. To develop polymer-drug

conjugates for the concurrent delivery of multiple chemotherapy drugs, the conjugation chemistry was first established with a characteristic non-biodegradable polymer, poly(vinyl alcohol) (PVA). The methodology was then applied to a CD44+ tumor-targeting biopolymer, hyaluronic acid (HA).

5.2. CPT- and DOX-PVA conjugates

Nucleophilic acyl substitution was utilized to conjugate CPT and DOX onto PVA (10 kDa), the same chemistry which is commonly employed in clinical formulations [152, 153].As shown in Reaction Scheme 5.1, this synthesis comprised of two steps. First, pendant hydroxyl groups of PVA (Sigma Aldrich) were partially succinylated (5%) by reaction with succinic anhydride (Sigma Aldrich) using4-(dimethylamino)pyridine(DMAP) as a catalyst in dry DMSO. The reaction was allowed to proceed overnight, under moderate heating and stirring. The succinylated PVA (S-PVA) was precipitated and rinsed multiple times in acetone, and finally re-dissolved in DMSO. The carboxyl groups on S-PVA were activated with EDC to further couple CPT and DOX, respectively through ester and amide bonds. The resulting polymer-drug conjugates were purified using size exclusion Sephadex G-25 PD-10 columns (GE Healthcare Life Sciences; Piscataway, NJ, USA) of MWCO 5,000 Da and concentrated with Amicon® Ultra centrifugal filters of MWCO 3kDa (EMD Millipore; Billerica, MA, USA). CPT-PVA and DOX-PVA are the designations utilized for CPT- and DOX- conjugated PVA, respectively, synthesized via Reaction Scheme 5.1. Conjugated CPT and DOX concentrations were determined via absorbance at 366 nm and 480 nm, respectively, of vehicle serial dilutions using a

Tecan Infinite M200 Pro plate reader. The resultant single drug incorporations were 0.39mol% CPT or 0.16mol% DOX relative to PVA. These conjugation efficiencies are expected, since both reaction steps of Reaction Scheme 5.1, the succinic anhydride modification of PVA and the esterification of succinic acid, are known to be thermodynamically limited [154, 155].

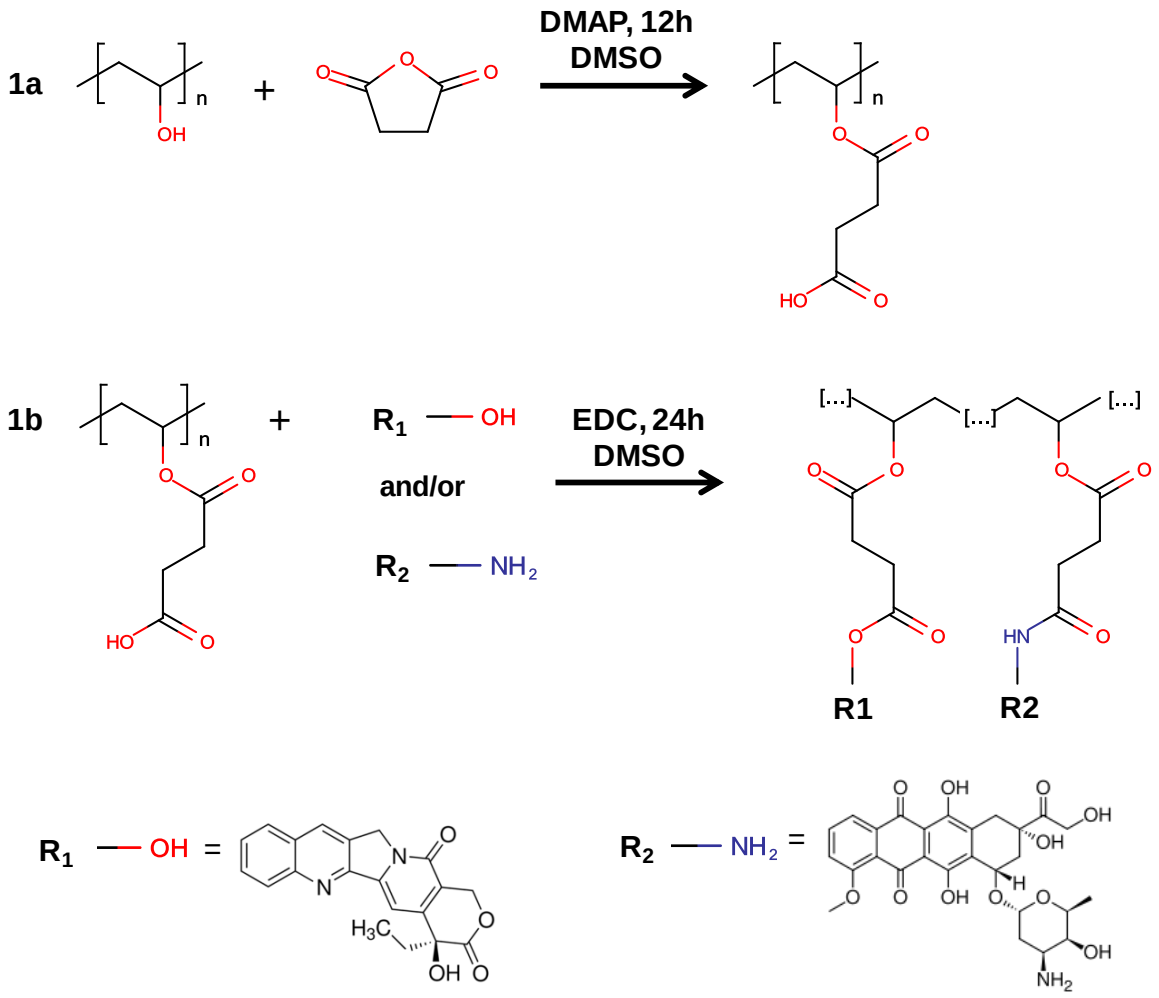

Reaction Scheme 5.1. Reactions utilized for incorporation of DOX and/or CPT on PVA.

Reaction 1a activates PVA hydroxyl groups with succinic anhydride to form EDC-reactive carboxylic acid side chains. Reaction 1b shows further conjugation to nucleophilic drugs (designated as R_1-OH or R_2-NH_2), with either hydroxyl or amine moieties. Reaction Scheme 5.1 was utilized for the synthesis of CPT-PVA, DOX-PVA, and CPT-PVA-DOX.

In order to assess the impact of polymer conjugation on drug activity, initial studies evaluated the *in vitro* cancer cell growth inhibition of CPT-PVA and DOX-PVA. MTT cytotoxicity assays which were used to evaluate free drug activities in Chapter 3 were also applied to the polymer-drug conjugates. As seen in Figure 5.1, both PVA-drug conjugates were active at inhibiting BT-474 cancer cell growth. D_{50} concentrations of DOX-PVA and CPT-PVA were 1.5 μM DOX and 14 μM CPT, respectively. In comparison, D_{50} concentrations of free DOX and CPT reported in Sections 3.2 and 3.6 were 0.3 μM and 100 μM, respectively; hence, conjugation to PVA reduced activity of DOX, whereas it enhanced activity of CPT. The proposed cause of these shifts in drug activities are reduced intracellular availability of DOX, but improved intracellular concentrations of CPT, and these effects are investigated in Section 5.3.

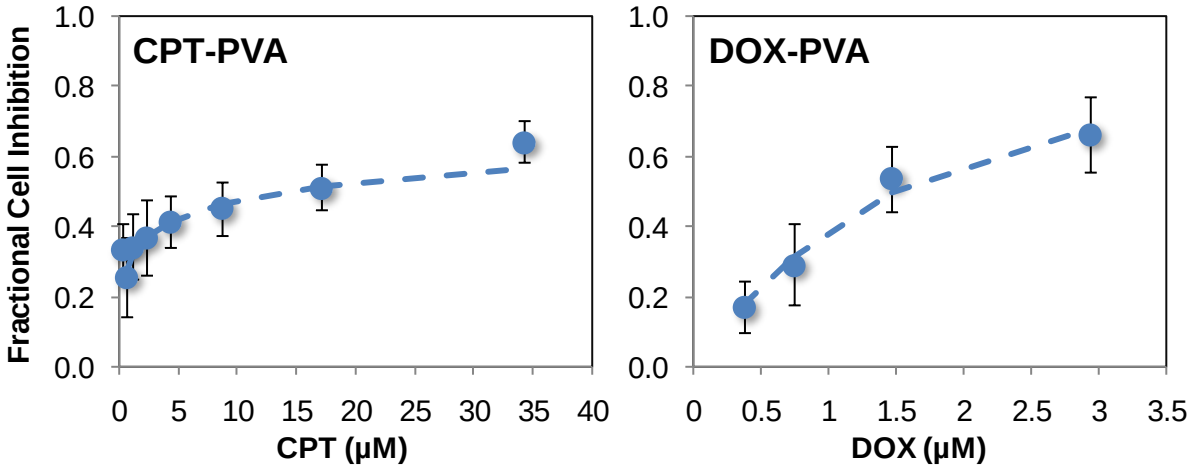

Figure 5.1. Cell inhibitory effects of CPT-PVA or DOX-PVA.

Cell inhibition of human breast cancer cell line BT-474 in the presence of CPT-PVA (left) or DOX-PVA (right). Cells were incubated with each polymer-drug conjugate for 72 hrs, then subsequently analyzed via MTT assay. Data expressed as mean ± SD (n≥12). Dashed lines represent dose-effect curves fit to experimental data using Chou and Talalay's median-effect model. D_{50} concentrations determined from the median-effect model are 1.5 ± 0.9 μM DOX (R^2=0.99) and 14 ± 0.9 μM CPT (R^2=0.97) for DOX-PVA and CPT-PVA, respectively.

After establishing that CPT-PVA and DOX-PVA are still active at inhibiting cancer cell growth, the two single-drug vehicles were simultaneously exposed to cancer cells at various ratios to see if CPT+DOX synergy was also preserved in the polymer-bound form. Combination interactions were evaluated and quantified utilizing the CI method (Section 2.3). As a reminder, free CPT and DOX were demonstrated in Section 3.6 to synergistically inhibit BT-474 cancer cell growth at R >0.1 M:M CPT:DOX, with the greatest synergy occurring at R > 2. Figure 5.2a-bshows that the same synergistic ratios hold true for the PVA-bound drugs; for R > 2.3, CI values were found to be « 1. The anticancer activities of single drug-conjugates which comprise the combinations are also seen in Figure 5.2a-b, and verifies that the combination of CPT-PVA + DOX-PVA is indeed more potent at inhibiting cancer cell proliferation than either of the individual constituents.

To determine whether drug synergy could be conserved in a single nano-vehicle rather than two separate entities, both CPT and DOX were conjugated to the same PVA polymer. The motivation behind these studies is that only multi-drug incorporated vehicles will ensure simultaneous drug exposure to tumors and be able to capture the combination's potency that is easily found *in vitro*. CPT-PVA-DOX was also synthesized via Reaction Scheme 5.1, where CPT was first made to react with PVA for 2 hours, followed by the addition of fresh EDC and DOX for 30 minutes. This synthesis resulted in the conjugation of CPT and DOX in the molar ratio of R = 1.5 (0.015 mol% CPT and 0.010 mol% DOX), which falls within the synergistic range (R > 0.1) of the free drugs (Figure 3.8). The anticancer activity of CPT-PVA-DOX conjugates against BT-474 cancer cell growth was evaluated via MTT

cytotoxicity assays, and compared to the anticancer activities of CPT-PVA and DOX-PVA. As seen in Figure 5.2c-d, CPT-PVA-DOX exhibited more than double the potency of either CPT-PVA or DOX-PVA alone. These studies suggest that CPT and DOX synergy can be conserved upon polymer conjugation, provided that the polymer-bound drugs are still active and that the two drugs are combined in optimal ratios.

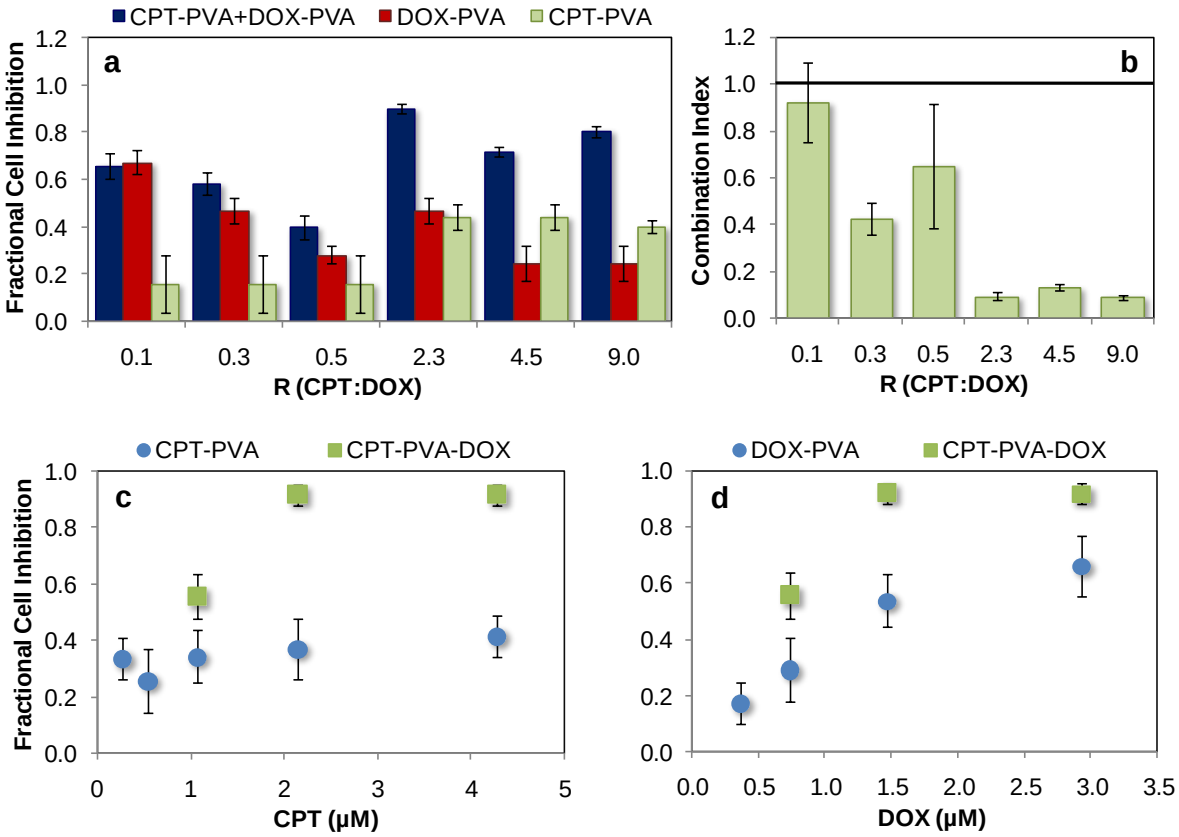

Figure 5.2. Anticancer activity of CPT-PVA + DOX-PVA and CPT-PVA-DOX.

(a) Cell inhibition of human breast cancer cell line BT-474 treated with combinations of CPT-PVA and DOX-PVA at various molar ratios (blue, left bars). Single PVA-conjugate treatments of DOX-PVA (red, middle bars) and CPT-PVA (green, right bars) at concentrations which make-up the combination are juxtaposed for direct comparison. Drug concentrations (μM) of CPT and DOX respectively corresponding to each R ratio were: 0.1 (0.53, 5.34), 0.3 (0.53,1.89), 0.5 (0.53,1.07), 2.2 (4.27, 1.90), 4.5 (4.27,0.95), and 9.0 (8.54,0.95). Data is represented as mean ± SD (n=6). (b) CI values calculated for CPT-PVA and DOX-PVA combinations seen in (a). BT-474 cell inhibition in the presence of CPT-PVA-DOX conjugates (squares) are compared to that of (c) CPT-PVA alone (circles) or (d) DOX-PVA alone (circles). Cells were incubated with formulations for 72 hours, and assessed for cell viability utilizing the MTT cytotoxicity assay. Data is reported as mean ± SD (n≥6).

5.3. CPT- and DOX- conjugated to HA

While CPT and DOX co-conjugated to PVA showed promising efficacy, PVA is not biodegradable *in vivo* and may elicit more treatment-related toxicities. Furthermore, the molecular weight of PVA utilized in Section 5.2. may not be suitable for *in vivo* purposes since polymers ≤ 10 kDa are rapidly cleared from systemic circulation [156, 157]. Rather, polymers of 50 kDa MW or higher have been shown to effectively accumulate in tumor tissue due to their renal retention and the EPR effect [148, 158, 159]. Hence, to assess the therapeutic potential of CPT and DOX co-delivery with a more clinically relevant polymer, the drugs were conjugated to the biocompatible, biodegradable, and larger (250 kDa) biopolymer hyaluronic acid (HA). HA was chosen not just for its biocompatibility, but also for its specificity for surface marker CD44, which is over-expressed on many cancer cells [160-162].

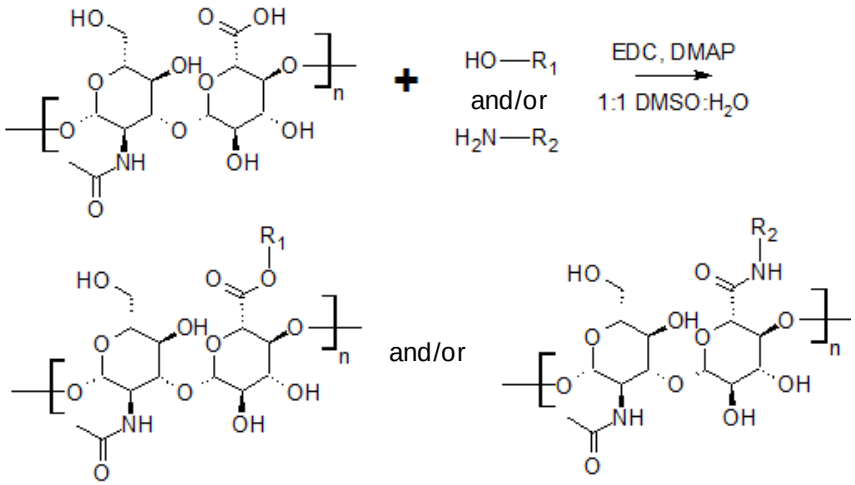

Reaction Scheme 5.2. Reactions utilized for incorporation of CPT and/or DOX on HA.

CPT- and DOX-conjugation to HA occurs via single-step reaction which involves nucleophilic acyl substitution. CPT-conjugation results from ester formation, and DOX-conjugation occurs from both aminolysis and ester formation with the glucoronic acid monomers present on HA. Either aminolysis or ester formation occurs with DOX-conjugation since DOX contains both free amine and hydroxyl moieties. In either case, the same reactants are utilized. Carboxylic acid moieties are activated with EDC and DMAP to catalyze conjugation to nucleophilic drugs (designated as R_1 and R_2), containing either hydroxyl or amine moieties. R_1 and R_2 correspond to the same groups in Reaction Scheme 5.1.

CPT and DOX were conjugated to HA (Creative PEGWorks; Winston Salem, NC, USA) via similar chemistry utilized for PVA conjugation, nucleophilic acyl substitution. However, as seen in Reaction Scheme 5.2, only a one-step synthesis was needed due to the naturally-occurring carboxylic acid moieties present in the D-glucoronic acid sugar. Specifically, the carboxylic acid moieties of HA were conjugated to CPT via ester formation [163] and to DOX via both ester formation and aminolysis [164]. For all reactions, 100 mg of HA was dissolved in a 10 mL mixture of DMSO/water (1:1 by volume) under stirring and slight heating (40˚C). DMAP and EDC were added at a molar ratio of 0.75:1 relative to HA monomers, and were allowed to activate the polymer for 1 hour under stirring. To synthesize CPT-conjugated HA (CPT-HA), CPT was slowly added to the reaction mixture at a molar ratio of 0.4:1 CPT:HA. In the case of DOX-conjugated HA (DOX-HA), DOX was dissolved in the reaction mixture in a molar ratio of 0.2:1 DOX:HA. The reactions proceeded under slight heating (40˚C) for 3 days. Afterwards, CPT-HA and DOX-HA were separated from unreacted free drugs, EDC and DMAP via size exclusion chromatography through Sephadex G-25 PD-10 desalting columns (5000 MWCO) equilibrated in phosphate buffered saline (PBS, pH 7.4). The reaction products were further concentrated in 0.5 mL centrifugal filter tubes (3000 NMWL) for a minimum of three runs, each at 16,000 g for 15 min. For the final centrifuge run, an additional 0.4 mL of PBS was added. Concentrations of CPT and DOX were determined by the same methods reported for the PVA-conjugates. In both CPT-HA and DOX-HA formulations, 1.6 mol% drug:HA was achieved. The drug encapsulation in CPT-HA-DOX was 5.9 mol% CPT and 1.8 mol% DOX.

To evaluate the impact of HA conjugation on drug activity, cancer cell viability post-incubation with CPT-HA or DOX-HA was analyzed via MTT cytotoxicity assays. As seen in Figure 5.3, conjugation to HA reduced the activity of DOX compared to free drug, whereas the activity of CPT-HA was reduced only slightly compared to that of free CPT. D_{50}concentrations of DOX-HA and CPT-HA were 95.8 ± 47.5 μM DOX and 399.5± 34.5 μM CPT, respectively. These correspond to a 322-fold and 4-fold augmentation, respectively, in D_{50} compared the free DOX and free CPT activities, and reflect the qualitative trends seen in Figure 5.3. These differences in HA-bound and free drug activities are similar to the results seen for PVA-conjugates in Section 5.2. This is expected since the chemical conjugations and linkers are the same in both PVA- and HA-conjugates. In the case of PVA-conjugates, however, CPT-PVA exhibited greater efficacy than free CPT, and this may be attributed to inherent differences in polymeric properties.

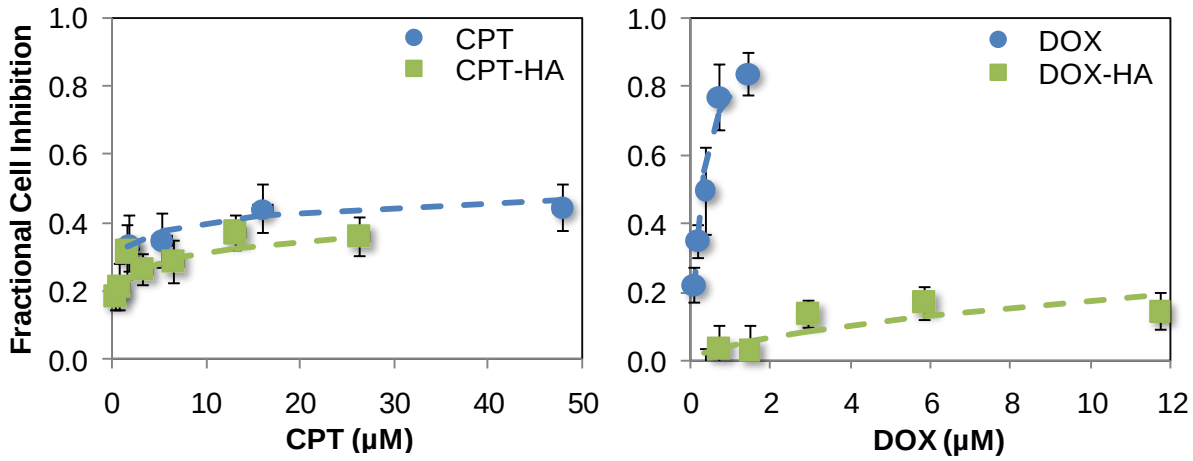

Figure 5.3. Cell inhibitory effects of CPT-HA or DOX-HA.

Cell inhibition of human breast cancer cell line BT-474 in the presence of CPT in free solution (circles) or CPT-HA (squares) (left) or DOX in free solution (circles) or DOX-HA (squares) (right). Cells were incubated with each drug for 72 hrs, then analyzed via MTT assay. Data expressed as mean ± SD (n≥8). Dashed lines represent fits to the ME model. D_{50} and R^2 corresponding to ME fits are (399.5 ± 34.5 μM CPT, R^2=0.99) for CPT-HA and (95.8 ± 47.5 μM DOX, R^2=0.82) for DOX-HA.

Internalization and release studies were performed to investigate the origins of shifts in drug activity upon HA conjugation. First, internalization of the carrier itself, HA, without drug was investigated via confocal laser scanning microscopy (Section 2.4). These studies provided insight as to whether drugs must first completely hydrolyze from the polymer extracellularly prior to cell internalization or if the HA-drug entity is capable of entering cancer cells as a whole. BT-474 cells were incubated with fluorescein-conjugated HA (Creative PEGworks; Winston Salem, NC, USA) for 6 hrs at 37˚C to mimic physiological conditions or 4˚C to prevent active endocytosis. Fluorescence was quantified in averaged 10 μm z-stacks, and was normalized to cell count per image. Results in Figure 5.4a show significantly more HA fluorescence, and hence cellular uptake, when exposed to cells at 37˚C as opposed to 4˚C. Incubation at 4˚C prevents energy-intensive internalization mechanisms, and resulted in a four-fold reduction of intracellular HA. Thus, cellular uptake of HA occurs via active internalization mechanisms, as confirmed by lack of internalization at 4˚C.

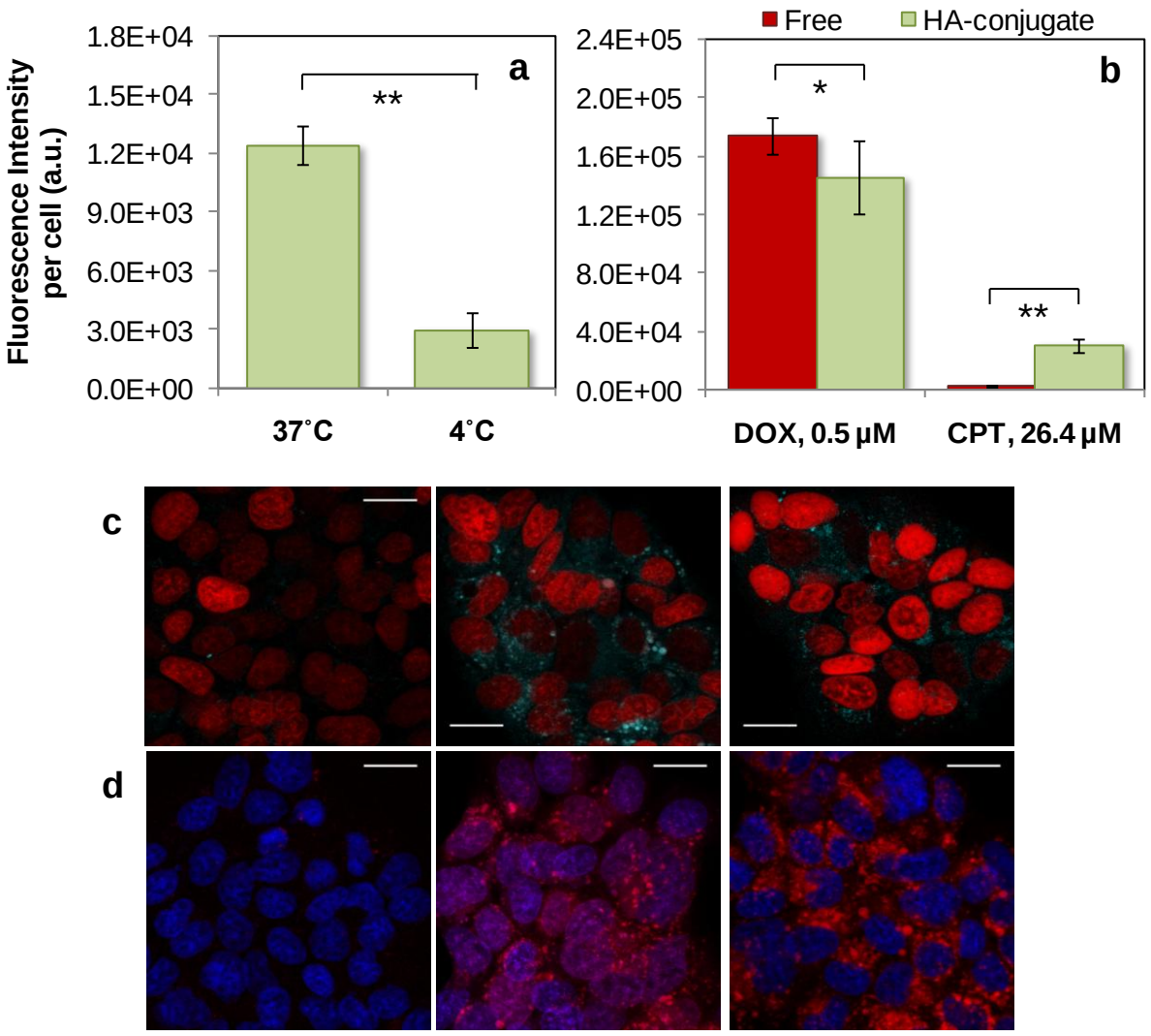

Figure 5.4. Internalization of HA, CPT-HA, or DOX-HA.

(a) Quantitative fluorescence of fluorescein-conjugated HA present in BT-474 cells after 6 hours of incubation at 37˚C or 4˚C and 5% CO_2. (b) Quantitative fluorescence of DOX or CPT in free solution (red, left bars) or as a HA-conjugate (green, right bars) present in BT-474 cells after 24 hours of incubation at 37˚C and 5% CO_2. Data expressed as mean ± SD (n=3). (c) Representative images of CPT (cyan) internalization when incubated as a free solution (middle) or as a HA-conjugate (right). Untreated cells are demonstrated on the left. Cells were labeled with DRAQ5 nuclear dye (red). (d) Representative images of DOX (red) internalization when incubated as a free solution (middle) or as a HA-conjugate (right). Untreated cells are on the left. Cells were labeled with Hoechst nuclear dye (blue). Scale bars = 20 µm.

After verification that the polymeric carrier is readily internalized by BT-474 cells, uptake of polymer-bound drugs were next investigated by visualizing the natively fluorescent drugs via confocal laser scanning microscopy. These studies illustrate the effect of polymer-conjugation on intracellular drug concentrations. Cells were exposed to the same drug concentration, the free drug D_{50}, of either the free drug solution or the HA-conjugate form for 24 hrs at 37˚C and 5% CO_2. CPT-HA exhibited significantly enhanced uptake compared to free CPT (Figure 5.4b), possibly due to its enhanced water solubility upon conjugation to HA. On the other hand, uptake of DOX-HA was only slightly less than that of free DOX (Figure 5.4b). Subsequent intracellular distribution of DOX-HA, however, was significantly different compared to that of free DOX (Figure 5.4c). HA-bound DOX was localized mostly in punctate spots surrounding nuclei, whereas free DOX was more diffuse and co-localized with cell nuclei. While free DOX is sufficiently small to permeate across the cell and nuclear membrane, DOX-HA is likely internalized via endocytosis and localized in endosomes.

Drug release from the polymer also plays a considerable role in intracellular drug distribution. Once internalized, DOX must release from the polymer via amide or ester hydrolysis and escape from the endosomes before reaching its nuclear target, top II. Drug release profiles (Figure 5.5) indicate slow DOX release surmounting to only 25% after 72 hours, and a fast CPT release with near complete hydrolysis within 24 hours. The difference in drug release rates may be attributed to greater stability of amide bonds compared to ester bonds in aqueous conditions. This alternate internalization pathway, slow drug release, and reduced

concentrations of free intracellular DOX may cause a time-lag between DOX internalization and activity, and may explain reduced cytotoxicity upon HA-conjugation. It is likely that the same shifts in DOX internalization and availability to top II occurs with PVA-conjugates, as DOX activity is also reduced upon PVA-conjugation. An exponential fit to the DOX release profile from DOX-HA reveals a half-life of 254 hours, and suggests that complete DOX release will be achieved on the order of 50-100 days. Therefore, in order to realize the full therapeutic potential of DOX-HA, drug incubations for longer time-periods than are reasonably utilized may be warranted.

HA-bound CPT, on the other hand, improved intracellular CPT concentrations with no hydrolysis limitations; nearly 95% was released after 24 hours. Despite this, CPT-HA was less active compared to free CPT, and suggests that HA-conjugation restricts CPT's ability to interact with its intracellular target, top I. It is likely that released CPT remains confined within endosomes or lysosomes, and results in reduced anticancer efficacy. On the contrary, PVA-bound CPT was more active at inhibiting cancer cell growth than free CPT, as seen in Section 5.2. Since the conjugation chemistry and linkers are similar for both HA- and PVA-bound CPT, CPT should release from both polymers at the same rates. Hence, it is probable that PVA-conjugation either improves CPT-internalization or its ability to interact with top I, compared to HA-conjugation. These enhancements further potentiate CPT's cancer cell inhibition when conjugated to PVA.

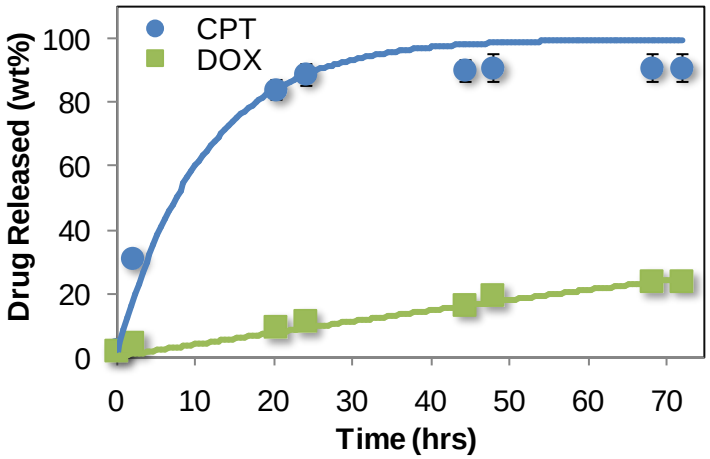

Figure 5.5. CPT or DOX release from HA-conjugates.

Release of CPT (circles) or DOX (squares) from CPT-HA or DOX-HA, respectively, determined as wt% of initial drug conjugated to HA. Lines represent exponential fits to release profiles ($t_{1/2,R}$= 11 hrs, $t_{1/2,R}$ = 254 hrs for CPT and DOX, respectively). Data represents mean ± SD (n=3).

5.4. Synergy of CPT- and DOX-conjugated HA

After confirming that CPT-HA and DOX-HA are readily internalized by cancer cells and can inhibit their growth, CPT-HA and DOX-HA were mixed at various molar ratios and incubated with BT-474 cells, followed by CI analysis. The combination inhibited more cancer cell growth than either CPT-HA or DOX-HA alone (Figure 5.6a). The CI of the mixed conjugates (Figure 5.6b) was less than 1 for $1 < R < 9$ CPT:DOX, indicating that CPT-HA and DOX-HA were indeed synergistic at the same ratios that free CPT and DOX elicited synergy (Figure 3.8c).

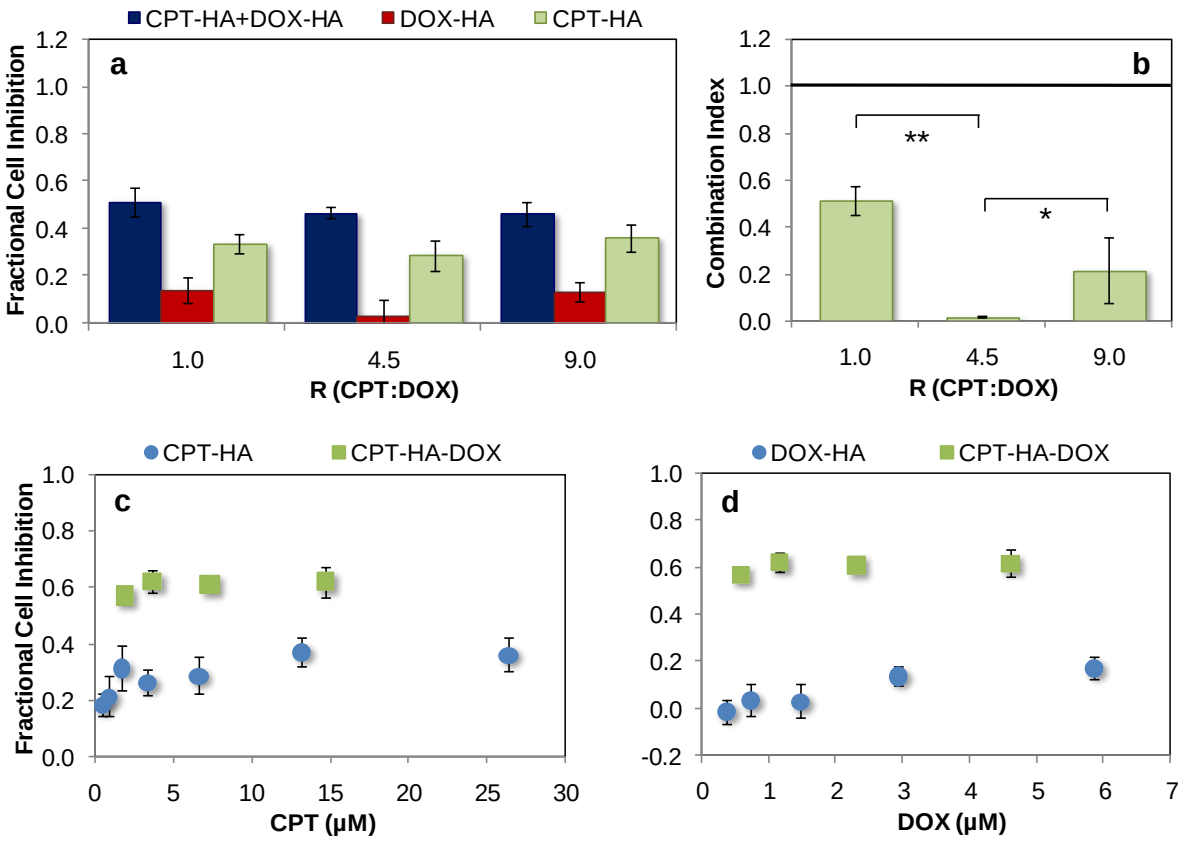

Figure 5.6. Anticancer activity of CPT-HA + DOX-HA and CPT-HA-DOX.

(a) Cell inhibition of human breast cancer cell line BT-474 treated with combinations of CPT-HA and DOX-HA at various molar ratios (blue, left bars). Single HA-conjugate treatments of DOX-HA (red, middle bars) and CPT-HA (green, right bars) at concentrations which make-up the combination are juxtaposed for direct comparison. Drug concentrations of CPT and DOX respectively in μM: 1 (11.7, 11.7), 4.5 (6.6, 1.5), 9 (26.4, 2.10), (b) CI values calculated for the CPT-HA and DOX-HA combinations shown in (a). (c) Cell inhibition of in the presence of CPT-HA (circles) or CPT-HA-DOX conjugates (squares). (d) Comparison of the cell inhibition of DOX-HA (circles) and CPT-HA-DOX conjugates of R = 3.2 CPT:DOX (squares). Cells were incubated with formulations for 72 hours, and assessed for cell viability utilizing the MTT cytotoxicity assay. Data is reported as mean ± SD (n≥6).

It should be noted that although CPT and DOX undergo distinct release profiles from HA (Figure 5.5), this differential release does not compromise their synergy. On the contrary, HA-conjugation may promote the pair's synergistic interactions against cancer cell proliferation. Whereas CPT and DOX in free solution only exhibit additive cancer cell kill at R = 1 (Figure 3.8c), their HA-bound

counterpart is synergistic (Figure 5.6b). One hypothesis for this finding is that slower DOX release causes an effective free R greater than that bound to the polymer. Thus, the intracellular free combination released from the polymer results in R > 2, meeting the synergistic requirement for CPT and DOX. Free CPT and DOX are more synergistic at greater R values (Figure 3.8c), with no apparent upper limit. In the case of polymer-bound CPT and DOX, however, there appears to be an optimal polymer-bound R, as indicated by a greater CI for R = 9 compared to R = 4.5. Although this finding is not completely understood, one possible explanation is that a minimum DOX-HA concentration is required in order for the concentration of released DOX to be therapeutically active and synergistic with CPT. Because only 25% of DOX is released from DOX-HA over a period of 72 hours, exposure of cancer cells to larger HA-bound R can significantly reduce the concentration of free DOX exposed to cancer cells. It may be possible that a threshold DOX concentration is required for synergistic interactions with CPT. Further studies will verify whether threshold drug concentrations exist for synergistic drug interactions. These initial results, however, demonstrate that CPT-HA and DOX-HA can deliver synergistic CPT and DOX ratios to cancer cells, despite the administration of a lower, bulk polymer-bound R.

CPT and DOX were then co-conjugated to HA to evaluate if potent cancer cell kill could be maintained when co-delivered in the same nano-vehicle. Without inclusion of both drugs in a single vehicle, the pair will undergo uncoordinated pharmacokinetics, and the tumor will not be exposed to the optimal drug ratio which maximizes potency. In the case of our particular chemotherapy combination, CPT

exhibits a distribution half life of 71-90 minutes in humans [15], whereas that of DOX is much shorter, approximately 4 minutes [14]. Therefore, it is proposed that co-conjugation to HA will ensure simultaneous arrival in tumors at the prescribed, synergistic ratio, and provide superior therapeutic effects compared to free drug administration. To synthesize CPT- and DOX-conjugated HA (CPT-HA-DOX), CPT was first conjugated to HA for 3 days via Reaction Scheme 5.2, followed by the subsequent reaction of DOX to CPT-HA for another 3 days. For the purpose of demonstrating a synergistic drug-loaded carrier, HA carrying a molar ratio of R = 3.2 CPT:DOX was investigated. The content of CPT and DOX was determined via UV-Vis spectroscopy to be 5.9 mol% and 1.8 mol%, respectively. *In vitro* cytotoxicity studies show that CPT-HA-DOX inhibited more cancer cell growth than either CPT-HA (Figure 5.6c) or DOX-HA (Figure 5.6d) alone. Cell inhibition studies performed with mixed HA-conjugates and drugs co-conjugated to HA reveal that polymer-conjugation preserved synergy between CPT and DOX. While both formulations conserved the drug pair's potency, only the latter can ensure simultaneous exposure to tumor cells, and can provide a means to capture the *in vitro* antitumor efficacy *in vivo*, as well.

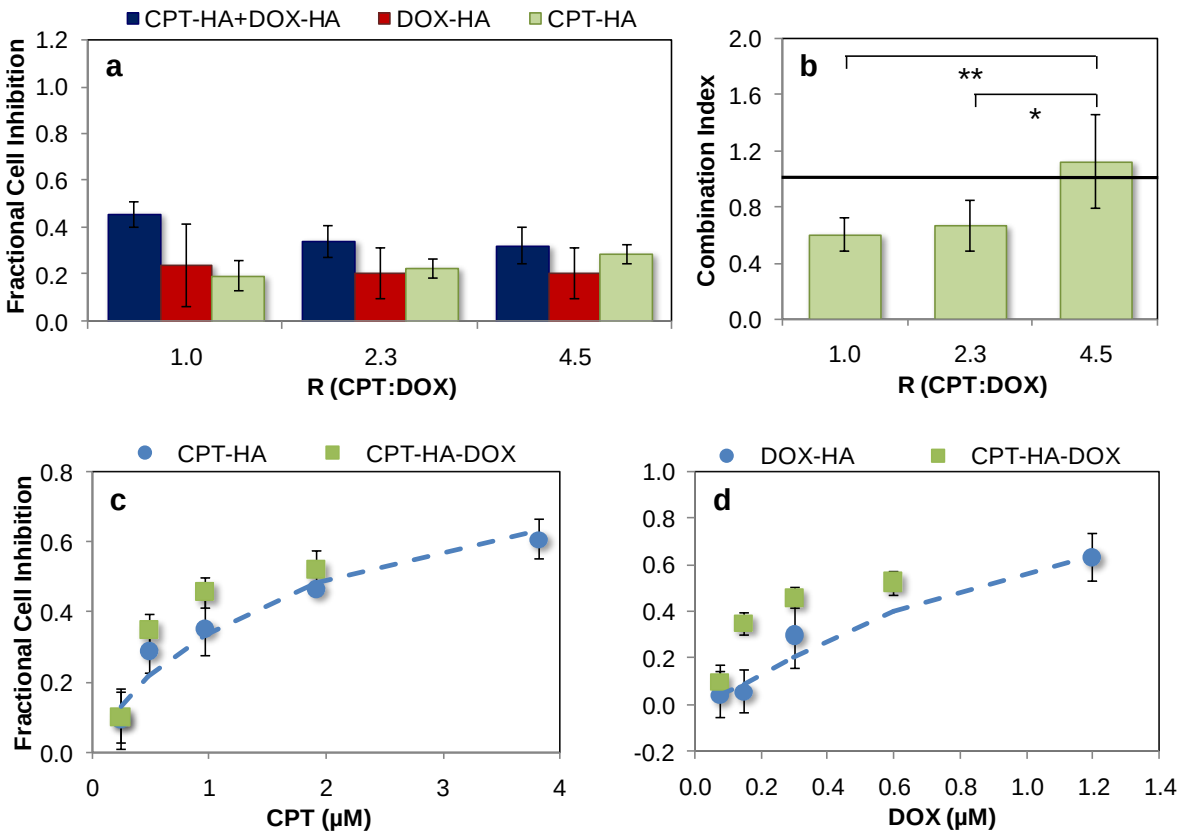

Figure 5.7. Activity of CPT-HA + DOX-HA and CPT-DOX-HA against murine 4T1 breast carcinoma cells.

(a) The cell inhibition of metastatic murine breast cancer cell line 4T1 treated with combinations of CPT-HA and DOX-HA at various molar ratios (blue, left bars). Single drug treatments of DOX (red, middle) and CPT (green, right) at concentrations which make-up the combination are juxtaposed for direct comparison. CPT and DOX concentrations (μM), respectively, which composed each ratio (R, CPT:DOX) were: 1.0 (0.30, 0.30), 2.3 (0.34, 0.15), 4.5 (0.68, 0.15). (b) CI values calculated for CPT-HA and DOX-HA combinations in (a). (c) Cell inhibition in the presence of CPT-HA (circles) or CPT-HA-DOX conjugates (squares). (d) Comparison of the cell inhibition of DOX-HA (circles) and CPT-HA-DOX conjugates of R = 3.2 CPT:DOX (squares). Dashed lines represent fits to the ME model. Cells were incubated with formulations for 48 hours, and assessed for cell viability utilizing the MTT cytotoxicity assay. Data is reported as mean ± SD (n≥4).

5.5. *In vivo* antitumor efficacy of CPT-HA-DOX

An orthotopic 4T1 breast cancer mouse model in BALB/c mice was utilized to assess the *in vivo* anticancer efficacy of CPT-HA-DOX. A 4T1 model was chosen for its robust tumor formation in mice [165], and to challenge the synergistic conjugate

with a highly metastatic, aggressive cancer [166]. While all *in vitro* studies focused on the cell inhibition of BT-474 human breast cancer cells, CPT and DOX synergy was also verified in 4T1 cells and occurred at the same ratios as BT-474 (Figure 3.9 and Figure 5.7). Mice were administered i.v. with designated formulations every other day for a total of 5 treatments (Days 3, 5, 7, 9, 11). Treatments consisted of either CPT-HA-DOX or free CPT+DOX in equivalent drug doses of 2 mg/kg CPT and 1.05 mg/kg DOX. To prepare the free drug formulation, CPT was first dissolved in 10 vol% Tween-80 in 0.9 wt/vol% NaCl to solubilize the highly hydrophobic drug. DOX was directly dissolved in 0.9 wt/vol% NaCl, and was subsequently mixed with the CPT solution. CPT-HA-DOX was freshly prepared in 0.9% NaCl prior to injections. For comparison, untreated tumor-bearing mice were observed as controls. Results in Figure 5.8a show as high as 70% tumor volume reduction achieved by the free drug combination, and 50% tumor reduction achieved with the co-conjugated polymer relative to control. This was surprising, as the free drug administration was projected to elicit lower therapeutic efficacy due to uncoordinated accumulation in tumors. However, since CPT+DOX synergistically inhibit cancer cell growth for a wide range of ratios, the antitumor activity of this particular pair may not be severely impacted by the uncoordinated drug pharmacokinetics when administered as a free solution. Thus, both HA-bound and free CPT+DOX elicited compelling therapeutic efficacies.

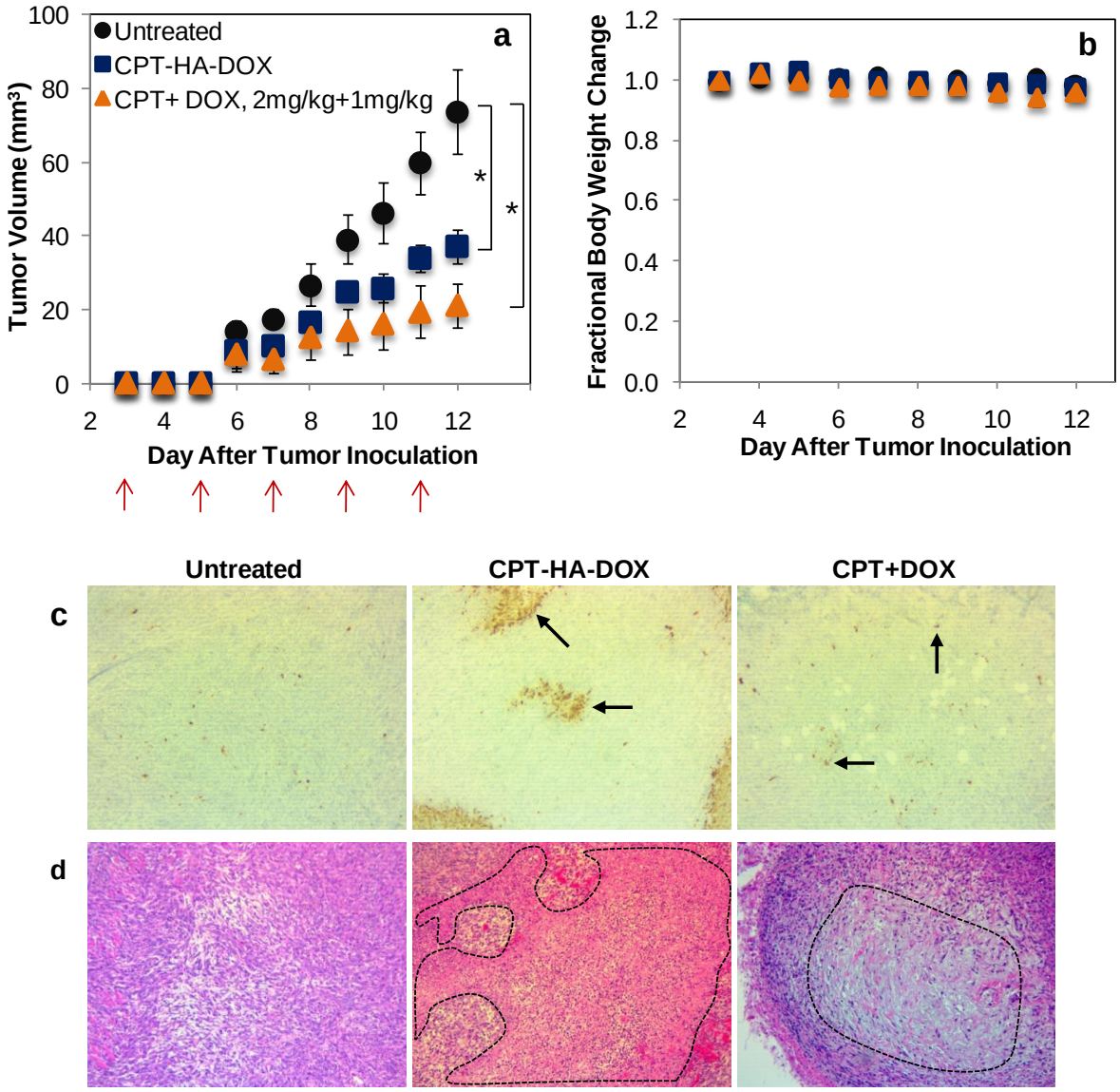

Figure 5.8. Tumor growth inhibition of CPT-HA-DOX or CPT+DOX.

(a) Tumor growth of mice bearing 4T1 breast cancer tumors, without treatment (circles), with IV injections of CPT-HA-DOX (squares), or free CPT+DOX in 0.9% saline (triangles). Mice were injected i.v. with CPT-HA-DOX or free CPT+DOX, at drug-equivalent concentrations of 1.05 mg/kg DOX and 2 mg/kg CPT. Red arrows indicate treatment days. (b) Change in body weight of control mice (circles), CPT-HA-DOX-treated mice (squares), or CPT + DOX-treated mice (triangles). Data is reported as mean ± SE (n≥8). (c) Immunohistochemistry analysis of excised control tumors (left), tumors treated with CPT-HA-DOX (middle) or free CPT+DOX (right) stained for cleaved caspase-3 (apoptosis indicator). Black arrows indicate representative stained apoptotic nuclei. (d) Histology analysis of tumors treated with H&E. Circled areas represent necrotic tissue. All images were taken at 100X magnification and are representative of each group (n=3).

Caspase 3 immunohistochemistry of tumor sections post-treatment was performed to further assess antitumor efficacy of CPT and DOX formulations. Despite greater gross tumor reduction in mice treated with free CPT+DOX, more apoptotic cells were found in CPT-HA-DOX-treated tumors (Figure 5.8c). Furthermore, H&E staining shows more necrosis in mice treated with CPT-HA-DOX compared to those treated with free CPT+DOX, as indicated by the greater occurrence of pyknotic (smaller) or missing nuclei (absence of purple staining) and overall pink rather than purple hue (Figure 5.8d). Histology analyses also suggest that, while macroscopic measurements indicate that free CPT+DOX mixture is more effective in reducing tumor size, CPT-HA-DOX was more effective in inducing both necrosis- and apoptosis-induced cell death. Whereas free CPT+DOX attacks tumor cells predominantly via apoptotic mechanisms, CPT-HA-DOX exploits both potent mechanisms. The implications of these two types of cell death for cancer therapies are unclear. Chemotherapy drugs commonly initiate cancer cell death via apoptosis, but there are many potential benefits in necrotic-inducing agents [167, 168]. In contrast to apoptosis, necrosis is a rapid cell death mechanism which does not require a complex cascade of biochemical events [168]. Necrosis is also indiscriminatory in that the affected cells need not be in a certain cycle phase or express certain genes, and once initiated, immune cells are recruited in an inflammatory response to further attack the tumor [167]. Hence, necrotic-inducing agents can result in more rapid and vigorous cancer cell death compared to apoptotic-inducing drugs. Our studies suggest that CPT-HA-DOX bears great potential for improving tumor growth inhibition compared to free CPT+DOX

administration, due to the added capability of necrosis-induced cancer cell death. Thus, although the gross tumor inhibition of CPT-HA-DOX was less than that of the free drugs, optimization of the current CPT-HA-DOX formulation may enhance therapeutic efficacy. Other factors that were not investigated in this study, but could be implemented to improve anticancer potency, are described in Chapter 6.

Despite room for formulation optimization, particular significance of our findings is drawn to the low doses utilized for these immense therapeutic effects, 2 mg/kg CPT and 1.05 mg/kg DOX. Previous literature reports of murine tumor models treated with intravenous free drug solutions show that 2 mg/kg of free DOX by itself is incapable of significantly reducing tumor volume [169, 170], and that 1.5 mg/kg free CPT administered alone results in 50% tumor reduction albeit with high variability [171]. In comparison, the studies reported here have identified a potent chemotherapy combination with high activity at low doses, and that HA-conjugation of synergistic ratios of CPT and DOX preserves the combination's potency *in vivo*.

5.6. CPT-HA-DOX tolerability *in vivo*

Apart from antitumor efficacy, tolerability of the treatment is equally important for clinical applicability. To translate a powerful cytotoxic drug pair to a therapeutic, not only is accumulation in tumor tissue required, but also minimal exposure to healthy organs. This feat can be mediated with HA-conjugation. Here, the delivery vehicle itself targets tumor tissue, and additional targeting ligands are not needed. CD44, a transmembrane glycoprotein overexpressed in many cancer types and in low expression in other tissues, is a principal receptor of HA; thus, drug

conjugation to HA can shift accumulation in tumors rather than healthy tissue [172-174]. The natural abundance of HA in the human body also renders it biocompatible and biodegradable.

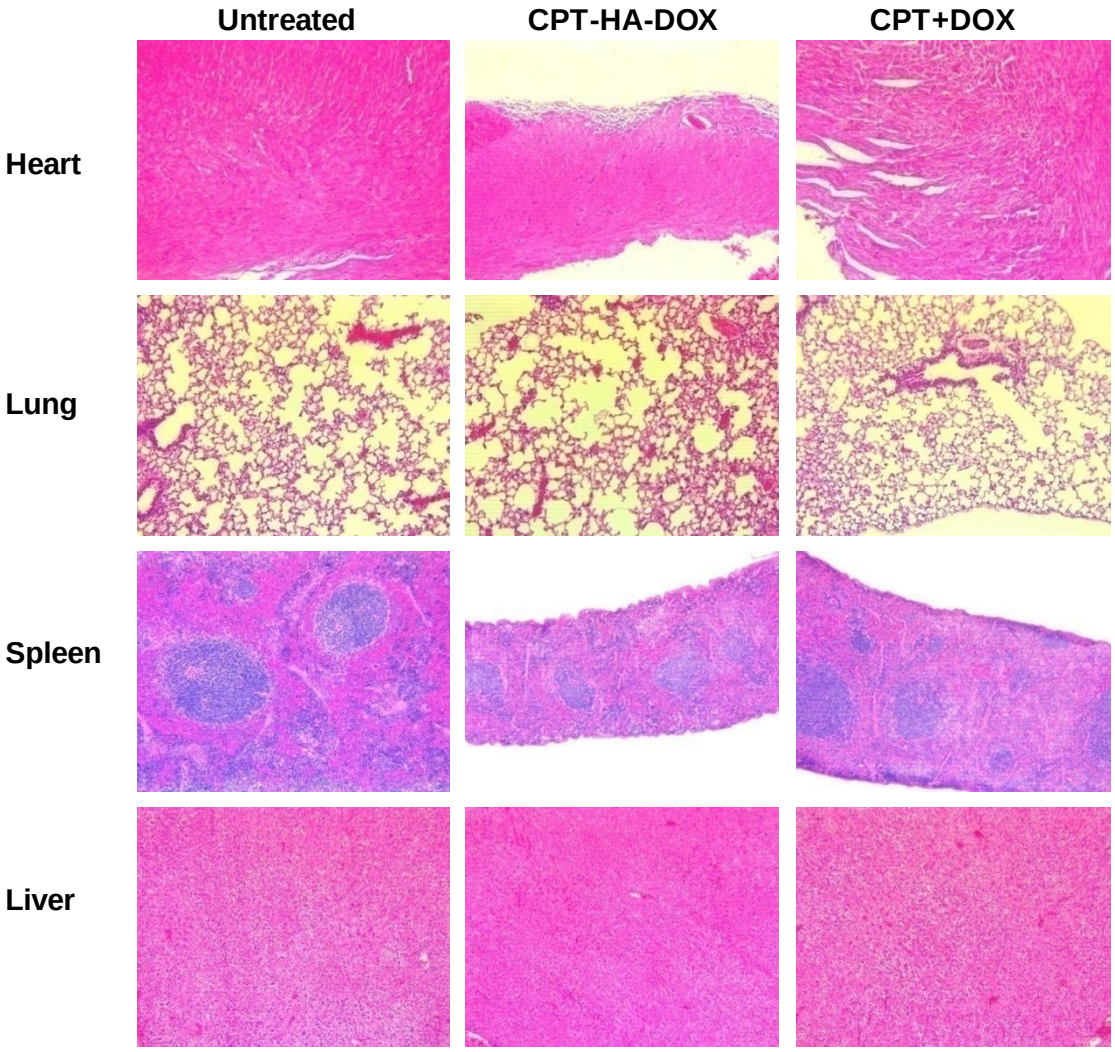

Figure 5.9. Histology analysis of excised tissues post-treatments.

Organs excised from control mice (left), mice treated with CPT-HA-DOX (middle), or CPT+DOX (right), and stained with H&E to assess formulation toxicity. Images were acquired at 100x magnification and are representative of each group (n=3).

In both CPT-HA-DOX and CPT+DOX treatments, negligible body weight change was observed (Figure 5.8b), and suggested no immediate toxicity concerns. To more extensively evaluate formulation toxicity, histology analyses of essential organs post-treatment were conducted. Lung, spleen, and liver organs in both CPT+DOX-treated and CPT-HA-DOX-treated mice showed no toxicity (Figure 5.9). Heart sections resected from CPT-HA-DOX-treated mice indicated mild inflammation. This may be explained by CD44 receptors and a large abundance of natural HA present in the heart [175]. Surprisingly, free solution CPT + DOX was also non-toxic to mice, with negligible body weight chances and no inflammation in the heart, lungs, liver, nor the spleen. The lack of chemotherapy toxicity may be attributed to the very low doses of CPT and DOX needed for synergistic tumor reduction. Collectively, negligible body weight changes and H&E analysis of essential organs suggest that both formulations were well-tolerated with no severe side effects.

While both CPT-HA-DOX and free CPT+DOX exhibited high therapeutic potential and minimal toxicity in mice, free solution combinations of top I and II inhibitors are notorious for inducing adverse side effects in humans. The most common repercussion of top I and II inhibitors, when administered as free drugs, is hematological toxicity [79, 81-83, 94, 176-180], and dose-limiting neutropenia has been reported to occur in as many as 50% of patients treated with top I and II poisons [83]. Polymer-conjugation to DOX, specifically DOX-HPMA, has already been shown to significantly reduce dose-limiting toxicities compared to free DOX [151], and is compelling evidence for the clinical use of polymer-bound drugs

compared to free drugs. Another advantage of the CPT+DOX combination administered here is the preferred cell kill of malignant cells over control endothelial cells, as demonstrated in Figure 3.9. By identifying optimal drug ratios which synergistically inhibit cancer cells and antagonistically affect healthy cells, it may be possible to administer low, non-toxic free drug doses of the combination, as demonstrated here. Conjugation of precise drug ratios to polymers ensures that this ratio is maintained in both tumor tissue and essential organs which cannot be avoided. Collectively, these findings suggest that CPT-HA-DOX has the potential of reducing life-threatening toxicities and improving therapeutic efficacy compared to free CPT+DOX, although additional studies are required for further assessment.

5.7. Summary of HA-conjugates for synergistic combinations delivery

Here, we developed plausible non-toxic methods for the delivery of the optimal ratios of top I and II inhibitors CPT and DOX identified in Chapter 3 which synergistically inhibit cancer cell growth. Due to the potent synergy between CPT and DOX, only low doses of each drug are required to significantly reduce tumor volumes in murine 4T1 models – doses which elicit no visible toxicity in healthy organs. Hence, free drug administration of the pair offers one method to elicit significant antitumor reduction. This is a remarkable finding, since free CPT elicits unpredictable side effects when administered at single drug therapeutic doses. By exploiting top I and top II poison collateral sensitivity, we have demonstrated a safe method to administer free CPT which is also therapeutically active. This finding alone highlights the power of combination chemotherapy.

HA-conjugation serves as another clinically translatable method for CPT and DOX administration, with the additional advantages of preserved synergistic drug ratios from the site of injection to tumor tissue, and enhanced tumor accumulation. This method can be broadly applied to various combination chemotherapies, since the conjugation chemistries are not specific to just top I and II inhibitors; the only prerequisite is the presence of nucleophilic moieties on the drug pair. HA co-conjugation can particularly be advantageous for combinations which elicit adverse effects in the free drug form, since it can direct the therapies to CD44+ tumors. Furthermore, precise ratios can be controlled via reactant concentrations, which will ensure the delivery of the most potent, synergistic ratio to tumors. This effect will be most impactful for chemotherapy combinations where synergistic interactions only occur for specific drug ratios.

Data was reprinted from Journal of Controlled Release, vol. 21, K.M. Camacho, S. Kumar, S. Menegatti, D.R. Vogus, A.C. Anselmo, S. Mitragotri, Synergistic antitumor activity of camptothecin–doxorubicin combinations and their conjugates with hyaluronic acid, 198-207, Copyright 2015, with permission from Elsevier.

Chapter 6

Impact of nano-carrier properties on therapeutic efficacy

6.1. Physical and chemical properties of nano-carriers

The previous two chapters focused on the development of two specific nano-vehicles for the co-encapsulation of synergistic chemotherapy pairs, with culminating evaluations of their *in vivo* efficacies. Along the path to their development, however, many fundamental studies were conducted to determine optimal physical and chemical properties for effective drug delivery. Tumor accumulation, nanoparticle internalization, drug release, and drug-target interactions must all occur in order for the carrier to be an effective drug vehicle. Because various nanoparticle properties can notably influence many or all of these factors, many literature efforts have focused on evaluating these interactions [50, 76, 124, 181-186]. Here, we summarize similar findings that were discovered during the development of polymer-drug conjugates and liposomes for multi-drug delivery. Specifically, polymer molecular weight, polymer-drug linkers, lipid membrane properties, particle stability, and ζ potential effects were assessed. Results reported here will unfold the impact of these particle parameters on combination chemotherapy efficacy.

6.2. Low molecular weight polymer-drug conjugates

Many literature reports demonstrate the superior tumor accumulation and plasma circulation of high molecular weight (~100 kDa) water-soluble polymers [148, 157-159], and for this reason, most biodegradable polymer-drug conjugates in clinical trials bear molecular weights >50 kDa [29, 187-189]. However, high overall tumor accumulation may not be enough to inhibit tumor growth. For example, micelles ranging between 30-100 nm have been found to equally penetrate highly permeable tumors in mice, but only sub-50 nm particles were found able to extravasate into tumor tissue with reduced vasculature and achieve greater tumor reduction [182, 190]. In another study, it was shown that low molecular weight polymers were more readily internalized by epithelial cells as compared to polymers greater than 80 kDa [191]; thus, high molecular weight polymers may impede conjugated drugs from reaching their intracellular targets. It is clear that carrier size governs drug distribution in tumor microenvironments, which further impacts drug activity. Therefore, although low molecular weight polymer-drug conjugates are less-explored, they may elicit significant therapeutic efficacy. We have previously demonstrated the tumor reduction capability of high molecular weight 250 kDa HA bound to CPT and DOX [192]. Here, we extend our approach to low molecular weight 10 kDa HA to investigate whether uncommonly utilized small MW polymers bear merit for improving *in vivo* efficacy of chemotherapy combinations.

The same reaction scheme used in Chapter 5 (Reaction Scheme 5.2) was employed to conjugate both CPT and DOX to 10 kDa HA. By varying reactant ratios, two CPT+DOX ratios were achieved: 7.5 and 2.8 CPT:DOX. The corresponding drug

incorporations were 14.4mol% CPT + 1.9mol% DOX for R=7.5, and 6.9mol% CPT+ 2.4 mol% DOX for R=2.8. It is noteworthy that the same chemistry and initial starting materials resulted in less than half as much CPT conjugation and hence a less synergistic ratio (R=3.2) in higher molecular weight 250 kDa HA; one possible reasoning is the reduced steric hindrance in smaller polymeric chains. Conjugation of chemotherapy drugs to polymers typically alters drug activity, as was evident in our previous study of 250kDa hyaluronic acid conjugated to CPT and DOX. However, drug activity should not be compromised so much as to entirely prevent its anticancer effects. Therefore, initial studies evaluated the *in vitro* cancer cell growth inhibition of 10 kDa CPT-HA-DOX.As seen in Figure 6.1, both R=2.8 and R=7.5 10 kDa CPT-HA-DOX inhibited more 4T1 mouse breast cancer cell growth than R=3.2 250 kDa HA, regardless of drug concentrations. D_{50} concentrations of the 10 kDa conjugates (0.50 μM CPT + 0.07 μM DOX for R=7.5 and 0.24 μM CPT + 0.09 μM DOX for R=2.8) were determined by fitting experimental data to the median-effect model, and are lower than those corresponding to the 250 kDa conjugates (5.8 μM CPT + 1.8 μM DOX). The D_{50} concentration of CPT is reduced as much as 24-times, and the DOX D_{50} dose is halved when the pair is exposed as a 10 kDa HA conjugate as opposed to a 250 kDa conjugate. This finding may be attributed to either the higher, more synergistic drug loading capabilities of the 10 kDa polymer, or due to a possible enhancement of cellular uptake with lower molecular weight polymers [193]. In either case, our studies indicate that low molecular weight polymers are capable of maintaining combination chemotherapy synergy, and are more effective than higher molecular weight polymers at inhibiting cancer cell growth *in vitro*. Also

noteworthy is the slightly lower activity of R=7.5 CPT-HA-DOX compared to R=2.8 CPT-HA-DOX. According to results in Chapter 3 (Figure 3.8), synergistic interactions between free CPT+DOX should increase with higher R, however the polymer-bound drugs here perform conversely. This effect seems consistent across the two molecular weights investigated. In Chapter 5 (Figure 5.6), it was shown that an optimal R (R=4.5) occurs when the CPT+DOX are bound to 250 kDa HA. R=9 yielded lower cell inhibition than R=4.5 and hence less synergy. As alluded to in Chapter 5, it is possible that a threshold DOX concentration is necessary for CPT+DOX to synergistically inhibit cancer cells. Due to poor DOX release, HA bearing a large R may significantly reduce the amount of DOX available for cancer cell kill. Therefore, while a clear R cut-off is not evident in free drug interactions, it is for both 10 kDa and 250 kDa HA conjugates. Despite this, polymer-bound CPT+DOX at R~3 perform better when conjugated to 10 kDa HA as opposed to the larger 250 kDa HA.

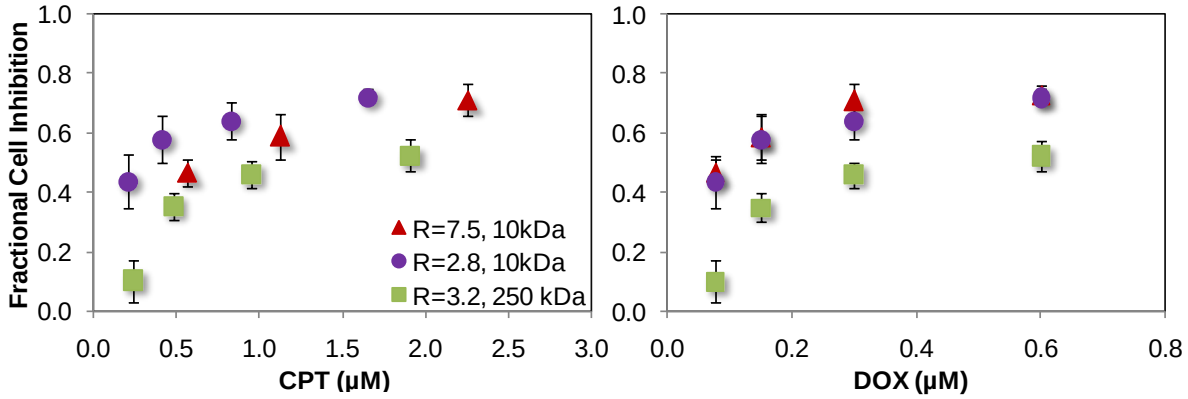

Figure 6.1. *In vitro* cancer cell inhibition of 10kDa CPT-HA-DOX.

4T1 cancer cell viability after incubation with 10 kDa CPT-HA-DOX of R=2.8 (circles) or R=7.5 (triangles) as a function of CPT (left) or DOX (right) concentration. For comparison, 250 kDa CPT-HA-DOX R=3.2 (squares) from Figure 5.7 is provided. Data expressed as mean ± SD (n≥6).

The more potent of the two 10 kDa formulations, R=2.8 CPT-HA-DOX, was further evaluated *in vivo* to investigate if low molecular weight HA could also effectively deliver the synergistic pair to tumor tissues when presented with biological barriers. Mice inoculated with 4T1 murine breast cancer cells were challenged with R=2.8 10 kDa CPT-HA-DOX at the same dosing schedule, i.v. tail vein injections on Days 3, 5, 7, 9, and 11 post-inoculation. For this study, two doses were investigated: low dose 2 mg/kg CPT + 1.2 mg/kg DOX (same as 250 kDa studies), or high dose 3 mg/kg CPT + 1.8 mg/kg DOX. Tumor growth inhibition, body weight changes, and survival rates elicited by these doses are reported in Figure 6.2. After 22 days, the low dose and high dose treatments respectively inhibited 47% and 37% tumor growth relative to untreated mice. While CPT-HA-DOX-treated tumor volumes were statistically different from control mice, volumes between the different doses were not. This suggests that, similar to 250 kDa CPT-HA-DOX, 10 kDa conjugates are capable of providing significant therapeutic effects. However, 10 kDa conjugates seemed to perform no better or worse than the 250 counterparts, since both inhibited ~50% tumor growth (Figure 5.8). However, the inhibition from 250 kDa CPT-HA-DOX occurred as early as 12 days, whereas that of 10 kDa CPT-HA-DOX appeared later, at 22 days post-inoculation. Therefore, small molecular weight HA delays therapeutic effect compared to larger molecular weight HA. Despite providing significant tumor reduction, 10 kDa CPT-HA-DOX was not able to prolong survival rates relative to control mice. Tumors inevitably grew to the same sizes as control mice, which was likely caused by the delay in antitumor activity.

Since tumor growth is exponential, it may be necessary to stagnate growth early in order to significantly improve overall survival.

One evident difference between 10 kDa and 250 kDa conjugates which may cause this disparity in antitumor activity is their size distributions. Dynamic light scattering of the two formulations tested *in vivo* (Table 6.1) provided multi-modal distributions, likely attributed to anisotropic polymeric backbone scattering. However, the size regimes exhibited by the two conjugates vary drastically. While 10 kDa conjugates exhibit tenths and tens of nanometer particulates, 250 kDa conjugates exhibit sizes of tens and hundreds of nanometers. Both exhibit micron-sized particulates, likely aggregates of pendant hydrophobic drug interactions. The differences in their nano-sized particles, however, may cause their discrepancies in therapeutic efficacies. Since renal filtration can remove particles in the tens of nanometers [21], 10 kDa CPT-HA-DOX can be cleared more rapidly than 250 kDa CPT-HA-DOX. Hence, 250 kDa conjugates may circulate longer and accumulate more in tumors. However, nanoparticles in the tens of nanometers can penetrate deeper into tumor tissue [190], and can induce cancer cell death where larger conjugates cannot. Although it is unclear how this difference in tumor distribution impacts antitumor efficacy, one hypothesis is that larger conjugates inhibit cancer cell growth in the peripheral tumor cells, while smaller conjugates inhibit cancer cell growth deeper within the tumor interstitium. It is unclear why these discrepancies in tumor cell inhibition would elicit different times or delays of treatment efficacy, but there is evidently an impact of polymer size on antitumor potency. It may also be possible to prevent growth earlier than 22 days or prolong survival if the drug doses

were increased, especially since the maximum tolerable dose of DOX (20 mg/kg) [194] is ten-fold what was administered, in both the 10 kDa and 250 kDa studies. Here, doses were limited by low chemical conjugation efficiencies, and dose optimization will further elucidate the therapeutic abilities of low molecular weight HA. Collectively, our findings encourage investigation of low molecular weight polymers for polychemotherapy delivery.

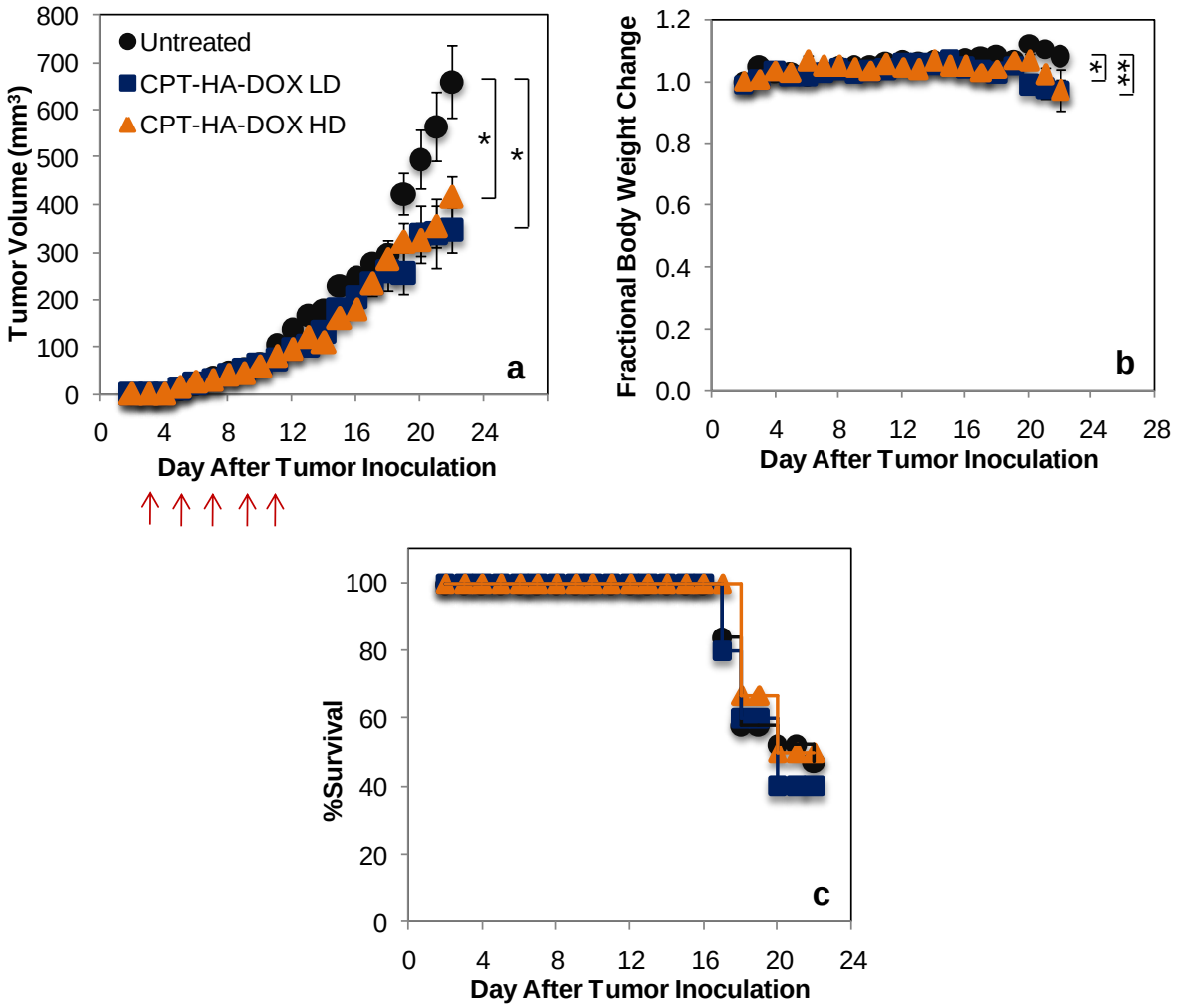

Figure 6.2. Tumor growth inhibition of 10kDa CPT-HA-DOX.

(a) Tumor growth of mice bearing 4T1 breast cancer tumors, without treatment (circles), with i.v. injections of low dose 10 kDa CPT-HA-DOX R=2.8 (squares), or high dose 10 kDa CPT-HA-DOX R=2.8 (triangles). Low dose CPT-HA-DOX treatments consisted of drug-equivalent doses of 2 mg/kg CPT + 1.2 mg/kg DOX, while high dose CPT-HA-DOX treatments consisted of 3 mg/kg CPT + 1.8 mg/kg DOX. Arrows indicate days of treatment. (b) Effect of treatment on body weight fluctuations. Data is reported as mean ± SE, n≥10 at start of study, and varied accordingly to survival rates. (c) Survival rates for all treatment groups.

	10 kDa			250 kDa		
	Size (nm)	%Intensity	StDev (nm)	Size (nm)	%Intensity	StDev (nm)
Peak 1	1036.0	84.6	554.1	275.2	90.3	136.2
Peak 2	0.8	8.7	0.2	52.0	4.9	10.4
Peak 3	61.8	6.7	18.1	4772.0	4.7	741.1

Table 6.1. Multi-modal intensity-based size distribution of CPT-HA-DOX conjugates.

6.3. Polymer-drug chemical linkers

The chemical linkage between the drug and polymer is another variable that can greatly impact drug activity. Depending on the chemical linker, the drug may be released from the polymer carrier at various rates or may not hydrolyze at all. With regards to combination chemotherapy delivery, drugs that are conjugated to a polymeric backbone via different linkers may release at distinct rates. This can have immense ramifications on the combination's potency, as therapeutic efficacy is heavily governed by the schedule and order of drugs administered [95, 195, 196]. In order to determine the effect of hydrolysis on drug activity, DOX was conjugated to 10 kDa PVA via ester, amide, or hydrazone linkers using Reaction Schemes 5.1, 6.1, or 6.2, respectively, and the cancer cell growth inhibition was evaluated *in vitro* for all conjugates. The conjugation achieved for the ester, amide and hydrazone-linked DOX were 0.25mol%, 0.81mol% and 0.03mol% DOX relative to PVA, respectively. Ester bonds are the most commonly used in literature due to ease of synthesis, and also represent hydrolytically labile bonds; amide-linked conjugates represent hydrolytically stable bonds, whereas hydrazone linkers are hydrolytically degraded at endosomal pH 5.0 but stable at physiological pH 7.4 [197, 198]. *In vitro* cancer cell cytotoxicity studies in Figure 6.3a show that the cleavable conjugates, ester-linked DOX (DOXePVA) and hydrazone-linked DOX (DOXhPVA), are active against cancer cells, whereas the non-cleavable amide-linked DOX (DOXaPVA) is not.

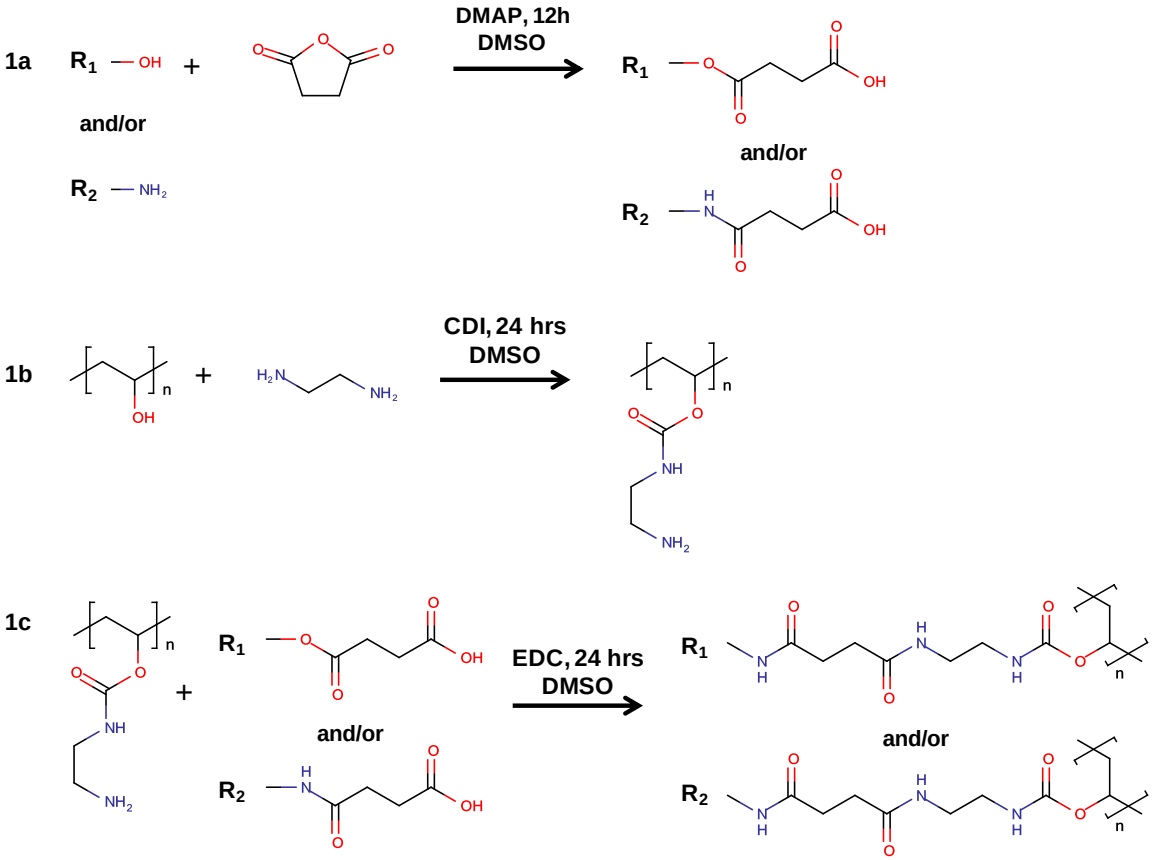

Reaction scheme 6.1. Chemical reactions utilized for incorporation of DOX and/or CPT onto PVA via amide linkers.

Reaction 1a activates nucleophilic drugs (designated as R_1-OH or R_2-NH_2) with succinic anhydride to form EDC-reactive drugs. Reaction 1b shows amination of PVA side chains, which is further reacted with products of 1a in reaction 1c. DOXaPVA was synthesized in this manner.

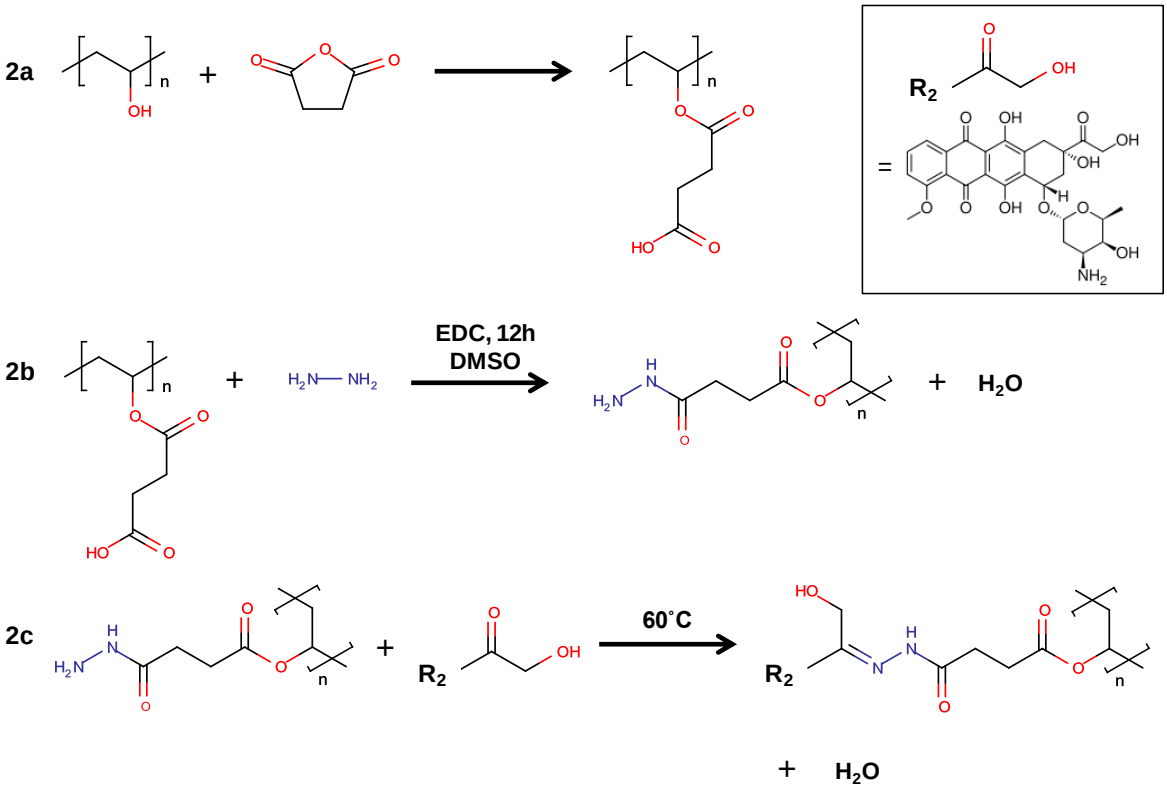

Reaction Scheme 6.2. Chemical reactions utilized for incorporation of DOX onto PVA via hydrazone bonds.

Reaction 2a activates PVA hydroxyl groups with succinic anhydride to form EDC-reactive carboxylic acid side chains. Reaction 2b shows hydrazine conjugation to activated PVA side chains. Hydrazine-conjugated PVA is further reacted with a ketone-containing drug (DOX) to form a hydrazine-linked PVA-drug conjugate. DOX is designated as R_2-$COCH_2OH$.

Confocal studies were implemented in order to assess the impact of chemical linkage on drug internalization and potential correlations with anticancer activity. As seen in Figure 6.3b-c, cell internalization of DOX in the form of DOXePVA and DOXaPVA is much lower than that of free DOX, which suggests that polymer-drug conjugates require active internalization, whereas free DOX can diffuse through the cell membrane. Furthermore, the internalization of polymer-bound DOX is dictated by the chemical linker, as indicated by the significant decline of drug internalization when introduced as DOXaPVA compared to DOXePVA. One possible reason for this sharp contrast is that drug hydrolysis may occur prior to cell entry in the case of the

ester-linked conjugate, which then allows DOX to become internalized via passive, non-energy intensive mechanisms. Also noteworthy is the difference in nuclear drug accumulation between the different conjugates. Since DOX inhibits topoisomerase II enzymes, drug co-localization within the nucleus may be directly correlated to its ability to inhibit proliferation. As a free drug, nuclear accumulation of DOX is evident through the purple nuclear hue (red and blue co-localization) in Figure 6.3c. Less purple, and hence nuclear DOX accumulation, is seen in cancer cells incubated with DOXePVA, and barely any is observed in cancer cells incubated with DOXaPVA. Therefore, it seems that non-cleavable conjugates prevent DOX from escaping endosomes and reaching the nucleus, which in turn hinders its anticancer activity. Both internalization studies and cancer cell growth inhibition results suggest that DOX must be cleaved from the polymer at physiological conditions in order to remain active at inhibiting cancer cell growth, and the polymer-bound drug is not active prior to drug hydrolysis.

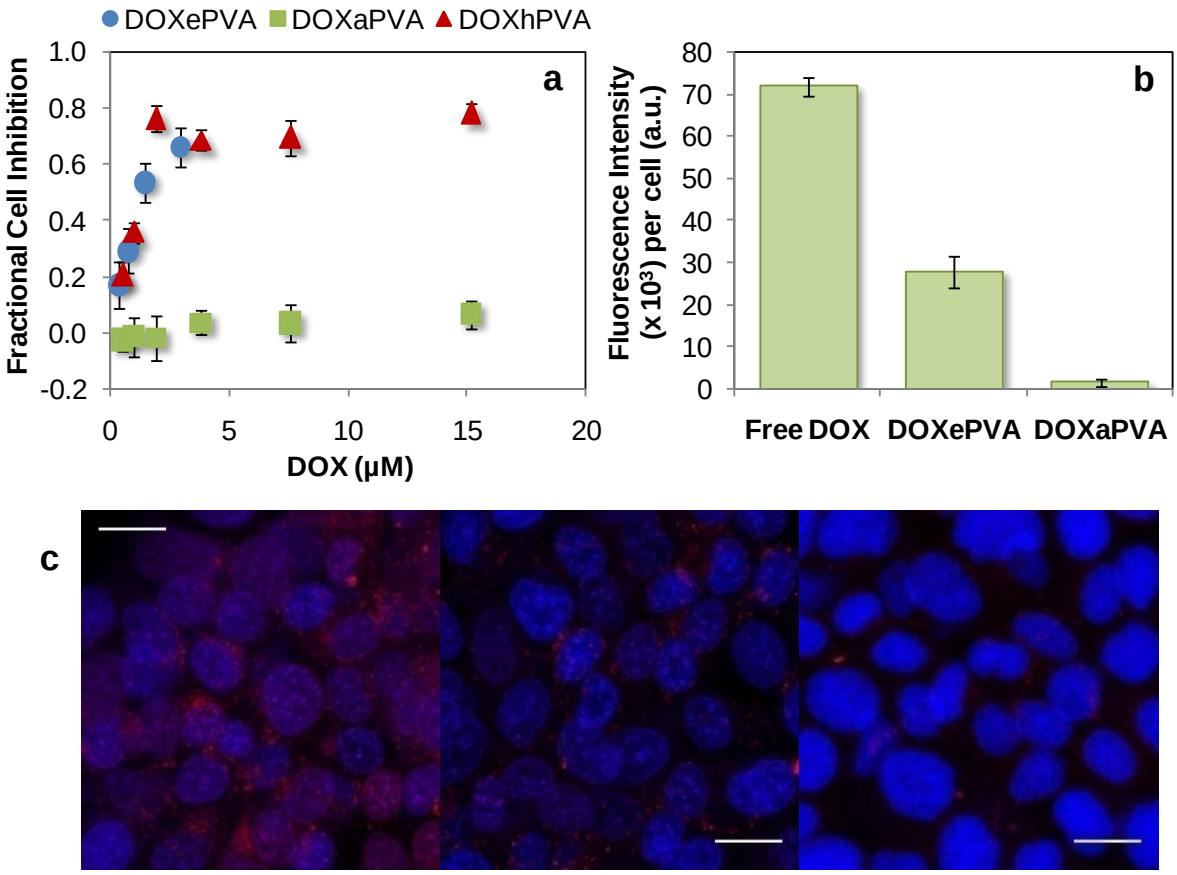

Figure 6.3. The impact of various PVA-drug linkers on drug activity and internalization.

DOXePVA refers to ester-linked drug, which was synthesized via Reaction Scheme 5.1; DOXaPVA refers to amide-linked drug, which was synthesized via Reaction Scheme 6.1, and DOXhPVA refers to hydrazone-linked drug, which was synthesized via Reaction Scheme 6.3. (a) Comparison of the *in vitro* BT-474 cancer cell growth inhibition of the various linkers. DOXePVA is indicated by circles, DOXaPVA is represented by squares, and DOXhPVA is indicated by triangles. (b) Fluorescence of DOX in free solution, DOXePVA, or DOXaPVA present in BT-474 cells after 24 hours of incubation at 37˚C and 5% CO_2. Initial drug loadings were 1 μM DOX-equivalents. Data expressed as mean ± SD (n=3). (c) Representative images of DOX (red) internalization from free solution (left), DOXePVA (middle), or DOXaPVA (right). Cells were labeled with Hoechst nuclear dye. Images are averages of 10 μm z-stacks. Scale bar=20 μm.

To further investigate the effect of chemical linker on combination chemotherapy efficacy, DOX and CPT were co-conjugated to PVA utilizing physiologically labile and non-labile tethers. CPT-PVA-DOX F1 utilized Reaction Scheme 6.1, which conjugated DOX and CPT via amide and ester bonds, respectively.

CPT-PVA-DOX F2 was synthesized with Reaction Scheme 5.1, which conjugated both drugs via ester bonds. In the case of CPT-PVA-DOX F1, only one drug was hydrolytically labile and capable of releasing from the polymer under physiological conditions; on the contrary, CPT-PVA-DOX F2 can release both drugs since ester linkages were used to conjugate CPT and DOX. Both schemes resulted in the conjugation of CPT and DOX in ratios at which the free drugs exhibited synergistic cancer cell kill, R > 0.1 (Figure 6.4a). Also noteworthy is the poor conjugation efficiency of Reaction Scheme 5.1 compared to Reaction Scheme 6.1. Whereas Reaction Scheme 6.1 achieved conjugations of 0.10 and 0.28 mol% CPT and DOX, respectively, Reaction Scheme 5.1 only yielded 0.01 mol% for both drugs. This can be attributed to the overall less favorable nature of hydroxyl esterification compared to amide formations.

The activity of these two CPT-PVA-DOX conjugates against BT-474 cancer cell growth was evaluated via MTT cytotoxicity assays, and compared to the anticancer activities of the single ester-linked PVA-conjugates (Figure 6.4b). CPT-PVA-DOX F1 showed similar efficacy as CPT-PVA and DOX-PVA, with no clear advantage over either single drug conjugate. On the other hand, CPT-PVA-DOX F2 exhibited more than double the potency of either CPT-PVA or DOX-PVA alone. While the two formulations bear different drug ratios, both ratios of 0.36 and 1.50 are expected to exhibit synergy in the polymer form, as demonstrated in Figure5.2a-b.Thus, the differences in cancer cell growth inhibition can be clearly attributed to differences in linker chemistry. Physiologically labile linkers such as esters and hydrazones enhance intracellular concentrations of drugs and thus maintain drug activity,

whereas hydrolytically stabile amide bonds significantly reduce drug activity as well as combination potency. These results further emphasize the necessity of drug hydrolysis from the polymer in order to preserve both drug activity and combination synergy.

a

Formulation	Reaction Scheme	R (CPT:DOX)	CPT (mol%)	DOX (mol%)
F1	6.1	**0.36**	0.10	0.28
F2	5.1	**1.50**	0.01	0.01

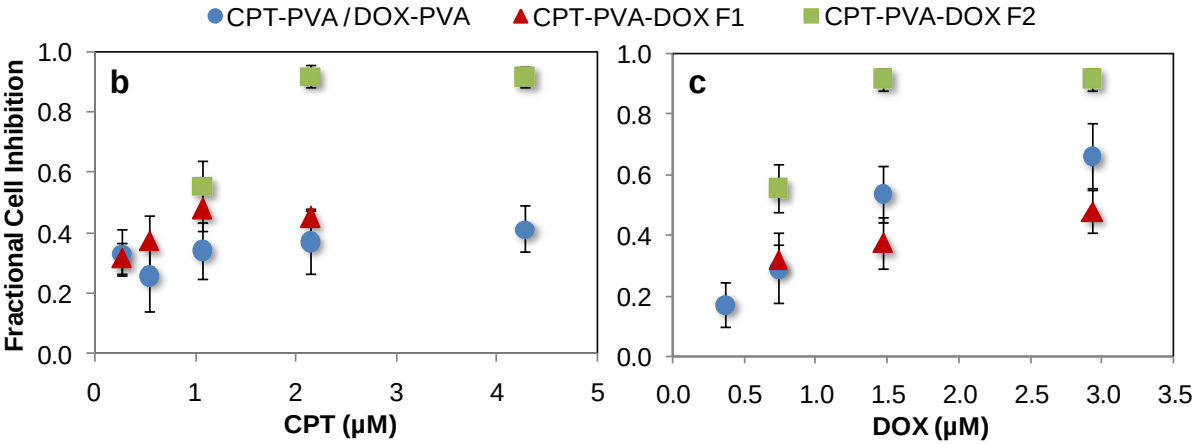

Figure 6.4. *In vitro* anticancer activity of CPT-PVA-DOX with non-hydrolyzable and hydrolyzable linkers.

(a) Properties of PVA-conjugates which utilized Reaction Schemes 5.1 or 6.1 to conjugate both CPT and DOX to the same polymer. Cell inhibition of BT-474 cells in the presence of CPT-PVA-DOX conjugates F1 (triangles) and F2 (squares) are compared to the cell inhibition of cells treated with (b) CPT-PVA alone (circles) or (c) DOX-PVA alone (circles). CPT-PVA-DOX F2, CPT-PVA and DOX-PVA were synthesized utilizing esterification (Reaction Scheme 5.1) and are the same as reported in Figure 5.2. Cells were incubated with formulations for 72 hours, and assessed for cell viability utilizing the MTT cytotoxicity assay. Data is reported as mean ± SD (n≥6).

6.4. Mass transport across lipid bilayer of liposomes

Poor drug release from liposomes is an inherent issue with the highly effective transmembrane ammonium sulfate gradient DOX encapsulation method [28, 112, 113]. Y. Barenholz describes this effect as "no free lunch", suggesting that adequate drug release and high drug encapsulation often come at the cost of the other [112]. As seen in the previous section, poor drug release from nano-vehicles can be detrimental to both single and combination therapeutic efficacies. To combat this challenge, a small amount of cationic lipids can be incorporated (Chapter 4) to facilitate intracellular DOX release. However, mass transport of drug from the inner aqueous core, across the lipid bilayer and to the extra-liposomal aqueous environment can be enhanced through a variety of liposomal property adjustments. Two alternatives were considered during the development of liposomes for chemotherapy co-delivery: reduction in ammonium sulfate concentration and cholesterol content. An analysis of mass transport barriers during DOX release will help reveal how these parameters can be tuned to accelerate drug release.

Inherently, slow DOX release is attributed to the highly efficient encapsulation method. As depicted in Figure 4.2, an ammonium sulfate gradient is formed such that $[(NH_4)_2SO_4]_{intra\text{-}liposomal} > [(NH_4)_2SO_4]_{extra\text{-}liposomal}$. DOX in its hydrochloride salt form is then co-incubated with the vesicles. Since DOX is weakly basic, it will be present in its neutral form outside of the vesicle. The high intra-liposomal proton concentration drives DOX inside, where it becomes protonated and associated with a sulfate ion to form a final precipitate, $(DOX\text{-}NH_3)_2SO_4$ [127]. Drug loading is performed above the phase transition temperature of the lipids (55˚C) to

facilitate transport across the lipid bilayer. All reactions are reversible, but the final precipitate cannot cross the liposomal barrier at physiological temperature, 37˚C. Thus, when liposomal DOX is delivered intravenously, the precipitated DOX must revert back to the soluble DOX-NH_2 before escaping the liposome. Here, there are two main aspects of mass transfer which influence drug release: dissolution of the precipitate and diffusion of the soluble form across the bilayer. We can address one aspect at a time, followed by a comparison of the consequences of each.

First, we consider mass transfer of soluble DOX, DOX-NH_2. DOX-NH_2 must first diffuse within the aqueous core to reach the surface of the lipid bilayer; then it must cross the lipid bilayer. The bilayer itself constitutes a resistance to mass transport; highly hydrophobic interactions and embedded cholesterol groups pose a barrier for a water soluble molecule to cross. For simplicity, we model the intra-liposomal space in 1-D, as seen in Figure 6.5. Here, z=0 represents the center of the liposome and z=R indicates the lipid bilayer. We model the bilayer as a membrane with permeability k_m. The concentration of DOX-NH_2 at the center is C_o, whereas the concentration at the surface is C_S.

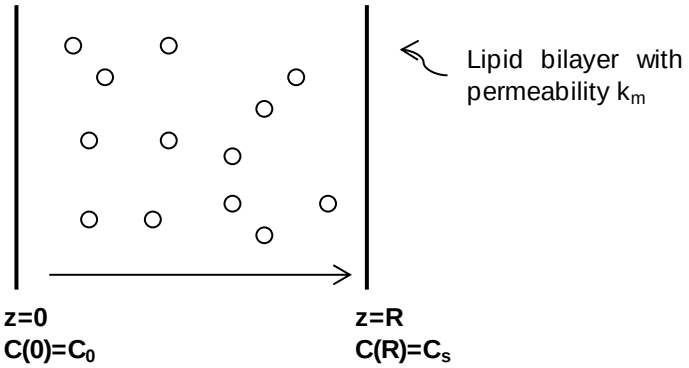

Figure 6.5. 1-D model of drug diffusion through intra-liposomal space.

The flux out of the lipid bilayer surface is:

$$J_{out} = k_m \Delta C \tag{6.1}$$

Since the extra-liposomal space has no DOX before drug release, we can say:

$$\Delta C = C_S - 0 = C_S \tag{6.2}$$

We can also find the diffusive flux within the liposome:

$$J_D = -D\nabla C \tag{6.3}$$

where D is the diffusivity of DOX within the aqueous core

$$\nabla C = \frac{C_S - C_0}{R} \tag{6.4}$$

At steady state, the flux out of the bilayer and the diffusive flux must be the same. By setting (6.1) and (6.3) equal, we find the relationship:

$$C_S = \frac{C_0}{1 + \frac{Rk_m}{D}} \tag{6.5}$$

The Damköhler naturally presents itself in the dominator, as the ratio of the lipid permeability rate to the diffusion rate:

$$Da_1 = \frac{Rk_m}{D} \tag{6.6}$$

By looking at the limiting cases of Da_1, we can find valuable information. In the case where $Da_1 \gg 1$, we see that $C_S \ll C_o$. Permeation through the lipid bilayer occurs rapidly, and diffusion within the liposome is slow. Thus, diffusion to the membrane surface limits the mass transfer of soluble DOX. In the other case, where $Da_1 \ll 1$, we see that $C_S \approx C_o$ and C_S is constant. Thus, the supply of DOX to the lipid membrane is constant, but the permeability through the membrane is slow and limiting. Given

that the diffusivity of DOX is approximately 4 x 10^{-6} cm^2/s [199] and the average diameter of our DOX-liposomes is 150 nm (Table 4.1), the rate of diffusivity is 0.53 cm/s. Thus, the time it takes DOX to traverse the intra-liposomal space and reach the lipid membrane is on the order of 10^{-5} s and is considerably fast. We expect that lipid permeability is the limiting mass transfer, where $k_m \ll D/R$ and therefore $Da_1 \ll 1$. We can now solve for the residence time of one DOX molecule in the liposome, τ_L. If C is given in molecules per volume,

$$N = \frac{4}{3}\pi R^3 C \tag{6.7}$$

Where N is the number of DOX molecules and $C=C_s=C_o$. The molecular flux of a DOX molecule will be the liposomal area multiplied by the steady state flux described by (6.1):

$$J_m = 4\pi R^2 k_m C \tag{6.8}$$

The residence time of one DOX molecule in the liposome is N divided by J_m:

$$\tau_L = \frac{1}{3}\frac{R}{k_m} \tag{6.9}$$

Thus, in the case where lipid membrane permeability limits the mass transfer of soluble DOX, the residence time of DOX in the liposome is inversely proportional to the membrane permeability k_m.

Now that we've discussed the liposomal escape of soluble DOX, it is necessary to consider how the reaction of precipitated DOX to soluble DOX affects drug release. We can think of precipitated DOX, $(DOX\text{-}NH_3)_2SO_4$, as a core in the center of the liposome that acts as a reservoir for soluble DOX, $DOX\text{-}NH_2$. A summary of the reactions occurring within the liposome is given below:

$$2DOX\text{-}NH_2 + 2H^+ \rightleftarrows 2(DOX\text{-}NH_3^+)$$
$$2(DOX\text{-}NH_3^+) + SO_4^{2-} \rightleftarrows (DOX\text{-}NH_3)_2SO_4\ (ppt)$$
$$2DOX\text{-}NH_2 + 2H^+ + SO_4^{2-} \rightleftarrows (DOX\text{-}NH_3)_2SO_4\ (ppt) \quad \text{Total Reaction (6.10)}$$

$$A + B + \tfrac{1}{2}D \underset{k_b}{\overset{k_f}{\rightleftarrows}} \tfrac{1}{2}C\ (ppt) \quad \text{Simplified Reaction (6.11)}$$

For simplicity, we denote A=DOX-NH_2, B=H^+, D=SO_4^{2-}, and C = $(DOX\text{-}NH_3)_2SO_4$, and ppt designates a precipitate. The forward reaction rate is k_f and the reverse reaction rate is k_b. At equilibrium, the concentrations of C and A are not changing in time. However, as A (soluble DOX) escapes the liposome and is depleted, the reaction is driven to dissolve more of C (precipitated DOX) by Le Chatelier's principle in order to compensate for lost A. As A escapes the liposome, this results in a small change δ in the concentration of A, [A], and we can determine the time required for the system to reach equilibrium again. Assuming stoichiometric reaction rates, we can define the change in [A] with time:

$$\frac{\partial[A]}{\partial t} = -k_f[A][B][D]^{1/2} + k_b[C]^{1/2} \tag{6.12}$$

We can define a small perturbation in equilibrium concentrations as such, where $[X]_o$ denotes an equilibrium concentration:

$$[A] = [A]_0 + \delta \tag{6.13}$$

$$[B] = [B]_0 + \delta \tag{6.14}$$

$$[C] = [C]_0 - 2\delta \tag{6.15}$$

$$[D] = [D]_0 + 2\delta \tag{6.16}$$

Plugging (6.13)-(6.16) into (6.12) and using Taylor expansion, we find the O(1) differential equation:

$$\frac{\partial [A]_0}{\partial t} = -k_f [A]_0 [B]_0 [D]_0{}^{1/2} + k_b [C]_0{}^{1/2} \tag{6.17}$$

Equation 6.13 is identically zero since it represents steady state. We can also find the O(δ) differential equation:

$$\frac{\partial \delta}{\partial t} = -k_f \delta \left([A]_0 [B]_0 [D]_0{}^{-\frac{1}{2}} + [A]_0 [D]_0{}^{\frac{1}{2}} + [B]_0 [D]_0{}^{\frac{1}{2}} \right) - k_b \delta [C]_0{}^{1/2} + O(\delta^2) \tag{6.18}$$

Integrating (6.18), we find:

$$\delta(t) = \delta_0 \exp[t \left(-k_f \left([A]_0 [B]_0 [D]_0{}^{-\frac{1}{2}} + [A]_0 [D]_0{}^{\frac{1}{2}} + [B]_0 [D]_0{}^{\frac{1}{2}} \right) - k_b [C]_0{}^{\frac{1}{2}} \right)] \tag{6.19}$$

Thus, the concentration profile of A after a small perturbation in equilibrium is:

$$A(t) = [A]_0 + \delta_0 \exp \left[t \left(-k_f \left([A]_0 [B]_0 [D]_0{}^{-\frac{1}{2}} + [A]_0 [D]_0{}^{\frac{1}{2}} + [B]_0 [D]_0{}^{\frac{1}{2}} \right) - k_b [C]_0{}^{\frac{1}{2}} \right) \right] \tag{6.20}$$

And the time required for the perturbation in equilibrium to dissipate, τ_R, is given in the exponential:

$$\tau_R = [\left(-k_f \left([A]_0 [B]_0 [D]_0{}^{-\frac{1}{2}} + [A]_0 [D]_0{}^{\frac{1}{2}} + [B]_0 [D]_0{}^{\frac{1}{2}} \right) - k_b [C]_0{}^{\frac{1}{2}} \right)]^{-1} \tag{6.21}$$

This says that the faster the reaction rates k_f and k_b are, the shorter the time required for the system to reach equilibrium again.

Through the individual analyses of the lipid membrane and the reaction limitations to mass transport, we have identified the time constants associated with

each limit, as seen in Equations 6.9 and 6.21. The ratio of Equation6.9 to 6.21 represents another Damköhler number which relates the reaction time scale to the lipid permeation time scale:

$$Da_2 = \frac{\left(-k_f\left([A]_0[B]_0[D]_0^{-\frac{1}{2}} + [A]_0[D]_0^{\frac{1}{2}} + [B]_0[D]_0^{\frac{1}{2}}\right) - k_b[C]_0^{\frac{1}{2}}\right)}{3\,\frac{k_m}{R}} \tag{6.22}$$

If $Da_2 \ll 1$, then the time for precipitated DOX to dissolve is much faster than the time required for soluble DOX to pass through the lipid membrane. In this case, drug release is limited by mass transport through the lipid bilayer. On the contrary, if $Da_2 \gg 1$, the time for soluble DOX to pass through the lipid bilayer is faster and the dissolution of DOX is rate limiting.

Without knowledge of reaction rates k_f and k_b or membrane permeability k_m, we can still estimate whether the reaction or the lipid membrane constitutes the highest mass transport barrier. As described by Equation 6.20, the release of DOX with respect to time should be exponential if reaction is limiting mass transfer. On the other hand, if lipid bilayer permeability is the limitation, the flux in Equation 6.1 suggests that the release of DOX should be linear in time with slope k_m. Thus, DOX concentrations released from liposomes can be collected over time and be utilized to estimate the mass transport limitation.

In an effort to determine the mass transfer limitations in our system, drug release data was collected. DOX-loaded liposomes were incubated in a dialysis tube which permits DOX transfer but no liposome transfer (Section 2.9). The dialysis tube was incubated at physiological temperature (37˚C) and samples of fluid surrounding the dialysis tube were analyzed at various time points for DOX. Samples

were compared to a DOX fluorescence standard curve to determine drug concentration. Two formulations with different liposomal ammonium sulfate concentrations were compared, as seen in Figure 6.6a. We see that at 250 mM $(NH_4)_2SO_4$, DOX release was linear with time, whereas at 10 mM $(NH_4)_2SO_4$, DOX release seemed nonlinear. Thus, if we assume that the system reached steady state within a day, DOX release was limited by lipid permeability at higher intra-liposomal ammonium sulfate concentrations. However, at lower intra-liposomal ammonium sulfate concentrations, dissolution of precipitated DOX limited drug release. This suggests that when less ammonium sulfate ions are available, DOX remains in the precipitated form. Therefore, the release of DOX can be modified by changing the intra-liposomal ammonium sulfate concentration. To promote exponential drug release with time, a low ammonium sulfate concentration can be utilized. However, by utilizing low concentrations of ammonium sulfate, one will sacrifice DOX encapsulation efficiency.

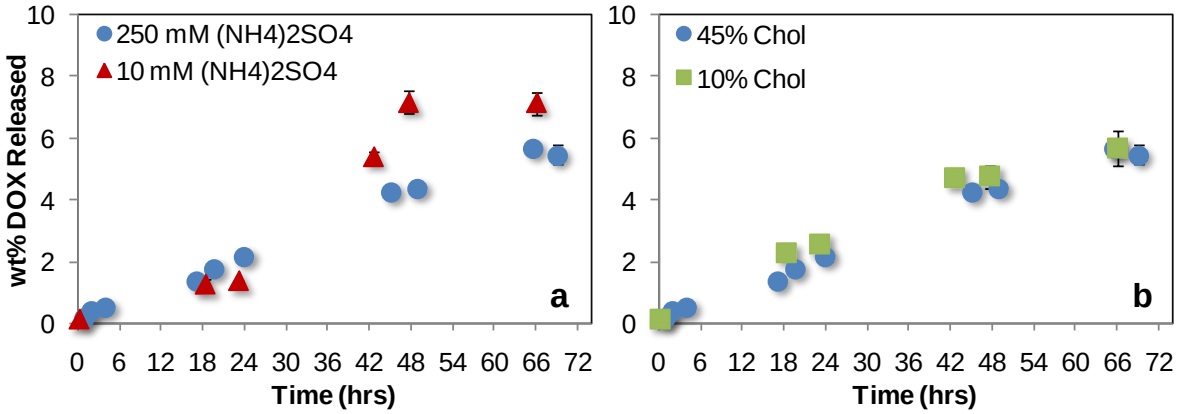

Figure 6.6. Effect of membrane properties on liposomal drug release.

Effect of (a) intra-liposomal ammonium sulfate concentration or (b) Chol content on DOX release from liposomes. Liposomes with 45% Chol content and rehydrated in 250 mM $(NH_4)_2SO_4$ buffer (circles) are compared to liposomes with 10% Chol content with 250 mM $(NH_4)_2SO_4$ buffer (squares) and liposomes with 45% Chol content rehydrated in 10 mM $(NH_4)_2SO_4$ buffer (triangles). Data expressed as mean ± SD (n=3).

High concentrations of ammonium sulfate are necessary for high DOX loading, but in this case, lipid membrane permeability poses the greatest barrier to DOX release. One possible method to increase membrane permeability, or k_m, is to reduce the cholesterol (Chol) content. Since Chol is embedded in the lipid bilayer, a reduction of Chol will reduce the hydrophobic interactions in the membrane and decrease the barrier for transport of water soluble molecules, including ammonium sulfate ions that maintain the transmembrane pH gradient. DOX liposomes were fabricated with 250 mM ammonium sulfate and two different cholesterol mol fractions: 45% and 10%. The release data are shown in Figure 6.6b. In both 45% and 10% Chol liposomes, DOX release was linear with time, and only slightly more DOX was released with 10% Chol at earlier time points. As a result, the slope relating DOX released and time was similar for both 10% and 45% Chol liposomes. As defined in Equation 6.1, k_m should have units of [m/s], but release data was collected as DOX mass rather than DOX concentration. Thus the slopes of the release data have units of [μg/day] and still qualitatively represent k_m. The slopes for 45% and 10% cholesterol liposomes were respectively 2.07 μg DOX/day and 2.06 μg DOX/day. The release data show that membrane permeability is not affected by Chol content within the range of 10-45 mol%.

Chol is known to exhibit multiple effects on lipid bilayer transport, which can account for this observed little difference in DOX release. On one hand, Chol reduces permeability of ions and small molecules across the phospholipid membrane and hence hinders the ability of such molecules to disorder the bilayer [32]. However, Chol has also been shown to prevent ordering of saturated lipid chains and

actually enhance membrane permeability [200]. The observed effects of Chol depend on both the saturation of phospholipids and amount of incorporated Chol relative to phospholipids. Specifically, Chol has been shown to prevent ordering at above 30 mol% content in a bilayer containing saturated lipids, such as the lipids utilized here (DSPC). Therefore, it is likely that 10 mol% Chol does not affect T_m of liposomes, but allows the diffusion of small molecules, whereas 45 mol% Chol reduces T_m but prevents the passage of small molecules. These two regimes may ultimately elicit identical effects on liposome permeability k_m, and hence result in similar drug release rates. Therefore, altering Chol content between 10-45 mol% in DSPC-comprised bilayer is not a practical method for accelerating drug release from liposomes.

DOX release from liposomes can be characterized as membrane transport-limited or reaction-limited. Considering the nano-size of the liposomes and relatively high DOX diffusivity, diffusion of soluble DOX to the membrane seems negligible compared to its transport though the lipid membrane barrier. Through mass transport analysis, it was found that in membrane-limited transport, the release of DOX with time should be linear. In reaction-limited transport, DOX release is exponential with time. Changing the ammonium sulfate concentration for DOX encapsulation can influence whether the release is membrane transport-limited or reaction-limited. Despite this change in DOX release profiles, the reduction in ammonium sulfate concentrations does not drastically improve overall drug release. It was also shown that decreasing cholesterol content offers little enhancement in membrane permeability. Therefore, to accelerate DOX release during cancer

treatments, other methods may need to be explored. Alternative methods which increase membrane permeability may be of interest, such as physical membrane alterations. Our studies in Chapter 4 involved the use of cationic lipids to promote ionic interactions with native negatively-charged lipids on cell membranes. Current literature efforts in this area also include ultrasound or photo-switchable lipids which create a more porous and leaky structure when exposed to a particular wavelength of light. Investigating stimuli for instantaneous membrane permeability can promote high local concentrations of toxic drugs at tumor sites and potentially more effective cancer treatments. An analysis of the mass transport limitations in our current system has revealed how certain parameters can influence DOX release, but that other methods may need to be explored in order to significantly impact DOX release from liposomes. Moreover, optimizing single drug release with various stimuli will allow for the development of multi-drug loaded liposomes that release both drugs at acceptable rates and hence do not alter combination potency.

6.5. Nanoparticle stability

Another chief determinant of the clinical applicability of nanoparticles is their shelf-life. Size and drug leakage from nanoparticles can alter depending on the pH, temperature, and time of storage. However, as nanoparticle fabrication is a time- and economically-consuming process, poor stability may render the nanoparticles impractical drug delivery solutions. Here, the storage shelf-lives of liposomes and polymer-drug conjugates developed on Chapters 4 and 5 are compared, with the intent of evaluating their ease of clinical translations. An efficient way to test

formulation stability is by determining D_{50} concentrations *in vitro* at various times after nanoparticle storage. Presumably, if drug is released during storage, D_{50} concentrations should become lower with increased storage time and should eventually mimic those of free drugs.

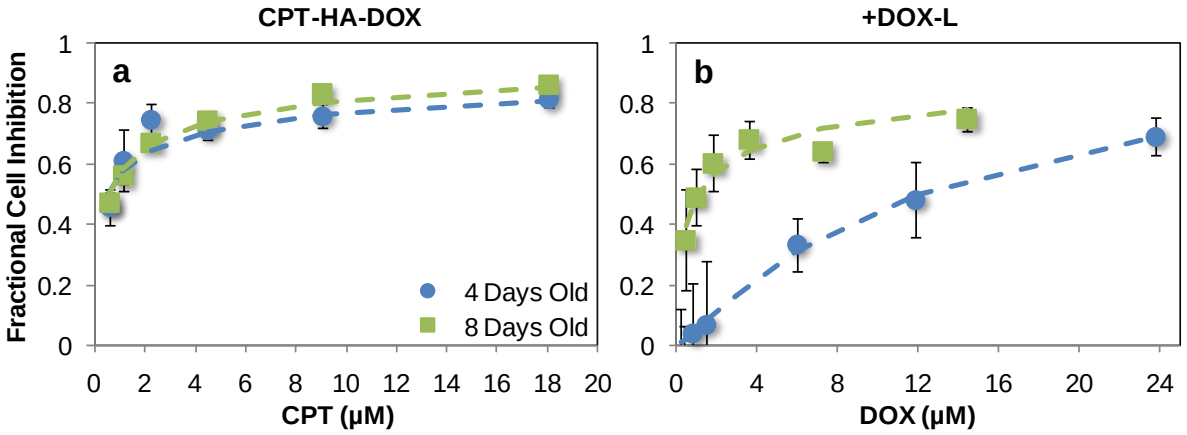

Figure 6.7. Effect of nanoparticle age on cancer cell cytotoxicity.

4T1 cancer cell viability after incubation with 4 day old (circles) or 8 day old (squares) (a) 10 kDa CPT-HA-DOX (R=7.5) or (b) +DOX-L. Data expressed as mean ± SD (n≥6). 4 days old or 8 days old refers to the age of nanoparticle at the time of incubation with cells. Dashed lines represent fits to the ME model. D_{50} and R^2 values corresponding to 4 and 8 days old CPT-HA-DOX, respectively, are (0.55 ± 0.04 μM, 0.98) and (0.59 ± 0.04 μM, 0.97). D_{50} and R^2 values corresponding to 4 and 8 days old +DOX-L, respectively, are (11.9 ± 0.6 μM, 0.99) and (1.07 ± 0.1 μM, 0.93).

As seen in Figure 6.7, CPT-HA-DOX exhibited a similar dose-effect relationship when stored for 4 or 8 days, while the cell inhibitory effects of +DOX-L dramatically increased after 8 days (vs. 4 days) of storage. ME model fits reflected little change in D_{50} of CPT-HA-DOX: 0.55 and 0.59 μM CPT after 4 and 8 days, respectively. However, the D_{50} of +DOX-L was reduced 11-fold (11.9 vs. 1.07 μM DOX) between 4 and 8 days of storage, suggesting that liposomal drug encapsulation was not as stable as polymer-drug incorporation. In both cases, nanoparticles were stored at 4°C to slow drug leakage. Ideally, nanoparticles should

exhibit shelf-lives on the order of months, so that large batches could be synthesized at a time without the need of unrealistic and costly continuous manufacture.

One approach to improving formulation stabilities is lyophilization. Lyophilization removes water through sublimation, and since the presence of water can hydrolyze polymer-drug conjugates or facilitate diffusion of drugs from liposomes, this process can significantly reduce drug release upon storage. In particular, liposomes can aggregate and fuse during aqueous storage [201]. However, it is necessary to verify that formulation properties are not altered during lyophilization and reconstitution in water prior to administration. Clinical polymer-drug conjugates have successfully been lyophilized and easily re-dissolved in water without altering physicochemical properties such as drug incorporation and size [30]. Liposomes, however, have been shown to lose as much as 70% encapsulated drug, as well as its monodispersed shapes after reconstitution [32]. These findings suggest that lyophilization affects the physical reformation of lipid bilayers, but does not compromise chemical linkers between polymers and drugs. Therefore, shelf-life may not be as presiding an issue for polymer-drug conjugates as it is for liposomes. To facilitate the implementation of liposomes for clinical combination chemotherapy delivery, efforts to improve stability and reduce drug release upon storage must be addressed.

6.6. Summary of nanoparticle property effects

In this Chapter, various characteristics of nanoparticles were evaluated for their impact on single and combination chemotherapy activity. For polymer-drug

conjugates, molecular weight and chemical tethers were investigated. Molecular weight dictates the distribution of polymers in tumor tissue, and as a result, influences therapeutic efficacy. Low molecular weight polymers can penetrate deeper into tumor interstitium, while higher molecular weight entities remain on the tumor periphery. Here, it was found that 10 kDa HA conjugates of CPT+DOX produced a lag in tumor reduction compared to 250 kDa HA conjugates of the same CPT+DOX ratio. However, both conjugates achieved the same 50% reduction in tumor volume relative to controls. Dose optimization studies of low and high molecular weight HA will further elucidate the therapeutic benefit of one over the other. It was also found that poorly hydrolyzable chemical linkers are detrimental to both single and combination chemotherapy potency. Amide-linked DOX abolished drug activity, and prevented synergistic cancer cell inhibition with ester-linked CPT. Hydrazone-linked and ester-linked DOX, however, represented highly biodegradable bonds, and resulted in high DOX activity, as well as preserved synergistic activity with CPT. These findings highlighted the therapeutic potential of low molecular polymer-drug conjugates for combination chemotherapy delivery, as well as illustrated the necessity of physiologically labile chemical linkers.

Similarly, release of DOX from liposomes bearing an ammonium sulfate gradient was explored, with an emphasis on membrane-limited and reaction-limited transport. Simply altering the concentration of ammonium sulfate in the lipid hydration solution can switch the mass transport limitation and dictate whether DOX release is linear or exponential. Despite these investigations, neither ammonium sulfate nor cholesterol content changes were found to significantly

improve drug release. Hence, these studies emphasize the need for innovative liposomes which can both encapsulate high drug payloads and trigger their release in tumors.

Lastly, nanoparticle stability was addressed. It was found that liposome-encapsulated drugs were more prone to release in storage than polymer-conjugated drugs. Moreover, lyophilization can prolong polymer-drug conjugate shelf-life without compromising drug incorporation, while it drastically reduces drug encapsulation of liposomes. Prolonged shelf-life is therefore an added challenge of liposome co-delivery that must be optimized for these nanoparticles to become a clinically viable option for chemotherapy combination drug delivery.

Chapter 7

Reflections and Future Directions

7.1. Challenges with multi-drug delivery

The highly coveted therapeutic potential of anticancer drug combinations has lead to a massive pursuit, amounting to a quarter of all oncology clinical trials [202]. Despite this, very few successful pairs exist that provide both therapeutic and toxicity benefits over single drug treatments [13]. In Chapter 3, we demonstrated the incredible potency of chemotherapy combinations when exposed to isolated cancer cells. Nearly 100% cancer cell kill can be achieved by drug combinations already implemented clinically, such as 5FU+DOX and top I + II inhibitors. The low prevalence of complete tumor regression in the clinic [8, 9, 68, 94, 96], however, illustrates the stark disconnect between combination potency *in vitro* and therapeutic efficacy *in vivo*. This disparity represents the highly unmet need for drug delivery carriers that can translate combinations into successful therapies. Research investigations throughout the course of my Ph.D. aimed to tackle this unmet need, and provide insight for future engineering of combination chemotherapy nano-vehicles.

It must be reiterated that chemotherapy drug delivery has not even been perfected for single drugs. Oncology therapeutics is a multi-disciplinary field diligently pursued by clinicians, pharmacists, chemists, chemical engineers, materials scientists, biologists, and many other professions, yet tumor environments

and cancer cells persist. High drug encapsulations, nanoparticle tumor accumulation, drug release and preservation of drug activity are all required for a successful single chemotherapy nanoparticle. These same challenges are amplified for multi-drug delivery. When considering concurrent chemotherapy drug delivery, multiple drugs need to be incorporated in the same nanoparticle, and not only do individual drug activities need to be conserved, but so do their synergy. If synergistic drug interactions are not maintained, there may not be merit to co-administering multiple drugs.

Nanoparticle encapsulation of a single drug is a challenge in itself, since loading techniques often rely on hydrophobic or ionic interactions that can easily be reversed. Empirical techniques are often derived to achieve high drug incorporations tuned to a specific drug, such as the transmembrane ammonium sulfate gradient for liposomal DOX entrapment [127], or copper ion complexation for 5FU liposomal incorporation [145]. However, different drugs bear unique chemical and physical properties, and a high encapsulation method for one drug may be ineffective for another. This became immediately evident in Chapter 4, when the transmembrane ammonium sulfate method yielded <1 mol% 5FU liposomal entrapment (Table 4.2), a technique which has been reported to achieve as high as 25 mol% DOX relative to lipid [14]. Therefore, identifying encapsulation methods which are compatible for both drugs in the combination, and are also not compromised by the presence of other drug, is a prominent challenge associated with multi-drug delivery.

As for maintaining combination synergy, one approach is to controllably encapsulate fixed drug ratios in nanoparticles. Chapter 3 demonstrated that two drugs can elicit synergistic, and antagonistic, or additive cancer cell kill depending on the drug ratio, R, exposed to cells. In particular, CPT+DOX exposed at R > 2 (M:M CPT:DOX) elicited CI « 1 (Figure 3.8c), indicating extreme synergistic cancer cell inhibition, with no apparent upper limit of R. However, when exposed as a mixture of polymer-drug conjugates, CPT-HA+DOX-HA exhibited a minimum CI at R = 4.5 (Figure 5.6b), suggesting that polymer-conjugation creates an upper limit of R for synergistic interactions. This finding demonstrates that synergy preservation upon nanoparticle encapsulation is a non-trivial feat, especially since optimal free drug synergistic R is not necessarily identical to that of nanoparticle-incorporated drugs. While free drug synergistic screens such as those presented in Chapter 3 are helpful in identifying promising drug pairs, the screen for synergistic ratios will most likely need to be repeated for combinations of nanoparticle-incorporated drugs in order to determine the optimal R to be co-loaded in multi-drug nanoparticles.

Also imperative is the release of drugs once accumulated in tumor tissue, in order to allow the drugs to reach their intracellular targets and thereby initiate cascades for cell death. In Chapter 6, DOX conjugated via stabile amide bonds to PVA was incapable of inhibiting cancer cell growth for a range of doses that ester-conjugated DOX was considerably active (Figure 6.3a). As a result, amide-conjugated DOX bound to the same polymer as ester-conjugated CPT was only as active as CPT-PVA (Figure 6.4), and their synergistic interactions were abolished. For the two co-loaded nano-vehicles developed during my Ph.D., DAFODIL and

CPT-HA-DOX, uncoordinated release profiles were discovered (Figure 4.7c and 5.5). One drug would release faster than the other, and this differential drug release can potentially impact synergistic interactions. In our studies, however, differential drug releases worked in the favor of synergy, and did not compromise the pair's ability to inhibit cancer cell growth. For the development of multi-drug loaded nano-vehicles, however, uncoordinated drug release profiles must be generally assessed for their impact on combination therapeutic efficacy.

7.2. Comparison of liposomes and polymer-drug conjugates

After arduously developing both liposomes and polymer-drug conjugates for combination chemotherapy delivery, the multi-drug encapsulation challenges addressed above were assessed for each particle type. A summary of our findings is provided in Table 7.1.

	Liposomes	**Polymer-drug conjugates**
Encapsulation methods	Gradient across lipid bilayer must be tuned to chemical properties of each drug	Requires reactive chemical moieties (i.e. -OH, -NH_2)
Encapsulation yield	25 mol% drug:lipid	15 mol% drug:polymer
Size control	Monodisperse	Multi-modal DLS size distributions
Stability	Drug releases rapidly at 4C, Cannot be lyophilized	Slow drug release at 4C, Can be lyophilized

Table 7.1. Comparative properties of liposomes and polymer-drug conjugates for combination chemotherapy delivery.

Drug encapsulations in liposomes are less intuitive than polymer-drug conjugations because it requires trial and error to develop appropriate gradients across the lipid bilayer. The gradient must be created in order for the drug to prefer the inner aqueous phase rather than the outer one, and the type of gradient required is unique for each drug, depending on its chemical properties. If the drug is basic, the liposome core should contain an excess of available protons, and vice versa. During our investigations, rather than modifying the well-established transmembrane ammonium sulfate gradient, we created pro-drugs of 5FU with proposed moieties to facilitate its compatibility with the gradient. We super-imposed chemical signatures required for encapsulation into an ammonium sulfate core onto a nucleobase analogue. While this required more methodological tests and troubleshooting compared to polymer-drug conjugations, it also resulted in double the encapsulation yields observed for HA-conjugates.

Conjugation of drugs to polymers, on the other hand, is more straightforward as simple chemical reactions can be applied to various drugs. The only prerequisite is that the drugs contain reactive chemical moieties, such as the nucleophilic hydroxyl and free amines found in CPT and DOX. Because this does not require methodological empirical studies for the introduction of a new drug, polymer-drug conjugates are more universal than liposomes, and provides a broader platform for high throughput testing of chemotherapy combinations. Combinations consisting of more than 2 drugs can also be conceivably incorporated in polymer-drug conjugates, while it would be considerably more challenging with liposomes. Incorporation is, however, limited by chemical reaction efficiency, which may require more

troubleshooting to improve. Another limitation of polymer-drug conjugates is poor size control. Unlike liposomes, which can be extruded to a certain size range, polymer-drug conjugations can result in polymer cross-linking or hydrophobic drug aggregates that cause size polydispersity. Because size can govern nanoparticle and hence drug fate *in vivo*, polydispersity can have immense ramifications on therapeutic efficacy. However, additional fabrication steps such as differential centrifugation and surfactant inclusion can be integrated with polymer-drug conjugates to control their size.

Lastly, stability is a greater issue with liposomes, as most incorporation methods rely on passively-loaded drugs, compared to polymer-bound drugs which are conjugated via strong chemical bonds. In our studies, four day storage at 4°C resulted greater liposome drug leakage than polymer-drug cleavage. This was evident in the reduction of liposome drug D_{50} after storage compared to that of polymer-conjugated drugs (Figure 6.7). Moreover, cryopreservation has been found in literature to prolong shelf-life of polymer-drug conjugates, but alters both size and drug encapsulation of liposomes. Therefore, to translate multi-drug loaded liposomes to clinically viable therapeutics, their shelf-life must be enhanced.

As evident from the discussion above, it is difficult to clearly say which nanoparticle is better for multi-drug delivery. Both liposomes and polymer-drug conjugates exhibit advantages where the other does not, and each of these advantages are detrimental for their clinical translation. Further studies to improve stability, size, and drug encapsulations will allow for better assessment. However, it is also probable that one nanoparticle is not truly better than the other for

combinatorial drug delivery. Through ester-conjugated tryptophan modifications, we have shown that a nucleobase analogue and doxorubicin can be simultaneously incorporated in liposomes. This method can be applied to all other nucleobase analogues, and may be a better fit for concurrent delivery than polymer-drug conjugates due to the high encapsulation yields. Drugs which possess nucleophilic moieties, however, may be readily conjugated to polymers and should be co-delivered via polymer-drug conjugates. We have shown that both types of vehicles are successful at inhibiting tumor growth *in vivo* when armed with a well-designed synergistic chemotherapy combination.

7.3. New methodology for developing combination chemotherapy nano-vehicles

Experiences from the development of two multi-drug loaded nanoparticles has led to a new proposed, and hopefully more efficient, methodology for combination chemotherapy drug delivery. Investigations of free drug combinations *in vitro* (Chapter 3) demonstrated that various drugs can be synergistic if exposed to cancer cells in the correct ratio. Studies with combinations of chemotherapy nanoparticles also suggested (Chapters 4 and 5) that the optimal synergistic R of single drug-loaded nanoparticles do not always correlate with those of free drugs. Liposome studies also elucidated the challenge of combining chemically distinct drugs in the same vehicle. To mediate these challenges, we propose that the development of combination chemotherapy nano-vehicles should start with synergy screens between single drug-loaded nanoparticles. These screens will allow for the

facile determination of optimal synergistic R, which can then be co-incorporated into a single nanoparticle.

By screening for synergy among single-drug nanoparticles, only combinations which can be easily co-loaded in drug carriers are considered. Therefore, only drugs whose pharmacokinetics can be unified, and whose concurrent accumulation in tumor tissue can be controlled will be assessed for combinations. Concurrent tumor exposure will ensure that both drug mechanisms of cancer cell kill will be activated simultaneously. This will also help mimic the *in vitro* concurrent drug exposure studies that often result in near perfect cell inhibition, and may help bridge the stark disconnect between *in vitro* and *in vivo* combination potency. Furthermore, the effect of differential drug release from nanoparticles is embedded in the synergy screen among single drug nano-vehicles. By testing various ratios of single drug nanoparticles for synergy, the differential drug release is already accounted for, and will not need to be further analyzed for impact on combination potency.

To clarify, however, this new approach does not suggest that all drugs which cannot be easily incorporated in nano-vehicles be excluded from combination studies. Drugs which exhibit poor encapsulation yields must first be developed to achieve high single drug nanoparticle incorporation. After these empirical studies, such as our 5FU analogue investigations, synergy screens among single drug-loaded nanoparticles can proceed. However, the feat of high single drug encapsulation must first be accomplished. Otherwise, encapsulation will need to be optimized after the identification of synergistic drug pairs, where the presence of the other drug may compound the challenge even further. Due to the numerous classes and chemical

variations of drugs, an infinite number of combinations to be investigated exists. It is our hope, that by imparting this new methodology for combination chemotherapy delivery, more efficient screens can be conducted, and lead to a more rapid discovery of successful therapies.

7.4. Extension of our approach

The remarkable therapeutic efficacies of polychemotherapy nano-vehicles developed here has ignited new and exciting prospects within the Mitragotri lab. New studies are assessing the effect of drug scheduling and order on combination potency, which can theoretically be tuned and achieved *in vivo* by certain linkers in polymer-drug conjugates. Targeting these potent, synergistic combinations specifically to tumors is also necessary as the combinations may be equally toxic to healthy tissue. Therefore, additional studies focus on conjugating drug pairs to aptamers which can specifically identify surface markers over-expressed on certain cancer cells. In this manner, the aptamer acts as a tumor-honing vehicle. A third effort is towards the development of nanoemulsions which can efficiently incorporate both hydrophobic and hydrophilic drugs. Nanoemulsions can be made to comprise other emulsions, and potentially create a large barrier for drug release, a greater barrier than is currently achievable for hydrophobic drugs embedded in the lipid bilayer of liposomes. By developing another vehicle for combination chemotherapy delivery, the repertoire of nanoparticles available for multi-drug delivery will expand and potentially encompass a wider variety of encapsulation methods to facilitate the assessment of even more chemotherapy combinations.

Outside of the Mitragotri lab, studies performed during my Ph.D. can help emphasize challenges that should be considered during future investigations of combination chemotherapies. First, identifying synergy should be prioritized, as antagonistic effects can result in poorer therapeutic efficacy in exchange for heightened adverse side effects - two outcomes which will automatically, and possibly falsely, negate the combination. Ratio can govern synergistic interactions and must be assessed amongst mixtures of single drug-loaded nanoparticles; free drug combination studies will not suffice, as nanoparticle encapsulation can alter the optimal R. Lastly, trial and error of drug encapsulations here elucidate common challenges in multi-drug delivery, such as the development of pro-drugs or optimal chemical linkers. While only liposomes and polymer-drug conjugates were explored, the lessons learnt have wide applicability to other systems and provide immense insight into the general development of nanoparticles for combination chemotherapies.

References

1. American Cancer, S., *A Guide to Cancer Surgery* S. American Cancer, Editor. 2014: http://www.cancer.org.
2. American Cancer, S., *Radiation Therapy What It Is, How It Helps*, S. American Cancer, Editor. 2014: http://www.cancer.org.
3. American Cancer, S., *Chemotherapy What It Is, How It Helps* S. American Cancer, Editor. 2013: http://www.cancer.org.
4. Matsumura, Y. and H. Maeda, *A new concept for macromolecular therapeutics in cancer chemotherapy: mechanism of tumoritropic accumulation of proteins and the antitumor agent smancs*. Cancer research, 1986. **46**(12 Part 1): p. 6387-6392.
5. Brannon-Peppas, L. and J.O. Blanchette, *Nanoparticle and targeted systems for cancer therapy*. Advanced drug delivery reviews, 2004. **56**(11): p. 1649-59.
6. Devita Jr, V.T., R.C. Young, and G.P. Canellos, *Combination versus single agent chemotherapy: a review of the basis for selection of drug treatment of cancer*. Cancer, 1975. **35**(1): p. 98-110.
7. Frei, E., E.J. Freireich, and E. Gehan, *Studies of sequential and combination antimetabolite therapy in acute leukemia: 6-mercaptopurine and methotrexate*. blood, 1961. **18**: p. 431-454.
8. Vanhoefer, U. and P. Rougier, *Final results of a randomized phase III trial of sequential high-dose methotrexate, fluorouracil, and doxorubicin versus etoposide, leucovorin, and fluorouracil versus*. Journal of Clinical Oncology, 2000. **18**(14): p. 2648-2657.
9. Xenidis, N., et al., *A multicenter phase II study of pegylated liposomal doxorubicin in combination with irinotecan as second-line treatment of patients with refractory small-cell lung cancer*. Cancer chemotherapy and pharmacology, 2011. **68**(1): p. 63-8.
10. Chan, S., et al., *Phase III study of gemcitabine plus docetaxel compared with capecitabine plus docetaxel for anthracycline-pretreated patients with metastatic breast cancer*. Journal of Clinical Oncology, 2009. **27**(11): p. 1753-60.
11. Gehl, J., et al., *Combined doxorubicin and paclitaxel in advanced breast cancer: effective and cardiotoxic*. Annals of oncology, 1996. **7**(7): p. 687-687.
12. Joensuu, H., et al., *Combination chemotherapy versus single-agent therapy as first- and second-line treatment in metastatic breast cancer: a prospective randomized trial*. Journal of Clinical Oncology, 1998. **16**(12): p. 3720-3720.
13. Carrick, S., et al., *Single agent versus combination chemotherapy for metastatic breast cancer (Review)*. The Cochrane Library, 2009(1).
14. Gabizon, A., et al., *Prolonged circulation time and enhanced accumulation in malignant exudates of doxorubicin encapsulated in polyethylene-glycol coated liposomes*. Cancer Research, 1994. **54**: p. 987-992.

15. Gottlieb, J.A., et al., *Preliminary pharmacologic and clinical evaluation of camptothecin sodium (NSC-100880).* Cancer chemotherapy reports. Part 1, 1970. **54**(6): p. 461.
16. Buzzoni, R., et al., *Adjuvant chemotherapy with doxorubicin plus cyclophosphamide, methotrexate, and fluorouracil in the treatment of resectable breast cancer with more than three positive axillary nodes.* Journal of clinical oncology : official journal of the American Society of Clinical Oncology, 1991. **9**(12): p. 2134-40.
17. Kuenen, B.C., L. Rosen, and E.F. Smit, *Dose-finding and pharmacokinetic study of cisplatin, gemcitabine, and SU5416 in patients with solid tumors.* Journal of Clinical Oncology, 2002. **20**(6): p. 1657-1667.
18. Holmes, F.A., T. Madden, and R.A. Newman, *Sequence-dependent alteration of doxorubicin pharmacokinetics by paclitaxel in a phase I study of paclitaxel and doxorubicin in patients with metastatic breast cancer.* Journal of Clinical Oncology, 1996. **14**(10): p. 2713-2721.
19. Li, S.D. and L. Huang, *Pharmacokinetics and biodistribution of nanoparticles.* Molecular Pharmaceutics, 2008. **5**(4): p. 496-504.
20. Cho, K., et al., *Therapeutic nanoparticles for drug delivery in cancer.* Clinical Cancer Research, 2008. **14**(5): p. 1310-6.
21. Soo Choi, H., et al., *Renal clearance of quantum dots.* Nat Biotech, 2007. **25**(10): p. 1165-1170.
22. Hu, C.M.J. and S. Aryal, *Nanoparticle-assisted combination therapies for effective cancer treatment*. Therapeutic Delivery, 2010. **1**(2): p. 323-334.
23. Liboiron, B.D., et al., *Nanoscale Delivery Systems for Combination Chemotherapy*. 2012, Wiley-VCH Verlag GmbH & Co. KGaA: Weinheim, Germany. p. 1013-1050.
24. Feldman, E.J., et al., *First-in-man study of CPX-351: a liposomal carrier containing cytarabine and daunorubicin in a fixed 5:1 molar ratio for the treatment of relapsed and refractory acute myeloid leukemia.* Journal of clinical oncology : official journal of the American Society of Clinical Oncology, 2011. **29**(8): p. 979-85.
25. Lammers, T., et al., *Simultaneous delivery of doxorubicin and gemcitabine to tumors in vivo using prototypic polymeric drug carriers.* Biomaterials, 2009. **30**(20): p. 3466-75.
26. Maleki, A., A.-L. Kjøniksen, and B. Nyström, *Effect of pH on the Behavior of Hyaluronic Acid in Dilute and Semidilute Aqueous Solutions.* Macromolecular Symposia, 2008. **274**(1): p. 131-140.
27. Duncan, R., *Polymer conjugates as anticancer nanomedicines.* Nature Reviews Cancer, 2006. **6**(9): p. 688-701.
28. Barenholz, Y., *Doxil®--the first FDA-approved nano-drug: lessons learned.* Journal of Controlled Release, 2012. **160**(2): p. 117-34.
29. Davis, M.E., *Design and development of IT-101, a cyclodextrin-containing polymer conjugate of camptothecin.* Advanced drug delivery reviews, 2009. **61**(13): p. 1189-92.

30. Duncan, R., *Development of HPMA copolymer-anticancer conjugates: clinical experience and lessons learnt*. Advanced drug delivery reviews, 2009. **61**(13): p. 1131-48.
31. Chou, T.C. and P. Talalay, *Quantitative analysis of dose-effect relationships: the combined effects of multiple drugs or enzyme inhibitors*. Advances in enzyme regulation, 1984. **22**: p. 27-55.
32. Szoka Jr, F. and D. Papahadjopoulos, *Comparative properties and methods of preparation of lipid vesicles (liposomes)*. Annual review of biophysics and bioengineering, 1980. **9**(1): p. 467-508.
33. Greco, W.R., G. Bravo, and J.C. Parsons, *The search for synergy: a critical review from a response surface perspective*. Pharmacological Reviews, 1995. **47**(2): p. 331-331.
34. American Cancer, S., *Cancer Facts & Figures 2015*. 2015, American Cancer Socity: http://www.cancer.org.
35. Miles, D., et al., *Survival Benefit with Capecitabine/Docetaxel Versus Docetaxel Alone: Analysis of Therapy in a Randomized Phase III Trial*. Clinical Breast Cancer, 2004. **5**(4): p. 273-278.
36. O'Shaughnessy, J., *Superior Survival With Capecitabine Plus Docetaxel Combination Therapy in Anthracycline-Pretreated Patients With Advanced Breast Cancer: Phase III Trial Results*. Journal of Clinical Oncology, 2002. **20**(12): p. 2812-2823.
37. Johnston, S., et al., *Lapatinib combined with letrozole versus letrozole and placebo as first-line therapy for postmenopausal hormone receptor-positive metastatic breast cancer*. Journal of clinical oncology : official journal of the American Society of Clinical Oncology, 2009. **27**(33): p. 5538-46.
38. Bonadonna, G., et al., *Adjuvant cyclophosphamide, methotrexate, and fluorouracil in node-positive breast cancer—the results of 20 years of follow-up*. New England Journal of Medicine, 1995. **332**(14): p. 901-906.
39. Mu, C.-F., et al., *The effects of mixed MPEG-PLA/Pluronic copolymer micelles on the bioavailability and multidrug resistance of docetaxel*. Biomaterials, 2010. **31**(8): p. 2371-9.
40. Gangemi, R.M., et al., *Late apoptotic effects of taxanes on K562 erythroleukemia cells: apoptosis is delayed upstream of caspase-3 activation*. International Journal of Cancer, 2000. **85**(4): p. 527-33.
41. Fabbri, F., et al., *Sequential events of apoptosis involving docetaxel, a microtubule-interfering agent: a cytometric study*. BMC cell biology, 2006. **7**(6).
42. Budman, D.R. and A. Calabro, *Zoledronic acid (Zometa) enhances the cytotoxic effect of gemcitabine and fluvastatin: in vitro isobologram studies with conventional and nonconventional cytotoxic agents*. Oncology, 2006. **70**(2): p. 147-53.
43. Zhang, D., et al., *Activity of lapatinib is independent of EGFR expression level in HER2-overexpressing breast cancer cells*. Molecular Cancer Therapeutics, 2008. **7**(7): p. 1846-50.

44. Chen, X., T.K. Yeung, and Z. Wang, *Enhanced drug resistance in cells coexpressing ErbB2 with EGF receptor or ErbB3*. Biochemical and Biophysical Research Communications, 2000. **277**(3): p. 757-63.
45. American Cancer, S., *Breast Cancer Facts & Figures 2013-2014*, S. American Cancer, Editor. 2013: http://www.cancer.gov.
46. Liu, Y., et al., *Codelivery of Doxorubicin and Paclitaxel by Crosslinked Multilamellar Liposome Enables Synergistic Antitumor Activity*. Molecular pharmaceutics, 2014. **11**: p. 1651-1661.
47. Tardi, P., et al., *In vivo maintenance of synergistic cytarabine:daunorubicin ratios greatly enhances therapeutic efficacy*. Leukemia research, 2009. **33**(1): p. 129-39.
48. Mayer, L.D., et al., *Ratiometric dosing of anticancer drug combinations: controlling drug ratios after systemic administration regulates therapeutic activity in tumor-bearing mice*. Molecular Cancer Therapeutics, 2006. **5**(7): p. 1854-63.
49. Shaikh, I.M., et al., *Liposome co-encapsulation of synergistic combination of irinotecan and doxorubicin for the treatment of intraperitoneally grown ovarian tumor xenograft*. Journal of controlled release : official journal of the Controlled Release Society, 2013. **172**(3): p. 852-861.
50. Gabizon, a. and D. Papahadjopoulos, *The role of surface charge and hydrophilic groups on liposome clearance in vivo*. Biochimica et biophysica acta, 1992. **1103**(1): p. 94-100.
51. Owens, D.E. and N.a. Peppas, *Opsonization, biodistribution, and pharmacokinetics of polymeric nanoparticles*. International journal of pharmaceutics, 2006. **307**(1): p. 93-102.
52. Peters, G.J., et al., *Sensitivity of human, murine, and rat cells to 5-fluorouracil and 5′-deoxy-5-fluorouridine in relation to drug-metabolizing enzymes*. Cancer research, 1986. **46**(1): p. 20-28.
53. Wang, S., et al., *Doxorubicin induces apoptosis in normal and tumor cells via distinctly different mechanisms. intermediacy of H(2)O(2)- and p53-dependent pathways*. The Journal of biological chemistry, 2004. **279**(24): p. 25535-43.
54. Efferth, T., et al., *Artesunate Induces ROS-Mediated Apoptosis in Doxorubicin-Resistant T Leukemia Cells*. PLoS ONE, 2007. **2**(8): p. e693.
55. Mookerjee, A., et al., *A novel copper complex induces ROS generation in doxorubicin resistant Ehrlich ascitis carcinoma cells and increases activity of antioxidant enzymes in vital organs in vivo*. BMC cancer, 2006. **6**(1): p. 267.
56. Lewin, F., et al., *Effect of 5-fluorouracil on the cell growth and cell cycle kinetics of a mouse ascites tumor growing in vivo*. Acta Oncologica, 1987. **26**(2): p. 125-131.
57. Mirjolet, J.F., et al., *G(1)/S but not G(0)/G(1)cell fraction is related to 5-fluorouracil cytotoxicity*. Cytometry, 2002. **48**(1): p. 6-13.
58. Li, M.-H., et al., *Effect of 5-fluorouracil on G1 phase cell cycle regulation in oral cancer cell lines*. Oral oncology, 2004. **40**(1): p. 63-70.

59. Yoshiba, S., et al., *Hypoxia induces resistance to 5-fluorouracil in oral cancer cells via G 1 phase cell cycle arrest*. Oral oncology, 2009. **45**(2): p. 109-115.
60. Ling, Y.H., et al., *Cell cycle-dependent cytotoxicity, G2/M phase arrest, and disruption of p34cdc2/cyclin B1 activity induced by doxorubicin in synchronized P388 cells*. Molecular pharmacology, 1996.
61. Longley, D.B. and P.G. Johnston, *5-Fluorouracil: Molecular Mechanisms of Cell Death*. 2007, Human Press Inc.: Totawa, NJ. p. 263-278.
62. Tyagi, A.K., et al., *Silibinin strongly synergizes human prostate carcinoma DU145 cells to doxorubicin-induced growth Inhibition, G2-M arrest, and apoptosis*. Clinical Cancer Research, 2002. **8**(11): p. 3512-3519.
63. Wils, J.A. and H.O. Klein, *Methotrexate and fluorouracil combined with doxorubicin--a step ahead in the treatment of advanced gastric cancer: a trial of the European Organization for Research*. Journal of Clinical ..., 1991. **9**(5): p. 827-831.
64. Murad, a.M., et al., *Modified therapy with 5-fluorouracil, doxorubicin, and methotrexate in advanced gastric cancer*. Cancer, 1993. **72**(1): p. 37-41.
65. Levi, J.A., et al., *Analysis of a prospectively randomized comparison of doxorubicin versus 5-fluorouracil, doxorubicin, and BCNU in advanced gastric cancer: implications for future studies*. Journal of Clinical Oncology, 1986. **4**(9): p. 1348-1355.
66. Cazap, E., et al., *Phase II trials of 5-FU, doxorubicin, and cisplatin in advanced, measurable adenocarcinoma of the lung and stomach*. Cancer treatment reports, 1986. **70**(6): p. 781-783.
67. Klein, H.O., M. Buyse, and J.A. Wils, *Prospective randomized trial using 5-fluorouracil, adriamycin and methotrexate (FAMTX) versus FAM for treatment of advanced gastric cancer*. Oncology Research and Treatment, 1992. **15**: p. 364-367.
68. Webb, A. and D. Cunningham, *Randomized trial comparing epirubicin, cisplatin, and fluorouracil versus fluorouracil, doxorubicin, and methotrexate in advanced esophagogastric cancer*. Journal of Clinical Oncology, 1997. **15**(1): p. 261-267.
69. Cullinan, S.A., et al., *A comparison of three chemotherapeutic regimens in the treatment of advanced pancreatic and gastric carcinoma: fluorouracil vs fluorouracil and doxorubicin vs fluorouracil, doxorubicin, and mitomycin*. Jama, 1985. **253**(14): p. 2061-2067.
70. Hortobagyi, G.N. and G.P. Bodey, *Evaluation of high-dose versus standard FAC chemotherapy for advanced breast cancer in protected environment units: a prospective randomized study*. Journal of Clinical ..., 1987. **5**(3): p. 354-364.
71. Gabra, H., D.A. Cameron, and L.E. Lee, *Weekly doxorubicin and continuous infusional 5-fluorouracil for advanced breast cancer*. British journal of cancer, 1996. **74**: p. 2008-2012.
72. Krauze, M.T., et al., *Convection-enhanced delivery of nanoliposomal CPT-11 (irinotecan) and PEGylated liposomal doxorubicin (Doxil) in rodent intracranial brain tumor xenografts*. Neuro-oncology, 2007. **9**(4): p. 393-403.

73. Shaikh, I.M., et al., *Liposome co-encapsulation of synergistic combination of irinotecan and doxorubicin for the treatment of intraperitoneally grown ovarian tumor xenograft*. Journal of Controlled Release, 2013. **172**(3): p. 852-861.
74. Hanada, M., T. Noguchi, and T. Yamaoka, *Amrubicin, a novel 9-aminoanthracycline, enhances the antitumor activity of chemotherapeutic agents against human cancer cells in vitro and in vivo*. Cancer science, 2007. **98**(3): p. 447-54.
75. Takigawa, N., et al., *The combination effect of amrubicin with cisplatin or irinotecan for small-cell lung cancer cells*. 2006: p. 837-842.
76. Barua, S. and S. Mitragotri, *Synergistic targeting of cell membrane, cytoplasm, and nucleus of cancer cells using rod-shaped nanoparticles*. ACS nano, 2013. **7**(11): p. 9558-70.
77. Sugimoto, Y., et al., *Elevated expression of DNA topoisomerase II in camptothecin-resistant human tumor cell lines*. Cancer research, 1990. **50**: p. 7962-7965.
78. Oguro, M., et al., *Collateral drug sensitivity induced in CPT-11 (a novel derivative of camptothecin)-resistant cell lines*. Biomedicine & pharmacotherapy, 1990. **44**: p. 209-216.
79. Hotta, K., et al., *Phase I Study of Irinotecan and Amrubicin in Patients with Advanced Non-Small-Cell Lung Cancer*. 2005. **2434**: p. 2429-2434.
80. Ryan, C.W., et al., *A phase I study of liposomal doxorubicin (Doxil) with topotecan*. American journal of clinical oncology, 2000. **23**(3): p. 297-300.
81. Goff, L.W., et al., *A phase I trial of irinotecan alternating with epirubicin in patients with advanced malignancies*. American journal of clinical oncology, 2008. **31**(5): p. 413-6.
82. Harada, T., et al., *A phase I/II trial of irinotecan plus amrubicin supported with G-CSF for extended small-cell lung cancer*. Japanese journal of clinical oncology, 2014. **44**(2): p. 127-33.
83. Oshita, F., H. Saito, and K. Yamada, *Dose escalation study of amrubicin in combination with fixed-dose irinotecan in patients with extensive small-cell lung cancer*. Oncology, 2008. **74**(1-2): p. 7-11.
84. Slichenmyer, W.J., *The current status of camptothecin analogues as antitumor agents*. Journal of the ..., 1993. **85**(4): p. 271-291.
85. Guarino, A., et al., *Pharmacologic studies of camptothecin (NSC-100880): distribution, plasma protein binding, and biliary excretion*. Cancer chemotherapy reports. Part 1, 1973. **57**(2): p. 125-140.
86. Moertel, C.G., et al., *Phase II study of camptothecin (NSC-100880) in the treatment of advanced gastrointestinal cancer*. Cancer chemotherapy reports. Part 1, 1972. **56**(1): p. 95.
87. Kaneda, N., et al., *Metabolism and pharmacokinetics of the camptothecin analogue CPT-11 in the mouse*. Cancer research, 1990. **50**(6): p. 1715-1720.
88. Erickson-Miller, C.L., et al., *Differential toxicity of camptothecin, topotecan and 9-aminocamptothecin to human, canine, and murine myeloid progenitors (CFU-GM) in vitro*. Cancer chemotherapy and pharmacology, 1997. **39**(5): p. 467-472.

89. Pavillard, V., et al., *Effects of the combination of camptothecin and doxorubicin or etoposide on rat glioma cells and camptothecin-resistant variants*. British journal of cancer, 2001. **85**(7): p. 1077-83.
90. Budman, D.R. and A. Calabro, *In vitro search for synergy and antagonism: evaluation of docetaxel combinations in breast cancer cell lines*. Breast Cancer Research and Treatment, 2002. **74**(1): p. 41-6.
91. Budman, D.R., A. Calabro, and W. Kreis, *In vitro evaluation of synergism or antagonism with combinations of new cytotoxic agents*. Anti-cancer drugs, 1998. **9**(8): p. 697-697.
92. Clements, M.K., S. Wasi, and S.S. Daoud, *Camptothecin exhibits selective cytotoxicity towards human breast carcinoma as compared to normal bovine endothelial cells in vitro*. Anti-cancer drugs, 1996.
93. Jones, C.B. and K. Clements, *Sensitivity to camptothecin of human breast carcinoma and normal endothelial cells*. 1997: p. 475-483.
94. Morgensztern, D., et al., *A phase I study of pegylated liposomal doxorubicin and irinotecan in patients with solid tumors*. Chemotherapy, 2009. **55**(6): p. 441-5.
95. Nishimura, S., et al., *Phase II study of irinotecan plus doxorubicin for early recurrent or platinum-refractory ovarian cancer: interim analysis*. International journal of gynecological cancer : official journal of the International Gynecological Cancer Society, 2007. **17**(1): p. 159-63.
96. Macdonald, J.S., *5-Fluorouracil, doxorubicin, and mitomycin (FAM) combination chemotherapy for advanced gastric cancer*. Annals of internal medicine, 1980. **93**: p. 533-536.
97. Slingerland, M., H.-J. Guchelaar, and H. Gelderblom, *Liposomal drug formulations in cancer therapy: 15 years along the road*. Drug discovery today, 2012. **17**(3): p. 160-166.
98. Torchilin, V.P., *Recent advances with liposomes as pharmaceutical carriers*. Nature reviews. Drug discovery, 2005. **4**(2): p. 145-60.
99. Bangham, A.D., *Surrogate cells or Trojan horses. The discovery of liposomes*. BioEssays, 1995. **17**(12): p. 1081-1088.
100. Lyass, O., et al., *Correlation of toxicity with pharmacokinetics of pegylated liposomal doxorubicin (Doxil) in metastatic breast carcinoma*. Cancer, 2000. **89**(5): p. 1037-47.
101. Safra, T., et al., *Pegylated liposomal doxorubicin (doxil): Reduced clinical cardiotoxicity in patients reaching or exceeding cumulative doses of 500 mg/m2*. Annals of Oncology, 2000. **11**(8): p. 1029-1033.
102. Muggia, F.M., et al., *Phase II study of liposomal doxorubicin in refractory ovarian cancer: antitumor activity and toxicity modification by liposomal encapsulation*. Journal of Clinical Oncology, 1997. **15**(3): p. 987-993.
103. Maurer, N., D.B. Fenske, and P.R. Cullis, *Developments in liposomal drug delivery systems*. Expert opinion on ..., 2001: p. 1-25.
104. Levchenko, T.S. and R. Rammohan, *Liposome clearance in mice: the effect of a separate and combined presence of surface charge and polymer coating*. International journal of ..., 2002. **240**: p. 95-102.

105. Judson, I., et al., *Randomised phase II trial of pegylated liposomal doxorubicin (DOXIL®/CAELYX®) versus doxorubicin in the treatment of advanced or metastatic soft tissue sarcoma: a study by the EORTC Soft Tissue and Bone Sarcoma Group*. European Journal of Cancer, 2001. **37**(7): p. 870-877.
106. O'Brien, M.E.R., N. Wigler, and M. Inbar, *Reduced cardiotoxicity and comparable efficacy in a phase III trial of pegylated liposomal doxorubicin HCl (CAELYXTM/Doxil") versus conventional doxorubicin for first-line treatment of metastatic breast cancer*. Annals of Oncology, 2004. **15**(3): p. 440-449.
107. Ellerhorst, J., et al., *Phase II trial of doxil for patients with metastatic melanoma refractory to frontline therapy*. Oncology reports, 1999. **6**(5): p. 1097-1106.
108. Halford, S., et al., *A phase II study evaluating the tolerability and efficacy of CAELYX (liposomal doxorubicin, Doxil) in the treatment of unresectable pancreatic carcinoma*. Annals of Oncology, 2001. **12**(10): p. 1399-1402.
109. Muggia, F.M., et al., *Phase II trial of the pegylated liposomal doxorubicin in previously treated metastatic endometrial cancer: a Gynecologic Oncology Group study*. Journal of clinical oncology, 2002. **20**(9): p. 2360-2364.
110. Mayer, L.D., et al., *Influence of vesicle size, lipid composition, and drug-to-lipid ratio on the biological activity of liposomal doxorubicin in mice*. Cancer research, 1989. **49**: p. 5922-5930.
111. Cabanes, A., D. Tzemach, and D. Goren, *Comparative study of the antitumor activity of free doxorubicin and polyethylene glycol-coated liposomal doxorubicin in a mouse lymphoma model.* Clinical Cancer Research, 1998. **4**: p. 499-505.
112. Barenholz, Y., *Liposome application: problems and prospects*. Current opinion in colloid & interface science, 2001. **6**(1): p. 66-77.
113. Zhao, Y., et al., *A simple way to enhance Doxil® therapy: drug release from liposomes at the tumor site by amphiphilic block copolymer*. Journal of Controlled Release, 2013. **168**(1): p. 61-69.
114. Bennett, C.F., et al., *Cationic lipids enhance cellular uptake and activity of phosphorothioate antisense oligonucleotides*. Molecular Pharmacology, 1992. **41**(6): p. 1023-1033.
115. Zelphati, O. and F.C. Szoka, *Mechanism of oligonucleotide release from cationic liposomes*. Proceedings of the National Academy of Sciences of the United States of America, 1996. **93**(21): p. 11493-8.
116. Wrobel, I. and D. Collins, *Fusion of cationic liposomes with mammalian cells occurs after endocytosis*. Biochimica et Biophysica Acta (BBA) - Biomembranes, 1995. **1235**(2): p. 296-304.
117. Friend, D.S., D. Papahadjopoulos, and R.J. Debs, *Endocytosis and intracellular processing accompanying transfection mediated by cationic liposomes*. Biochimica et Biophysica Acta (BBA) - Biomembranes, 1996. **1278**(1): p. 41-50.
118. Liu, Y., et al., *Factors influencing the efficiency of cationic liposome-mediated intravenous gene delivery*. Nat Biotech, 1997. **15**(2): p. 167-173.

119. Xu, Y. and F.C. Szoka, *Mechanism of DNA release from cationic liposome/DNA complexes used in cell transfection*. Biochemistry, 1996. **2960**(96): p. 5616-5623.
120. Zhou, X. and L. Huang, *DNA transfection mediated by cationic liposomes containing lipopolylysine: characterization and mechanism of action*. Biochimica et Biophysica Acta (BBA) - Biomembranes, 1994. **1189**(2): p. 195-203.
121. Filion, M.C. and N.C. Phillips, *Toxicity and immunomodulatory activity of liposomal vectors formulated with cationic lipids toward immune effector cells*. Biochimica et Biophysica Acta (BBA) - Biomembranes, 1997. **1329**(2): p. 345-356.
122. Thurston, G., et al., *Cationic liposomes target angiogenic endothelial cells in tumors and chronic inflammation in mice*. The Journal of clinical investigation, 1998. **101**(7): p. 1401-13.
123. Kalra, A.V. and R.B. Campbell, *Development of 5-FU and doxorubicin-loaded cationic liposomes against human pancreatic cancer: Implications for tumor vascular targeting*. Pharmaceutical research, 2006. **23**(12): p. 2809-17.
124. Campbell, R.B., D. Fukumura, and E.B. Brown, *Cationic charge determines the distribution of liposomes between the vascular and extravascular compartments of tumors*. Cancer Research, 2002. **62**: p. 6831-6836.
125. Ouchi, T., H. Kobayashi, and T. Banba, *Design of poly (α-malic acid)-5FU conjugate exhibiting antitumor activity*. Reactive Polymers, 1992. **15**: p. 153-163.
126. Costa, C.A.M.D. and A.M. Moraes, *Encapsulation of 5-fluorouracil in liposomes for topical administration*. Acta Sci Technol, 2003(1): p. 53-61.
127. Haran, G., et al., *Transmembrane ammonium sulfate gradients in liposomes produce efficient and stable entrapment of amphipathic weak bases*. Biochimica et biophysica acta, 1993. **1151**(2): p. 201-15.
128. Barenholz, Y., et al., *Stability of liposomal doxorubicin formulations: problems and prospects*. Medicinal research reviews, 1993. **13**(4): p. 449-491.
129. Kaiser, N., et al., *5-Fluorouracil in vesicular phospholipid gels for anticancer treatment: entrapment and release properties*. International Journal of Pharmaceutics, 2003. **256**(1-2): p. 123-131.
130. Markova, N., V. Enchev, and G. Ivanova, *Tautomeric equilibria of 5-fluorouracil anionic species in water*. The journal of physical chemistry. A, 2010. **114**(50): p. 13154-62.
131. Klibanov, A.L. and K. Maruyama, *Activity of amphipathic poly (ethylene glycol) 5000 to prolong the circulation time of liposomes depends on the liposome size and is unfavorable for immunoliposome*. Biochimica et Biophysica Acta (BBA), 1991. **1062**: p. 142-148.
132. Diasio, R.B. and B.E. Harris, *Clinical pharmacology of 5-fluorouracil*. Clinical pharmacokinetics, 1989.
133. Unezaki, S., K. Maruyama, and O. Ishida, *Enhanced tumor targeting and improved antitumor activity of doxorubicin by long-circulating liposomes containing amphipathic poly (ethylene glycol)*. International Journal of Pharmaceutics, 1995. **126**: p. 41-48.

134. Sun, Y., et al., *Bioreducible PAA-g-PEG graft micelles with high doxorubicin loading for targeted antitumor effect against mouse breast carcinoma.* Biomaterials, 2013. **34**(28): p. 6818-28.
135. Charrois, G.J.R. and T.M. Allen, *Multiple injections of pegylated liposomal doxorubicin: pharmacokinetics and therapeutic activity.* Journal of Pharmacology and Experimental Therapeutics, 2003. **306**(3): p. 1058-1067.
136. Du, G., et al., *Quercetin greatly improved therapeutic index of doxorubicin against 4T1 breast cancer by its opposing effects on HIF-1α in tumor and normal cells.* Cancer chemotherapy and pharmacology, 2010. **65**(2): p. 277-287.
137. Bandyopadhyay, A., et al., *Doxorubicin in combination with a small TGFbeta inhibitor: a potential novel therapy for metastatic breast cancer in mouse models.* PLOS ONE, 2010. **5**(4): p. e10365-e10365.
138. Wang, H., et al., *Dexamethasone as a chemosensitizer for breast cancer chemotherapy: potentiation of the antitumor activity of adriamycin, modulation of cytokine expression, and pharmacokinetics.* International journal of oncology, 2007. **30**(4): p. 947-953.
139. Wang, J., et al., *Star-shape copolymer of lysine-linked di-tocopherol polyethylene glycol 2000 succinate for doxorubicin delivery with reversal of multidrug resistance.* Biomaterials, 2012. **33**(28): p. 6877-6888.
140. Liu, C.-M., et al., *Comparison of the therapeutic efficacy of 188Rhenium-liposomes and liposomal doxorubicin in a 4T1 murine orthotopic breast cancer model.* Oncology reports, 2012. **27**(3): p. 678-684.
141. Mastria, E.M., et al., *Doxorubicin-conjugated polypeptide nanoparticles inhibit metastasis in two murine models of carcinoma.* Journal of Controlled Release, 2015. **208**: p. 52-58.
142. Yang, T., et al., *Antitumor effect of paclitaxel-loaded PEGylated immunoliposomes against human breast cancer cells.* Pharmaceutical research, 2007. **24**(12): p. 2402-11.
143. Riondel, J., M. Jacrot, and F. Picot, *Therapeutic response to taxol of six human tumors xenografted into nude mice.* Cancer chemotherapy ..., 1986. **17**: p. 137-142.
144. Yang, Y., et al., *Biodegradable and amphiphilic block copolymer–doxorubicin conjugate as polymeric nanoscale drug delivery vehicle for breast cancer therapy.* Biomaterials, 2013. **34**(33): p. 8430-8443.
145. Thomas, A.M., et al., *Development of a liposomal nanoparticle formulation of 5-fluorouracil for parenteral administration: Formulation design, pharmacokinetics and efficacy.* Journal of Controlled Release, 2011. **150**(2): p. 212-9.
146. Lammers, T., et al., *Effect of physicochemical modification on the biodistribution and tumor accumulation of HPMA copolymers.* Journal of controlled release : official journal of the Controlled Release Society, 2005. **110**(1): p. 103-18.
147. Sadekar, S., et al., *Comparative biodistribution of PAMAM dendrimers and HPMA copolymers in ovarian-tumor-bearing mice.* Biomacromolecules, 2011. **12**(1): p. 88-96.

148. Tabata, Y., Y. Murakami, and Y. Ikada, *Tumor accumulation of poly(vinyl alcohol) of different sizes after intravenous injection*. Journal of controlled release : official journal of the Controlled Release Society, 1998. **50**(1-3): p. 123-33.
149. Kopecek, J., et al., *Water soluble polymers in tumor targeted delivery*. Journal of controlled release : official journal of the Controlled Release Society, 2001. **74**(1-3): p. 147-58.
150. Young, C., et al., *CRLX101 (formerly IT-101)– A Novel Nanopharmaceutical of Camptothe- cin in Clinical Development*. 2011. **101**: p. 8-14.
151. Vasey, P.A., et al., *Phase I clinical and pharmacokinetic study of PK1 [N-(2-hydroxypropyl) methacrylamide copolymer doxorubicin]: first member of a new class of chemotherapeutic agents—drug-polymer conjugates*. Clinical Cancer Research, 1999. **5**(1): p. 83-94.
152. Dvorák, M., P. Kopecková, and J. Kopecek, *High-molecular weight HPMA copolymer-adriamycin conjugates*. Journal of controlled release : official journal of the Controlled Release Society, 1999. **60**(2-3): p. 321-32.
153. Cheng, J., et al., *Synthesis of linear, β-cyclodextrin-based polymers and their camptothecin conjugates*. Bioconjugate chemistry, 2003. **14**(5): p. 1007-1017.
154. Sánchez-Chaves, M., F. Arranz, and M. Cortazar, *Poly (vinyl alcohol) functionalized by monosuccinate groups. Coupling of bioactive amino compounds*. Polymer, 1998. **39**(13): p. 2751-2757.
155. Orjuela, A., et al., *Diethyl succinate synthesis by reactive distillation*. Separation and Purification Technology, 2012. **88**: p. 151-162.
156. Seymour, L.W. and R. Duncan, *Effect of molecular weight (Mw) of N-(2-hydroxypropyl) methacrylamide copolymers on body distribution and rate of excretion after subcutaneous, intraperitoneal, and*. Journal of biomedical ..., 1987. **21**: p. 1341-1358.
157. Sugahara, S.S., et al., *Characteristics of Tissue Distribution of Various Polysaccharides as Drug Carriers : Influences of Molecular Weight and Anionic Charge on Tumor Targeting*. 2001. **24**(May).
158. Seymour, L.W., et al., *Influence of molecular weight on passive tumour accumulation of a soluble macromolecular drug carrier*. European journal of cancer, 1995. **31A**(5): p. 766-770.
159. Park, K., et al., *Effect of polymer molecular weight on the tumor targeting characteristics of self-assembled glycol chitosan nanoparticles*. Journal of Controlled Release, 2007. **122**(3): p. 305-314.
160. Platt, V.M. and F.C.S. Jr, *Anticancer therapeutics: targeting macromolecules and nanocarriers to hyaluronan or CD44, a hyaluronan receptor*. Molecular pharmaceutics, 2008(1): p. 36777-36781.
161. Journo-Gershfeld, G., et al., *Hyaluronan oligomers-HPMA copolymer conjugates for targeting paclitaxel to CD44-overexpressing ovarian carcinoma*. Pharmaceutical research, 2012. **29**(4): p. 1121-33.
162. Choi, K.Y., et al., *Self-assembled hyaluronic acid nanoparticles for active tumor targeting*. Biomaterials, 2010. **31**(1): p. 106-14.

163. Lee, H., K. Lee, and T.G. Park, *Hyaluronic acid-paclitaxel conjugate micelles: synthesis, characterization, and antitumor activity*. Bioconjugate chemistry, 2008. **19**(6): p. 1319-25.
164. Minko, T., P. Kopecková, and J. Kopecek, *Efficacy of the chemotherapeutic action of HPMA copolymer-bound doxorubicin in a solid tumor model of ovarian carcinoma*. International journal of cancer. Journal international du cancer, 2000. **86**(1): p. 108-17.
165. Pulaski, B.A., et al., *Mouse 4T1 breast tumor model*. Current protocols in Immunology, 2001. **20**(2): p. 1-16.
166. Fantozzi, A. and G. Christofori, *Mouse models of breast cancer metastasis*. Breast cancer research : BCR, 2006. **8**(4): p. 212-212.
167. Amaravadi, R.K. and C.B. Thompson, *The roles of therapy-induced autophagy and necrosis in cancer treatment*. Clinical cancer research : an official journal of the American Association for Cancer Research, 2007. **13**(24): p. 7271-9.
168. Kiaris, H. and A.V. Schally, *Apoptosis versus necrosis: which should be the aim of cancer therapy?* Experimental Biology and Medicine, 1999: p. 87-88.
169. Ottewell, P.D., et al., *Antitumor effects of doxorubicin followed by zoledronic acid in a mouse model of breast cancer*. Journal of the National Cancer Institute, 2008. **100**(16): p. 1167-78.
170. Chen, Y., et al., *Multifunctional nanoparticles delivering small interfering RNA and doxorubicin overcome drug resistance in cancer*. The Journal of biological chemistry, 2010. **285**(29): p. 22639-50.
171. Watanabe, M., et al., *In vivo antitumor activity of camptothecin incorporated in liposomes formulated with an artificial lipid and human serum albumin*. Journal of controlled release : official journal of the Controlled Release Society, 2008. **127**(3): p. 231-8.
172. Bourguignon, L.Y.W., *Hyaluronan-mediated CD44 activation of RhoGTPase signaling and cytoskeleton function promotes tumor progression*. Seminars in cancer biology, 2008. **18**(4): p. 251-9.
173. Mero, A. and M. Campisi, *Hyaluronic Acid Bioconjugates for the Delivery of Bioactive Molecules*. Polymers, 2014. **6**(2): p. 346-369.
174. Mackay, R. and H. Stark, *Expression and Modulation of CD44 Variant Isoforms in Humans*. The Journal of cell biology, 1994. **124**(January): p. 71-82.
175. Hellström, M., B. Johansson, and A. Engström-Laurent, *Hyaluronan and its receptor CD44 in the heart of newborn and adult rats*. The anatomical record. Part A, Discoveries in molecular, cellular, and evolutionary biology, 2006. **288**(6): p. 587-92.
176. Garcia, A.a., et al., *Phase I clinical trial of topotecan and pegylated liposomal doxorubicin*. Cancer investigation, 2005. **23**(8): p. 665-70.
177. Lau, D., et al., *Population-based phase I trial of irinotecan and epirubicin*. American journal of clinical oncology, 2008. **31**(3): p. 226-30.
178. Shoji, T., et al., *A phase I study of irinotecan and pegylated liposomal doxorubicin in recurrent ovarian cancer (Tohoku Gynecologic Cancer Unit*

104 study). Cancer chemotherapy and pharmacology, 2014. **73**(5): p. 895-901.
179. Smith, S.M., et al., *Sequential doxorubicin and topotecan in relapsed/refractory aggressive non-Hodgkin's lymphoma: results of CALGB 59906*. Leukemia & lymphoma, 2006. **47**(8): p. 1511-7.
180. Wagner, S., et al., *Pegylated-liposomal doxorubicin and oral topotecan in eight children with relapsed high-grade malignant brain tumors*. Journal of neuro-oncology, 2008. **86**(2): p. 175-81.
181. Alexis, F. and E. Pridgen, *Factors affecting the clearance and biodistribution of polymeric nanoparticles*. Molecular ..., 2008. **5**(4): p. 505-515.
182. Cabral, H., et al., *Accumulation of sub-100 nm polymeric micelles in poorly permeable tumours depends on size*. Nature Nanotechnology, 2011. **6**(12): p. 815-823.
183. Charrois, G.J. and T.M. Allen, *Drug release rate influences the pharmacokinetics, biodistribution, therapeutic activity, and toxicity of pegylated liposomal doxorubicin formulations in murine breast cancer*. Biochimica et Biophysica Acta (BBA)-Biomembranes, 2004. **1663**(1): p. 167-177.
184. Geng, Y., et al., *Shape effects of filaments versus spherical particles in flow and drug delivery*. Nature nanotechnology, 2007. **2**(4): p. 249-55.
185. Barua, S., et al., *Particle shape enhances specificity of antibody-displaying nanoparticles*. Proceedings of the National Academy of Sciences, 2013. **110**(9): p. 3270-3275.
186. Kolhar, P., et al., *Using shape effects to target antibody-coated nanoparticles to lung and brain endothelium*. Proceedings of the National Academy of Sciences of the United States of America, 2013. **110**(26): p. 10753-8.
187. Brown, T.J., *Hyaluronan-chemotherapeutic agent formulations for the treatment of colon cancer*. 2013, Google Patents.
188. Danhauser-Riedl, S., et al., *Phase I clinical and pharmacokinetic trial of dextran conjugated doxorubicin (AD-70, DOX-OXD)*. Investigational New Drugs, 1993. **11**(2-3): p. 187-195.
189. Singer, J.W., *Paclitaxel poliglumex (XYOTAX™, CT-2103): A macromolecular taxane*. Journal of Controlled Release, 2005. **109**(1–3): p. 120-126.
190. Wang, J., et al., *The Role of Micelle Size in Tumor Accumulation, Penetration, and Treatment*. ACS Nano, 2015.
191. Duncan, R., et al., *Effect of molecular size of 125I-labelled poly (vinylpyrrolidone) on its pinocytosis by rat visceral yolk sacs and rat peritoneal macrophages*. Biochem. J, 1981. **196**: p. 49-55.
192. Camacho, K.M., et al., *Synergistic Antitumor Activity of Camptothecin-Doxorubicin Combinations and their Conjugates with Hyaluronic Acid*. Journal of Controlled Release, 2015. **210**: p. 198-207.
193. Fischer, D., et al., *A novel non-viral vector for DNA delivery based on low molecular weight, branched polyethylenimine: effect of molecular weight on transfection efficiency and cytotoxicity*. Pharmaceutical research, 1999. **16**(8): p. 1273-1279.

194. Harasym, T.O., P.R. Cullis, and M.B. Bally, *Intratumor distribution of doxorubicin following iv administration of drug encapsulated in egg phosphatidylcholine/cholesterol liposomes*. Cancer chemotherapy and pharmacology, 1997. **40**(4): p. 309-317.
195. Fujimoto-Ouchi, K., Y. Tanaka, and T. Tominaga, *Schedule dependency of antitumor activity in combination therapy with capecitabine/5′-deoxy-5-fluorouridine and docetaxel in breast cancer models*. Clinical cancer research, 2001. **7**: p. 1079-1086.
196. Zoli, W., et al., *Schedule-dependent interaction of doxorubicin, paclitaxel and gemcitabine in human breast cancer cell lines*. International Journal of Cancer, 1999. **80**(3): p. 413-6.
197. D'Souza, A.J.M. and E.M. Topp, *Release from polymeric prodrugs: linkages and their degradation*. Journal of pharmaceutical sciences, 2004. **93**(8): p. 1962-1979.
198. Majumdar, S. and T.J. Siahaan, *Peptide-mediated targeted drug delivery*. Medicinal research reviews, 2012. **32**(3): p. 637-658.
199. Lankelma, J., et al., *A mathematical model of drug transport in human breast cancer*. Microvascular research, 2000. **59**(1): p. 149-61.
200. De Gier, J., J. Mandersloot, and L. Van Deenen, *The role of cholesterol in lipid membranes*. Biochimica et Biophysica Acta (BBA)-Biomembranes, 1969. **173**(1): p. 143-145.
201. Lichtenberg, D., *Liposomes - Preparation, Characterization, and Preservation*. Methods of Biochemical Analysis, 1988. **33**.
202. WU, M., et al., *CHARACTERISTICS OF DRUG COMBINATION THERAPY IN ONCOLOGY BY ANALYZING CLINICAL TRIAL DATA ON CLINICALTRIALS.GOV*, in *Biocomputing 2015*. 2014, WORLD SCIENTIFIC. p. 68-79.